

**ENGINEERING POLYMERIC MATRICES FOR CONTROLLED DRUG
DELIVERY APPLICATIONS: FROM BULK GELS TO NANOGELS**

by

Yingkai Liang

A dissertation submitted to the Faculty of the University of Delaware in partial fulfillment of the requirements for the degree of Doctor of Philosophy in Materials Science and Engineering

Summer 2016

© 2016 Yingkai Liang
All Rights Reserved

ProQuest Number: 10192030

All rights reserved

INFORMATION TO ALL USERS

The quality of this reproduction is dependent upon the quality of the copy submitted.

In the unlikely event that the author did not send a complete manuscript and there are missing pages, these will be noted. Also, if material had to be removed, a note will indicate the deletion.



ProQuest 10192030

Published by ProQuest LLC (2016). Copyright of the Dissertation is held by the Author.

All rights reserved.

This work is protected against unauthorized copying under Title 17, United States Code
Microform Edition © ProQuest LLC.

ProQuest LLC.
789 East Eisenhower Parkway
P.O. Box 1346
Ann Arbor, MI 48106 - 1346

**ENGINEERING POLYMERIC MATRICES FOR CONTROLLED DRUG
DELIVERY APPLICATIONS: FROM BULK GELS TO NANOGELS**

by

Yingkai Liang

Approved: _____
Darrin J. Pochan, Ph.D.
Chair of the Department of Materials Science and Engineering

Approved: _____
Babatunde A. Ogunnaike, Ph.D.
Dean of the College of Engineering

Approved: _____
Ann L. Ardis, Ph.D.
Senior Vice Provost for Graduate and Professional Education

I certify that I have read this dissertation and that in my opinion it meets the academic and professional standard required by the University as a dissertation for the degree of Doctor of Philosophy.

Signed:

Kristi L. Kiick, Ph.D.
Professor in charge of dissertation

I certify that I have read this dissertation and that in my opinion it meets the academic and professional standard required by the University as a dissertation for the degree of Doctor of Philosophy.

Signed:

Darrin J. Pochan, Ph.D.
Member of dissertation committee

I certify that I have read this dissertation and that in my opinion it meets the academic and professional standard required by the University as a dissertation for the degree of Doctor of Philosophy.

Signed:

Xinqiao Jia, Ph.D.
Member of dissertation committee

I certify that I have read this dissertation and that in my opinion it meets the academic and professional standard required by the University as a dissertation for the degree of Doctor of Philosophy.

Signed:

R. Mark Jones, Ph.D.
Member of dissertation committee

ACKNOWLEDGMENTS

My science journey at the University of Delaware has been challenging yet incredibly rewarding. My time as a graduate student in the Department of Materials Science and Engineering has enabled me to push myself far beyond my mental limit and emerge stronger as a result. Over the past five years of Ph.D. training, I have become wiser, tougher, and more confident and comfortable in dealing with uncertainty and failure. Looking back, I realize that the improvements that I have made and the completion of this journey would not have been possible without the help and support I received along the way. For that, I am forever grateful.

First and foremost, I would like to thank my advisor, Dr. Kristi Kiick, for her mentorship. This dissertation work would not have been possible without her support, guidance and encouragement. Her remarkable erudition, strong enthusiasm for science, and high level of professionalism have set an example of an outstanding scholar and scientist, which has always been my motivation and inspiration throughout my graduate career. I am very grateful for the intellectual independence that she granted me and the projects and resources that she provided, which allowed me to expand my knowledge in materials science and obtain exposure to new areas and technologies. I am also very appreciative of the opportunities that she provided me to author scientific publications, attend conferences, and participate in interdisciplinary collaborations, which have been instrumental in my professional development as a scientist. I am honored and privileged to have the opportunity to work with a great mentor and educator like Dr. Kiick.

I would also like to thank my committee members, Dr. Darrin Pochan and Dr. Xinqiao Jia from the Department of Materials Science and Engineering at UD, and Dr. Mark Jones from Fraunhofer USA Center for Molecular Biotechnology, for their valuable suggestions and constructive feedback on my research. Specifically, I would like to thank Dr. Pochan for the helpful discussion on my research results and ideas, as well as his strong support on my external award application. I would also like to express my gratitude to Dr. Jia, for her instruction in polymer chemistry and the opportunity to teach the Polymer Synthesis and Characterization Laboratory. I am also deeply indebted to Dr. Jones, for the access to the state-of-the-art facilities and resources at Fraunhofer, his insightful comments on protein characterization, and valuable advice about career development.

Additionally, the help and support from friends and colleagues at UD and Fraunhofer have also been critical to my success as a graduate student. I am grateful to all current and past members for the Kiick group, for creating a supportive and motivating work environment. I would like to thank Linqing Li, Longxi Xiao, and Xian Xu, for their helpful conversations and suggestions regarding my work. I would like to thank Tianzhi Luo, Hang Kuen Lau, Ying Hao, and Wenwen Liu for their assistance in microscopy experiments as well as Dr. Chaoying Ni, Frank Kriss and Fei Deng for the access to the Keck Center for Advanced Microscopy and Microanalysis Facility. I am grateful to Dr. Shi Bai for his instruction in NMR spectroscopy and the access to the advanced NMR facility. I am very thankful to my colleagues and collaborators at Fraunhofer, Slobodanka (Dina) Manceva, Megan Coffin, and Jessica Chichester for their help and contribution in protein characterization, *in vitro* activity assays and animal experiments on the antibody release work. I would also like to thank all my friends and

colleagues for their friendship and support along this journey and making my time in graduate school a memorable experience of my life: Bradford Paik, Prathamesh Kharkar, Kevin Dicker, Kevin Jones, Cory Bomberger, Nandita Bhagwat, Christopher McGann, Morgan Urello, Haocheng Wu, Yu Tian, Shuang Liu, Aidan Zerdoum, Eric Fowler, He Zhang, Olivia George, Chris Koehler, Yingchao Chen, Jessie Sun and Michael Haider.

Furthermore, I am grateful to all current and past staff members in the Department of Materials Science and Engineering, especially Charles Garbini, Christine Williamson, Robin Buccos, Naima Hall, and Kathy Forwood, for ensuring lab safety and providing assistance with administrative needs.

Finally, I would like to express my sincere gratitude to my family and loved ones for their unconditional love, support and encouragement. I am most appreciative to my parents, my brother and my girlfriend for their care and emotional support as well as their respect and understanding of the decisions that I made in my life.

Once again, I would like to reiterate my gratefulness to everyone from the bottom of my heart. I will always be thankful for your help and support and remember the time we learned and grew together.

TABLE OF CONTENTS

| | |
|-----------------------|----|
| LIST OF TABLES | x |
| LIST OF FIGURES | xi |
| ABSTRACT | xx |

Chapter

| | | |
|--------|--|----|
| 1 | INTRODUCTION | 1 |
| 1.1 | Drug Delivery Systems..... | 1 |
| 1.2 | Hydrogels for Drug Delivery..... | 4 |
| 1.3 | Nanoparticle-Containing Hydrogels for Drug Delivery | 8 |
| 1.4 | Nanoparticles for Drug Delivery | 11 |
| 1.5 | Dissertation Summary | 15 |
| | REFERENCES | 18 |
| 2 | CONTROLLED RELEASE OF AN ANTHRAX TOXIN- NEUTRALIZING ANTIBODY FROM HYDROLYTICALLY DEGRADABLE POLYETHYLENE GLYCOL HYDROGELS | 30 |
| 2.1 | Introduction | 30 |
| 2.2 | Materials and Methods | 32 |
| 2.2.1 | Materials | 32 |
| 2.2.2 | Purification of Plant-Produced mAb PANG | 33 |
| 2.2.3 | Formation of Degradable PEG Hydrogels | 33 |
| 2.2.4 | Rheological Characterization of PEG Hydrogels..... | 34 |
| 2.2.5 | Swelling Experiments..... | 35 |
| 2.2.6 | <i>In Vitro</i> Protein Release Experiments | 35 |
| 2.2.7 | Size Exclusion Chromatography | 36 |
| 2.2.8 | Circular Dichroism Spectroscopy..... | 36 |
| 2.2.9 | Fluorescence Emission Spectroscopy..... | 37 |
| 2.2.10 | Anthrax Lethal Toxin Neutralization Assay..... | 37 |
| 2.3 | Results | 38 |
| 2.3.1 | Hydrogel Compositions and Formation | 38 |

| | | |
|------------------|---|-----------|
| 2.3.2 | Swelling Experiments..... | 40 |
| 2.3.3 | <i>In Vitro</i> Studies of PANG Release from PEG-Based Hydrogels | 42 |
| 2.3.4 | In-Gel and Post-Release Characterization of PANG..... | 45 |
| 2.3.5 | Biological Activity of Released PANG..... | 52 |
| 2.4 | Discussion..... | 53 |
| 2.5 | Conclusions | 55 |
| REFERENCES | | 57 |
| 3 | LIPOSOME-CROSSLINKED HYBRID HYDROGELS FOR GLUTATHIONE-TRIGGERED DELIVERY OF MULTIPLE CARGO MOLECULES | 62 |
| 3.1 | Introduction | 62 |
| 3.2 | Materials and Methods | 65 |
| 3.2.1 | Materials | 65 |
| 3.2.2 | Synthesis of Arylthiol End-Functionalized 4-Arm PEG | 66 |
| 3.2.3 | Preparation of Maleimide-Functionalized Liposomes | 67 |
| 3.2.4 | Preparation of Liposome-Crosslinked Hybrid Hydrogels | 67 |
| 3.2.5 | Rheological Studies | 68 |
| 3.2.6 | Scanning Electron Microscopy..... | 69 |
| 3.2.7 | Fluorescent Labeling and Confocal Microscopy..... | 70 |
| 3.2.8 | Mass Loss Studies | 70 |
| 3.2.9 | <i>In Vitro</i> DOX Encapsulation and Release | 71 |
| 3.2.10 | Co-Delivery of DOX and Cytochrome <i>c In Vitro</i> | 72 |
| 3.2.11 | Data Fitting of the Release Profiles of DOX and Cytochrome <i>c</i> | 72 |
| 3.2.12 | Data Analysis..... | 73 |
| 3.3 | Results and Discussion | 74 |
| 3.3.1 | Hydrogel Design..... | 74 |
| 3.3.2 | Rheological Characterization | 76 |
| 3.3.3 | Morphology of the Liposome-Crosslinked Hydrogels..... | 80 |
| 3.3.4 | Fluorescence Imaging of the Liposome-Crosslinked Hydrogels | 82 |
| 3.3.5 | Hydrogel Stability | 84 |
| 3.3.6 | Liposome Stability..... | 89 |
| 3.3.7 | <i>In Vitro</i> Release of DOX from Liposome-Crosslinked Hybrid Hydrogels | 93 |
| 3.3.8 | Co-Delivery of DOX and Cytochrome <i>c</i> | 98 |
| 3.4 | Conclusions | 103 |

| | |
|---|-----|
| REFERENCES | 105 |
| 4 MULTIFUNCTIONAL LIPID-COATED POLYMER NANOGELS CROSSLINKED BY PHOTO-TRIGGERED MICHAEL-TYPE ADDITION..... | 114 |
| 4.1 Introduction | 114 |
| 4.2 Materials and Methods | 117 |
| 4.2.1 Materials | 117 |
| 4.2.2 Synthesis of Photolabile, Protected PEG-SH | 118 |
| 4.2.3 Bulk Gel Preparation via Photo-Triggered Michael-type Addition and Subsequent Rheological Analysis | 118 |
| 4.2.4 Synthesis of Lipid-Coated Nanogels (NG)..... | 119 |
| 4.2.5 Surface Functionalization of Lipid-Coated Nanogels | 120 |
| 4.2.6 Dynamic Light Scattering (DLS) and Zeta Potential Analysis . | 121 |
| 4.2.7 Transmission Electron Microscopy (TEM) Characterization of Nanogel Morphology..... | 121 |
| 4.3 Results and Discussion | 122 |
| 4.3.1 Photodeprotection and Photo-Triggered Gelation..... | 122 |
| 4.3.2 Synthesis and Characterization of Lipid-Coated Nanogels (NGs) | 127 |
| 4.3.3 Surface Functionalization of Lipid-coated Nanogels | 131 |
| 4.4 Conclusions | 138 |
| REFERENCES | 139 |
| 5 CONCLUSIONS AND FUTURE DIRECTIONS | 146 |
| 5.1 Conclusions and Significance..... | 146 |
| 5.2 Future Directions | 148 |
| 5.2.1 Dual Responsive PEG-Collagen-Like Peptide Physical Hydrogels | 148 |
| 5.2.2 Glutathione(GSH)-Sensitive Crosslinked Liposomes | 152 |
| REFERENCES | 157 |
| Appendix | |
| COPYRIGHT PERMISSION FOR REPRINT OF PUBLISHED ARTICLES..... | 159 |

LIST OF TABLES

| | |
|--|----|
| Table 2.1 Formulations of different PEG hydrogels | 40 |
| Table 2.2 SEC analysis of the physical state of released PANG..... | 47 |

LIST OF FIGURES

- Figure 1.1 A comparison of drug concentration profiles between conventional drug delivery formulations (e.g. tablets or bolus injections) and controlled and sustained delivery systems (e.g. polymer implants or microspheres). Conventional drug delivery formulations commonly result in a bolus release of drugs followed by an immediate decrease of drug concentration below the therapeutic range. Controlled and sustained delivery systems can achieve prolonged therapeutic effect by continuously releasing the drugs over an extended period of time after administration of a single dose..... 2
- Figure 1.2 Controlled release of therapeutics from various drug delivery systems. (a) Solid polymer matrices composed of poly(ethylene-co-vinyl acetate) (EVA), where the therapeutic molecules diffuse through a tortuous network of interconnected pores that form during phase separation of drug/excipient from polymer. (b) Reservoir controlled release systems made from semi-permeable silicone rubber membranes (chemically cross-linked polydimethylsiloxane), through which the release of encapsulated therapeutics is regulated. (c) Water-swollen polymer hydrogels prepared from water-soluble polymers, such as poly(ethylene glycol) (PEG), where the rate of drug release is controlled by the mesh size of the swollen polymer network. Reprinted with permission from Ref.⁷, copyright (2016) American Chemical Society..... 3

| | | |
|------------|---|----|
| Figure 1.3 | <p>Various types of degradable hydrogel systems. (A) Hydrolytically degradable hydrogels that can control the release of therapeutics via hydrolysis over time. (B) Proteolytically degradable hydrogels that are formed based on guest-host interactions. Hydrogel degradation can be selectively triggered by cell-secreted enzymes such as matrix metalloproteinases (MMPs), releasing the encapsulated therapeutics (e.g., growth factors and proteins) within the matrix. (C) Photo-triggered release of green fluorescent protein (GFP) from dextran-based photodegradable hydrogels via the incorporation of the photolabile <i>o</i>-nitrobenzyl moiety. (D) Glutathione (GSH)-sensitive hydrogels that can undergo matrix degradation and offer targeted delivery of therapeutic molecules in GSH-containing environments. Reprinted with permission from (A) Ref.²⁶, copyright (2012) Nature Publishing Group; (B) Ref.²⁷, copyright (2015) American Chemical Society; (C) Ref.²⁸, copyright (2011) Royal Society of Chemistry; (D) Ref.²⁹, copyright (2012) Royal Society of Chemistry.</p> | 5 |
| Figure 1.4 | <p>Schematic of thiol Michael-type addition and reactivity of various vinyl groups (Michael acceptors) used in the reactions.</p> | 7 |
| Figure 1.5 | <p>Strategies in the formation of nanoparticle-containing hydrogels. (A) Physical encapsulation of nanoparticles during hydrogel formation. (B) Fabrication of self-assembled hydrogels employing polymer-nanoparticle physical interactions (e.g. hydrophobic or electrostatic interactions). (C) Hierarchical hybrid hydrogels prepared via the use of nanoparticles as covalent crosslinkers. Reprinted with permission from (A) Ref.⁸³, copyright (2014) American Chemical Society; (B) Ref.⁸⁴, copyright (2015) Nature Publishing Group; (C) Ref.⁸⁵, copyright (2012) Wiley.</p> | 10 |
| Figure 1.6 | <p>Nanoparticle agents are designed to utilize the enhanced permeability and retention (EPR) effect to exit leaky blood vessels and accumulate in the tumor, and to target tumor cells by functionalizing the surface of nanoparticles with ligands that promote cell-specific recognition and binding. The nanoparticles can (i) release their contents in close proximity to the target cells; (ii) attach to the membrane of the cell and act as an extracellular sustained-release drug depot; or (iii) internalize into the cell by endocytosis before releasing their drug payloads. Reprinted with permission from Ref.⁷⁰, copyright (2007) Nature Publishing Group.</p> | 13 |

| | | |
|------------|---|----|
| Figure 1.7 | Structure and synthetic strategies of polymer nanogels. (A) Crosslinked network structure of polymer nanogels. (B) Chemical synthesis of nanogels by inverse emulsion polymerization, where each droplet of polymer solution is isolated and crosslinked into nanoparticle. (C) Preparation of nanogels using liposome templated method, where crosslinked network is formed in the aqueous lumen of the liposome. Reprinted with permission from (A) Ref. ¹²⁸ , copyright (2011) American Chemical Society; (B) and (C) Ref. ¹¹⁷ , copyright (2010) Wiley..... | 15 |
| Figure 2.1 | Schematic representation of the formation and degradation of PANG-loaded PEG hydrogels. | 38 |
| Figure 2.2 | <i>In situ</i> gelation of 20wt% 8-arm 10/2K hydrogel, as characterized by oscillatory rheology. The evolution of G' (storage modulus) and G'' (loss modulus) was monitored as a function of time. | 39 |
| Figure 2.3 | Equilibrium swelling properties of various PEG hydrogels. (a) 4-arm 10/5K gels at different concentration; (b) 20wt% hydrogels prepared from polymer precursors with different functionalities and molecular weights..... | 41 |
| Figure 2.4 | <i>In vitro</i> cumulative release of PANG from various PEG hydrogels at a precursor concentration of 20wt%, with an initial loading concentration of 2.5 mg/mL, as a function of time. The release of protein was monitored by measuring the absorbance, at 280 nm, of the buffer solution above the gel at the indicated time intervals..... | 43 |
| Figure 2.5 | <i>In vitro</i> cumulative release of PANG from various 20wt% 4-arm hydrogels with different precursor molecular weights, with an initial loading concentration of 2.5 mg/mL, as a function of time. The release of protein was monitored by measuring the absorbance, at 280 nm, of the buffer solution above the gel at the indicated time intervals..... | 45 |
| Figure 2.6 | Normalized SEC trace of PANG controls and PANG released from the hydrogels after 28 days in PBS. Elution was monitored by UV absorbance at 280 nm. | 46 |
| Figure 2.7 | SDS-PAGE electrophoresis depicting protein release under (a) reducing and (b) non-reducing conditions. Lane 1: D35 sample from 10/2K; Lane 2: D35 PANG Control at 37°C; Lane 3: PANG Standard at -80°C; Lane 4: D56 sample from 10K/700; Lane 5: D56 PANG Control at 37°C; Lane 6: PANG Standard at -80°C..... | 48 |

| | | |
|-------------|---|----|
| Figure 2.8 | Conformational characterization of PANG control solutions and of PANG released from the hydrogels. (a) CD spectra of solutions of PANG control and PANG released from hydrogels; (b) Normalized fluorescence emission spectra of PANG control and PANG released from hydrogels. | 50 |
| Figure 2.9 | Conformational characterizations of PANG (5 mg/mL) when encapsulated within the hydrogels. (a) CD spectra of PANG control and encapsulated PANG; (b) Normalized fluorescence emission spectra of PANG control and encapsulated PANG. | 51 |
| Figure 2.10 | <i>In vitro</i> characterization of PANG released from PEG hydrogels. (a) Toxin-neutralizing activity of released PANG on J774A.1 cells incubated with LeTx; (b) Concentration profile of the <i>in vitro</i> released protein samples as characterized by UV-Vis at 280 nm. | 52 |
| Figure 3.1 | Chemical structures of the lipids used for liposome formulation (A) and the PEG-SH polymers employed for hybrid hydrogel formation (B). DOPC: 1,2-dioleoyl-sn-glycero-3-phosphocholine; DOPG: 1,2-dioleoyl-sn-glycero-3-phospho-(1'-rac-glycerol); MPB-PE: 1,2-dioleoyl-sn-glycero-3-phosphoethanolamine-N-[4-(p-maleimidophenyl) butyramide]. | 74 |
| Figure 3.2 | Schematic representation of the formation and degradation of the liposome-crosslinked hybrid hydrogels. The UD logos are used with permission from the University of Delaware. | 75 |
| Figure 3.3 | Representative oscillatory time sweep of the liposome-crosslinked hydrogels (1:2 Mal:SH ratio) in pH=7.0 bis-tris buffer at 37°C. | 77 |
| Figure 3.4 | Rheological characterization of liposome-crosslinked hybrid hydrogels at various crosslinking ratios (1:1, 1:2, and 1:4 Mal:SH ratios). A) Oscillatory frequency sweep of the hydrogels from 0.1 to 100 rad/s at 1% strain amplitude. B) Summary of storage moduli (G') of hydrogels prepared at different crosslinking ratios. | 79 |
| Figure 3.5 | Scanning electron microscopy (SEM) images of the liposome-crosslinked hybrid hydrogels after critical point drying. | 81 |
| Figure 3.6 | Scanning electron microscopy (SEM) images of 6wt% PEG hydrogel control lacking liposomes. | 81 |

| | | |
|-------------|--|----|
| Figure 3.7 | Chemical structures of the lipids used for fluorescent labeled liposome formulation. NBD-PC: 1-Oleoyl-2-[12-[(7-nitro-2-1,3-benzoxadiazol-4-yl)amino]dodecanoyl]-sn-Glycero-3-Phosphocholine; DOPC: 1,2-dioleoyl-sn-glycero-3-phosphocholine; DOPG: 1,2-dioleoyl-sn-glycero-3-phospho-(1'-rac-glycerol); MPB-PE: 1,2-dioleoyl-sn-glycero-3-phosphoethanolamine-N-[4-(p-maleimidophenyl)butyramide]..... | 82 |
| Figure 3.8 | Confocal images of fluorescent labeled liposome-crosslinked hydrogels. A) Liposomes are well distributed throughout the majority of the matrix, forming interconnected network. B) Slight aggregation of liposomes during gelation is observed within the matrix due to increased viscosity and evaporation of the solution during crosslinking. C) Overall Z-Stack of the fluorescent liposome distribution within the hydrogel to a depth of ~15 μm | 84 |
| Figure 3.9 | Evolution of storage modulus of the liposome-crosslinked hydrogel, as well as a PEG hydrogel control, when incubated with 10% Triton TM X-100 in water at 37°C, as monitored by oscillatory rheology. Mean and S.D. are shown (n = 3). Inset: visual inspection of the liposome-crosslinked hydrogel immersed in 10% Triton TM X-100 at 37°C over time. Both hydrogel images were taken with 10% Triton TM X-100 in the supernatant to mimic the conditions in the rheological measurements and to provide parallel comparisons. The UD logos are used with permission from the University of Delaware..... | 85 |
| Figure 3.10 | Mass loss studies of the liposome-crosslinked hybrid hydrogels in incubation with PBS and GSH in various concentrations at 37°C after initial equilibrium swelling in PBS for 24h. Mean and S.D. are shown (n = 3). | 86 |
| Figure 3.11 | Fitting of the degradation profiles from liposome-crosslinked hybrid hydrogels synthesized from arylthiol-PEG and alkylthiol-PEG respectively. A) Degradation kinetics of the aryl lipogel in 10 μM GSH; fitting is performed based on the rate law for second order kinetics ($-dM/dt = k[M][GSH] \approx kM^2$) considering the comparable concentration of GSH and crosslinks. B) Degradation kinetics of the aryl lipogel in 10 mM GSH; fitting is performed based on zero-order kinetics ($-dM/dt = k$) given the almost linear release observed. C) Degradation kinetics of the alkyl lipogel in 10 mM GSH; fitting is performed based on first-order kinetics ($-dM/dt = k[M]$) because of the excess amount of GSH, which renders its concentration unchanged over the course of the experiment. | 88 |

| | |
|---|----|
| Figure 3.12 Hydrodynamic diameter of liposomes prior to hydrogel formation, released liposomes after complete network degradation in 10 mM GSH, and any particles in the gel supernatant after 10% Triton™ X-100 incubation at 37°C, as determined by dynamic light scattering (DLS)..... | 90 |
| Figure 3.13 Confocal images of fluorescently labeled liposomes prior to hydrogel formation (A) and released after network degradation (B). Insert: expanded view of the confocal images..... | 92 |
| Figure 3.14 <i>In vitro</i> release of DOX from the liposome-crosslinked hydrogels at 37°C as assessed via visual inspection and fluorimetry. (A) Image of DOX-loaded liposome-crosslinked hydrogels incubated in 10 mM GSH (left, diffuse boundary observed) and PBS (right, clear boundary maintained) solutions on day 1; (B) Cumulative release profiles of DOX from liposome-crosslinked hydrogels in 10 mM GSH or in PBS solutions. * indicates the time point where ~90% hydrogel dissolution was observed. Mean and S.D. are shown (n = 3). | 92 |
| Figure 3.15 Fitting of the DOX release profiles from the liposome-crosslinked hybrid hydrogels (A) with network degradation and (B) lacking network degradation. A) Fitting of DOX release data is based on the the Ritger-Peppas equation (n=1). Data plotted as M_t / M_∞ versus t . B) Fitting of DOX release data is based on the early-time approximation of Fickian diffusion. Data plotted as M_t / M_∞ versus $t_{1/2}$ | 94 |
| Figure 3.16 <i>In vitro</i> DOX release profiles from 6wt% PEG hydrogel control prepared by reacting 4-arm aryl PEG-SH and 4-arm PEG-maleimide. Release experiments were carried out in 10 mM GSH in PBS and PBS solutions alone respectively at 37°C. Mean and S.D. are shown (n = 2)..... | 95 |
| Figure 3.17 <i>In vitro</i> release of DOX from the liposome-crosslinked hydrogels at 37°C in PBS. 10% Triton™ X-100 was applied to the aryl lipogels incubated in PBS at Day 10, resulting in the liberation of more liposome-encapsulated DOX. Mean and S.D. are shown (n = 3). | 96 |
| Figure 3.18 <i>In vitro</i> release of freely diffusing DOX from the liposome-crosslinked hydrogels in 10 mM GSH solutions, as monitored after dialysis in a cup-like mini dialysis device (MWCO 3.5K) at 37°C. Mean and S.D. are shown (n = 3)..... | 97 |

| | | |
|-------------|---|-----|
| Figure 3.19 | SDS-PAGE electrophoresis of cytochrome c (Lane 1) and a mixture of cytochrome c and 4-arm PEG arylthiol (Lane 2). The cytochrome c was incubated with PEG arylthiol polymers (1mg cytochrome c and 3mg of PEG polymer, the same amount as was employed in hydrogel formation, were incubated for 1h at 37°C)..... | 99 |
| Figure 3.20 | Release profiles of DOX and cytochrome c from the liposome-crosslinked hydrogels in 10 mM GSH at 37°C. A) Co-delivery of DOX and cytochrome c from a single gel. B) Individual release of DOX and cytochrome c from separate gels (DOX release data replotted from Figure 3.13). M_t/M_∞ represents the cumulative fractional mass released at time t . Dashed lines indicate the fitted curves of the release profiles. The mean and S.D. are shown (n = 3). | 99 |
| Figure 4.1 | Schematic of the protection of 4-arm PEG-thiol with photolabile groups: 1) DMF, 24h, R.T.; 2) water, 365nm, 10 mW/cm ² | 122 |
| Figure 4.2 | ¹ HNMR spectrum of four-arm thiolated PEG protected with the nitrobenzyl group. Functionality is calculated based on the integration of the aromatic protons of the protecting group relative to the methylene protons of the polymer. | 123 |
| Figure 4.3 | Schematic representation of the photo-triggered formation of PEG-based hydrogels via Michael-type addition. | 124 |
| Figure 4.4 | Oscillatory rheology time sweeps of 15wt% PEG hydrogels formed by photo-triggered Michael-type addition with (a) continuous and (b) periodic irradiation (365nm and 10mW/cm ²). | 124 |
| Figure 4.5 | Oscillatory rheology time sweeps of 15wt% PEG hydrogels formed by photo-triggered Michael-type addition (plotted in log scale)..... | 125 |
| Figure 4.6 | Comparison of storage moduli of PEG-SH/Mal hydrogels at different concentrations, after irradiation at 365nm, 10mW/cm ² in aqueous solution, characterized via oscillatory rheology..... | 126 |
| Figure 4.7 | Schematic representation of the synthesis of PEG-based nanogels via liposome templates in aqueous solutions. 1) DI water, polycarbonate membrane; 2) 2h, 365nm, 10 mW/cm ² | 127 |
| Figure 4.8 | Dynamic light scattering analysis of the hydrodynamic size of liposomes and lipid-coated nanogels in water at room temperature. | 128 |

| | | |
|-------------|---|-----|
| Figure 4.9 | TEM images of the lipid-coated nanogels dried from aqueous solution. | 129 |
| Figure 4.10 | Dynamic light scattering analysis of the hydrodynamic size of lipid-coated nanogels in PBS at different temperatures. | 131 |
| Figure 4.11 | Schematic representation of the synthesis of carboxylic-acid-functionalized, lipid-coated nanogels and the surface conjugation of a reactive fluorescent dye. 1) DI water, polycarbonate membrane; 2) 2h, 365nm, 10 mW/cm ² ; 3) EDC/sulfo-NHS solution, 1-aminomethylpyrene (dissolved in DMSO), pH=7.2, 4h, R.T.. | 132 |
| Figure 4.12 | Fluorescence spectra of carboxylic-acid-functionalized, lipid-coated nanogels and dye-conjugated nanogels in aqueous solution; $\lambda_{exc}=333\text{nm}$, 20°C; spectra of nanogels were normalized to the o-nitrosobenzaldehyde peak at 360nm, which should be of similar intensity for the various nanogels. | 133 |
| Figure 4.13 | Dynamic light scattering and zeta potential analysis of functional lipid-coated nanogels. Size distribution (a) and surface charge density (b) of carboxylic-acid-functionalized liposomes, carboxylic-acid-functionalized lipid-coated nanogels and dye-conjugated nanogels in water at room temperature. | 134 |
| Figure 4.14 | Fluorescence microscopy image of dye-conjugated nanogels in aqueous solution, characterized by confocal laser scanning microscopy (CLSM). | 135 |
| Figure 5.1 | Schematic illustration of the thermo-reversible gelling behaviors and chemical degradation of the PEG-CLP physical hydrogels. | 149 |
| Figure 5.2 | Schematic illustration of the synthesis of glutathione(GSH)-sensitive PEG-CLP conjugates. | 150 |
| Figure 5.3 | Visual inspection of the reversible thermal gelling behaviors of the 5wt% PEG-CLP hydrogels. The hydrogel is weakened into a liquid-like state at 80°C. Upon cooling, the liquid-like state rapidly transforms into a solid-like, self-standing gel. | 151 |
| Figure 5.4 | Visual inspection of the GSH-triggered degradation of the 5wt% PEG-CLP hydrogels. Matrix degradation is observed in 10 mM GSH solutions after incubation at 37°C overnight whereas the hydrogels remain intact and stable in PBS under the same conditions. | 152 |

| | | |
|------------|--|-----|
| Figure 5.5 | Schematic illustration of the design of GSH-sensitive, surface-crosslinked liposomes..... | 153 |
| Figure 5.6 | Schematic illustration of the stability of surface-crosslinked liposomes against Triton X-100 and GSH-triggered particle disassembly in Triton X-100..... | 154 |
| Figure 5.7 | Dynamic light scattering (DLS) characterization of various liposome samples: a) surface crosslinked liposomes; b) surface crosslinked liposomes with 5 mM Triton X-100; c) surface crosslinked liposomes with 5 mM Triton X-100 and 10 mM GSH..... | 155 |
| Figure 5.8 | <i>In vitro</i> DOX release profiles from surface crosslinked liposomes at 37°C in 10 mM GSH and PBS respectively..... | 156 |

ABSTRACT

Over the past few decades, drug delivery systems have been designed using a wide array of materials and chemical strategies to improve the specificity of therapeutics by increasing drug stabilities, controlling release profiles and localizing therapeutic effects. Among various types of drug delivery systems, hydrogels have emerged as a promising class of materials for the controlled release of bioactive molecules. Composed of hydrophilic three-dimensional polymer networks, hydrogels have several advantageous properties including high water content, tunable viscoelasticity, and biocompatibility, which allow bioactive molecules to be protected against degradation and released from the hydrogel matrix in a controlled manner over an extended period of time. Particularly, polyethylene glycol (PEG) hydrogels have been extensively used for controlled drug delivery applications with encouraging preclinical and clinical results, owing to the non-immunogenic nature, hydrophilicity and chemical versatility of PEG polymers. PEG hydrogel-based materials have received approval for use in a number of medical products including wound healing matrices, medical implants, and drug delivery depots.

In this work, we have specifically engineered PEG hydrogel matrices from bulk to nanoscale, including bulk hydrogels, nanoparticle-crosslinked hybrid hydrogels and nanogels for different delivery applications. Firstly, a library of hydrophilic and hydrolytically degradable PEG hydrogels has been developed for the sustained delivery of an anthrax toxin-neutralizing monoclonal antibody from 14-56 days. The hydrogels were formed via a Michael-type addition between multi-arm PEG-SH and

hydrolytically degradable crosslinkers of linear PEG-diacrylate. By varying the polymer architectures and molecular weights of the precursors, the degradation rate of the matrix can be systematically tuned, which in turn tailors the rate of antibody release from the hydrogels. In-gel and post-release analysis of the antibody samples indicate that the conformational properties and biological activity of the protein were well maintained.

In addition to bulk hydrogels for the long-term delivery of therapeutics, stimuli-responsive, nanoparticle-crosslinked hybrid hydrogels have also been introduced for the triggered and targeted release of therapeutic molecules. These hybrid hydrogels were constructed using maleimide-functionalized liposomes (~100nm) as structural elements to crosslink with thiolated 4-arm PEG polymers via Michael-type addition. Degradation of these hydrogels was selectively triggered upon exposure to thiol-containing molecules such as glutathione (GSH), offering great advantages for controlled and triggered release of therapeutic cargos under reducing environments that are analogous to the GSH-overproduced tumor microenvironment. The hierarchical structure of these hybrid hydrogels allows dual encapsulation and prolonged, sequential delivery of multiple therapeutic molecules with different release mechanism.

Motivated by the significant impact of nanotechnology on the development of nanoscale drug delivery vehicles, PEG nanogels that combine the advantages of both nanoparticulate and polymeric hydrogel systems were prepared via the use of liposome templates. The nanogels were formed by photo-triggered Michael-type addition of PEG polymer precursors encapsulated within the aqueous lumen of liposomes under UV irradiation. The production of nanogels was confirmed via dynamic light scattering (DLS) and transmission electron microscopy (TEM). The surface functionality of the

lipid-coated nanogels was demonstrated by surface modification with a reactive fluorescent dye as a proof of concept.

These PEG-based polymeric matrices provide a powerful platform for different specific delivery applications. The bulk, hydrolytically degradable PEG hydrogels present a simple yet efficient strategy to provide protein stabilization and long-term delivery of therapeutic proteins. The liposome-crosslinked hybrid hydrogels, on the other hand, suggest significant potential in the triggered and temporal release of multiple therapeutic molecules. Lastly, the PEG nanogels offer a unique strategy for the development of multifunctional nanoparticle therapeutics.

Chapter 1

INTRODUCTION

1.1 Drug Delivery Systems

Drugs and therapeutics have long been used to treat disease and improve health. The therapeutic efficacy of drugs is directly related to the way by which they are administered. Administration can affect drug pharmacokinetics, absorption, duration of therapeutic effect and toxicity.¹ Despite the promise of pharmaceutical development and early-stage discovery, many drug candidates face significant challenges during preclinical and clinical evaluation due to poor efficacy and limited bioavailability. For example, small molecule drugs can suffer from low solubility, poor stability, short circulation time, and non-specific toxicity, which greatly compromises their therapeutic efficacy.² Bioactive macromolecules such as nucleic acids, peptides, and proteins are often limited by poor stability and rapid clearance from the body.^{3,4} These challenges, coupled with the complexity and diversity of new pharmaceuticals, have stimulated the evolution of drug delivery systems that overcome bioavailability and delivery obstacles.⁵

Drug delivery systems based on the use of a wide array of materials and chemical strategies can improve the pharmacokinetics and pharmacodynamics of therapeutics by controlling the rate at which a drug is released and the location in the body where it is released.^{6,7} For example, polymer carriers loaded with therapeutics enable controlled temporal and spatial release of a drug by manipulating the diffusion of drug, the rate of dissolution, or degradation of the carrier, which maintains drug concentration within the

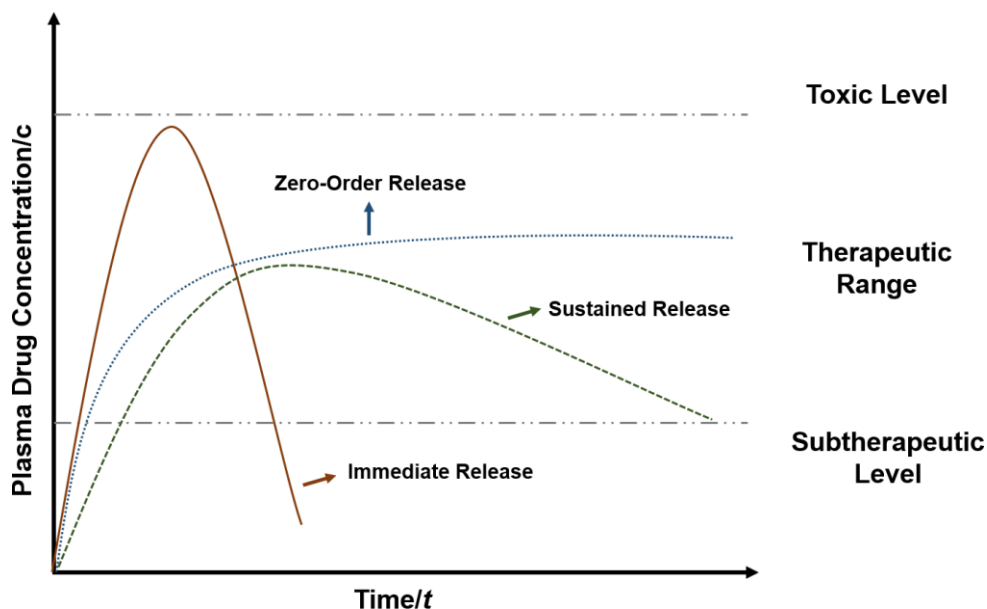


Figure 1.1 A comparison of drug concentration profiles between conventional drug delivery formulations (e.g. tablets or bolus injections) and controlled and sustained delivery systems (e.g. polymer implants or microspheres). Conventional drug delivery formulations commonly result in a bolus release of drugs followed by an immediate decrease of drug concentration below the therapeutic range. Controlled and sustained delivery systems can achieve prolonged therapeutic effect by continuously releasing the drugs over an extended period of time after administration of a single dose.

therapeutic window (effective dose, see Figure 1.1). By coating or conjugating the carrier with affinity reagents such as nucleic acids, peptides, antibodies, or ligands that could bind to specific cell receptors, therapeutic efficacy can be enhanced and off-target toxicity can be minimized by localization of the drug-loaded carrier at the pathological sites.⁸ Additionally, drug delivery systems can also be formulated to improve the *in vivo* solubility of lipophilic and hydrophobic drugs by encapsulation in a drug delivery carrier or by covalent conjugation or sequestration with a polymer.^{9,10}

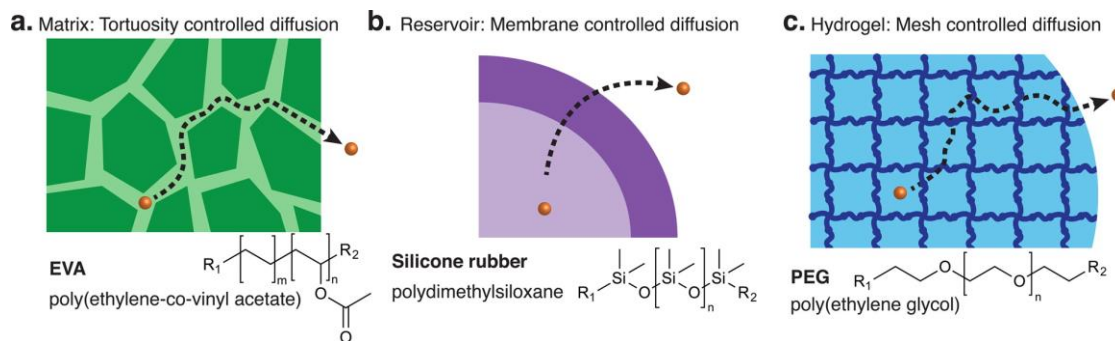


Figure 1.2 Controlled release of therapeutics from various drug delivery systems. (a) Solid polymer matrices composed of poly(ethylene-co-vinyl acetate) (EVA), where the therapeutic molecules diffuse through a tortuous network of interconnected pores that form during phase separation of drug/excipient from polymer. (b) Reservoir controlled release systems made from semi-permeable silicone rubber membranes (chemically cross-linked polydimethylsiloxane), through which the release of encapsulated therapeutics is regulated. (c) Water-swollen polymer hydrogels prepared from water-soluble polymers, such as poly(ethylene glycol) (PEG), where the rate of drug release is controlled by the mesh size of the swollen polymer network. Reprinted with permission from Ref.⁷, copyright (2016) American Chemical Society.

Over the past few decades, varieties of drug delivery systems have been developed (Figure 1.2), including diffusion-controlled solid polymer matrices and reservoirs (e.g. poly(ethylene-co-vinyl acetate) and silicone rubber (chemically crosslinked polydimethylsiloxane)),¹¹ water-swollen polymer hydrogels (e.g. poly(ethylene glycol) (PEG), polysaccharides, and polypeptides),^{12, 13} and polymer-based colloidal carriers (e.g. micro/nanoparticles, micelles, and micro/nanogels).^{14, 15} The choice of drug delivery system determines the drug loading capacity, the time span of release, and the route best suited for administration. Solid polymer matrices and reservoirs have shown great potential in long-term delivery of bioactive agents for up to 5 years but usually need to be implanted through a surgical intervention.¹⁶ Hydrogels

are advantageous for localized delivery as they could potentially be injected through syringes and needles and offer a broad range of release timeframes from days to months, although the size and solubility of drugs may limit the utility of these water-swollen polymer networks.¹⁷ Micro and nanoparticles can encapsulate a variety of drugs and achieve sustained release through systemic administration, yet non-specific uptake and local toxicity may induce undesired side effects.¹⁸ Therefore, selection of a drug delivery system must be driven by the nature of the drug and the inherent properties of the drug delivery system.

1.2 Hydrogels for Drug Delivery

Composed of cross-linked networks of hydrophilic polymers, hydrogels are capable of retaining large amounts of water yet remaining insoluble and maintaining their three-dimensional structure.^{19, 20} They are generally considered as biocompatible materials due to their high water content and mechanical softness, similar to natural extracellular matrices.²¹ Furthermore, the porous structures and tunable viscoelasticity of hydrogels provide great opportunity for the encapsulation of water-soluble therapeutics (e.g. proteins and peptides), allowing these bioactive molecules to be protected against degradation and released from the hydrogel matrix in a controlled manner over an extended period of time.²²

Proteins that are physically incorporated in the hydrogel matrix can be released via several mechanisms, such as diffusion, swelling, erosion or degradation, or a combination of these mechanisms.²³ Hydrogels allow fine-tuning of the protein release by tailoring their cross-link density via changes in polymer architecture, concentration, and molecular weight.²⁴ Over the years, varieties of stimuli-responsive hydrogels have

been developed via the incorporation of degradable functional groups in the backbones, crosslinks, and pendant groups. Hydrogel degradation permits systematic variations in the permeability of the network via engineering of the degradation rates and modes, offering great opportunities for the on-demand/target release of bioactive cargos (Figure 1.3).²⁵

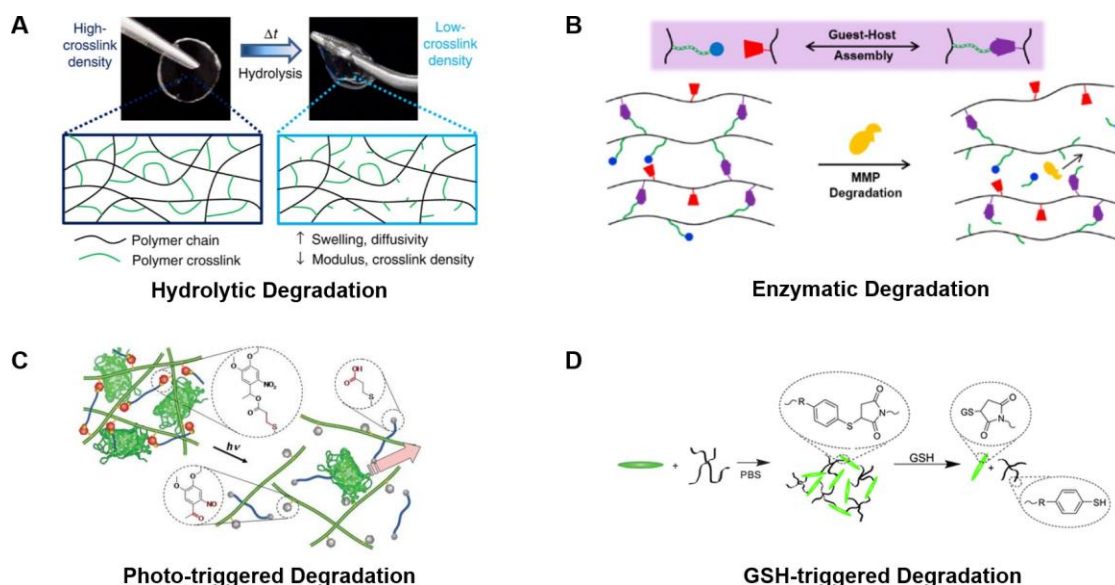
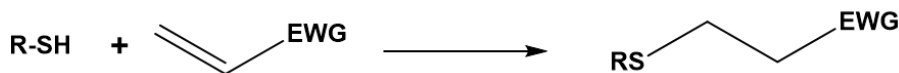


Figure 1.3 Various types of degradable hydrogel systems. (A) Hydrolytically degradable hydrogels that can control the release of therapeutics via hydrolysis over time. (B) Proteolytically degradable hydrogels that are formed based on guest-host interactions. Hydrogel degradation can be selectively triggered by cell-secreted enzymes such as matrix metalloproteinases (MMPs), releasing the encapsulated therapeutics (e.g., growth factors and proteins) within the matrix. (C) Photo-triggered release of green fluorescent protein (GFP) from dextran-based photodegradable hydrogels via the incorporation of the photolabile *o*-nitrobenzyl moiety. (D) Glutathione (GSH)-sensitive hydrogels that can undergo matrix degradation and offer targeted delivery of therapeutic molecules in GSH-containing environments. Reprinted with permission from (A) Ref.²⁶, copyright (2012) Nature Publishing Group; (B) Ref.²⁷, copyright (2015) American Chemical Society; (C) Ref.²⁸, copyright (2011) Royal Society of Chemistry; (D) Ref.²⁹, copyright (2012) Royal Society of Chemistry.

Hydrolytically degradable hydrogels incorporated with labile ester linkages in the polymer backbone or crosslinker provide a simple approach to introduce temporal changes in the network crosslink density, which can influence properties such as diffusivity, swelling and mechanics (Figure 1.3A).³⁰⁻³² Enzymatically degradable hydrogels pioneered by Hubbell and Lutolf³³⁻³⁵ can be easily prepared via the use of matrix metalloproteinases (MMPs)-cleavable peptide motifs as crosslinkers, offering tunable release of the encapsulated bioactive factors via enzymatic activities and cellular cues (Figure 1.3B). Photocleavable degradation based on photolabile *o*-nitrobenzyl derivatives have been pioneered by Anseth³⁶⁻³⁸ and others^{28, 39-41} to engineer photodegradable hydrogels, which allow real-time manipulation of the materials properties and photocontrolled, on-demand release of proteins (Figure 1.3C). The incorporation of thiol-sensitive linkages such as disulfide bonds⁴²⁻⁴⁴ and arylthioether succinimide adducts^{29, 45} in hydrogels is also of significant interest in drug delivery (Figure 1.3 D), since hydrogel degradation can be selectively triggered in the presence of thiol-containing species such as glutathione (GSH), an antioxidant commonly found in normal and malignant cells and usually overproduced in tumor microenvironments.⁴⁶ These thiol-sensitive hydrogels can undergo cleavage reactions (disulfide cleavage or retro-Michael reaction) that lead to matrix degradation upon exposure to GSH, allowing the targeted release and stimuli-triggered delivery of therapeutic molecules.⁴⁷⁻⁴⁹

Thiol Michael-Type Addition



Commonly Utilized Vinyl Groups in Thiol Michael-Type Addition Reactions

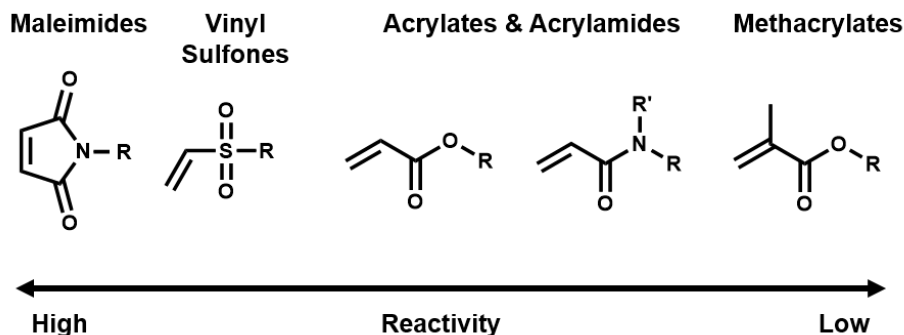


Figure 1.4 Schematic of thiol Michael-type addition and reactivity of various vinyl groups (Michael acceptors) used in the reactions.

Another major focus of hydrogel-based technology is the development of injectable hydrogels, which can be administered in a minimally invasive manner as polymer solutions and rapidly form viscoelastic network at the site of administration upon injection.^{50,51} Gelation of these materials can be triggered by external stimuli (such as temperature, pH, and ionic strength) or physical and chemical crosslinking methods (e.g. hydrogen bonding, stereocomplexation, radical polymerization, and Michael-type addition).⁵²⁻⁵⁴ Particularly, thiol Michael-type addition (Figure 1.4), a nucleophilic reaction typically between thiols and α,β -unsaturated carbonyl groups (e.g., maleimides, vinyl sulfones, acrylates, and methacrylates),^{55,56} has attracted significant attention in the preparation of injectable hydrogels, owing to its high selectivity, spontaneous reaction kinetics and physiologically relevant reaction conditions.^{25,56-58} Over the past

decade, varieties of injectable hydrogels prepared by Michael-type addition have been developed based on the use of synthetic polymers,⁵⁹⁻⁶² polysaccharides,^{63, 64} and polypeptides.^{65, 66} For instance, Hubbell and co-workers have developed various injectable matrices via the Michael-type addition of PEG thiols and PEG acrylates, PEG vinyl sulfones and cysteine-functionalized peptides for the controlled delivery of bovine serum albumin and vascular endothelial growth factor, respectively.^{67, 68} Similarly, Kiick and co-workers have synthesized heparin-functionalized hydrogels for the controlled release of basic fibroblast growth factor based on the thiol-maleimide Michael-type addition of PEG thiols and maleimide-functionalized heparin.⁶³ These heparin-functionalized hydrogels were subsequently injected subcutaneously in rabbits and demonstrated sustained anticoagulant release *in vivo*.⁶⁹ The rapid and *in situ* gelation of these materials enabled by thiol Michael-type addition allows facile encapsulation of bioactive molecules and suggests great potential for direct injection applications.

1.3 Nanoparticle-Containing Hydrogels for Drug Delivery

Parallel to the development of hydrogel strategies in drug delivery, nanotechnology has also made a significant impact on the advances in nanoscale delivery vehicles.^{15,70} In recent years, there has been an increasing interest in combining therapeutic nanoparticles with other biomaterials such as hydrogels to form hybrid nanostructures for improved therapeutic efficacy (Figure 1.5). The innovative combination of these two distinct types of materials not only provides structural diversity, but also introduces a plurality of property enhancements, resulting in improved tissue localization, minimized burst release, and multi-stage delivery.⁷¹⁻⁷³

Nanoparticles can be incorporated into hydrogel network by triggering gelation of monomer solutions in nanoparticle suspensions (Figure 1.5A).⁷⁴ Furthermore, inorganic nanoparticles (e.g., Au and Ag) can be formed in situ within the gel matrix by the reduction reactions of nanoparticle precursors loaded in the hydrogel.^{75, 76} Various types of nanoparticles including metallic nanoparticles,^{77, 78} liposomes^{79, 80} and polymeric nanoparticles^{81, 82} have been physically embedded within the hydrogel network, offering tailored physical properties and custom-made functionalities for improved therapeutic efficacy. For example, Zhang and co-workers⁷⁴ have developed hydrogels containing gold nanoparticle-stabilized liposomes for topical antimicrobial delivery. The nanoparticle-stabilized liposomes were physically encapsulated in a chemically crosslinked polyacrylamide gel by initiating gelation of the solution mixture of the acrylamide monomers and poly (ethylene glycol) dimethacrylate crosslinkers in the liposome suspensions. These hydrogel formulations can not only preserve the structural integrity of the nanoparticle-stabilized liposomes, but also offer tunable release kinetics of the incorporated liposomes that can subsequently fuse with bacterial membrane, providing a unique and robust hybrid formulation for topical drug delivery against microbial infections. Similarly, Shoichet and co-workers⁸² have prepared poly (lactico-glycolic acid) (PLGA) nanoparticle-loaded composite hydrogel for sustained release of bioactive proteins. Neurotrophin-3 (NT-3), a neural regenerative protein, was encapsulated in PLGA nanoparticles that were dispersed in an injectable hydrogel of hyaluronan and methyl cellulose (HAMC), exhibiting linear and more sustained release with minimal initial burst over 28 days compared to release from PLGA nanoparticles or HAMC hydrogels alone.

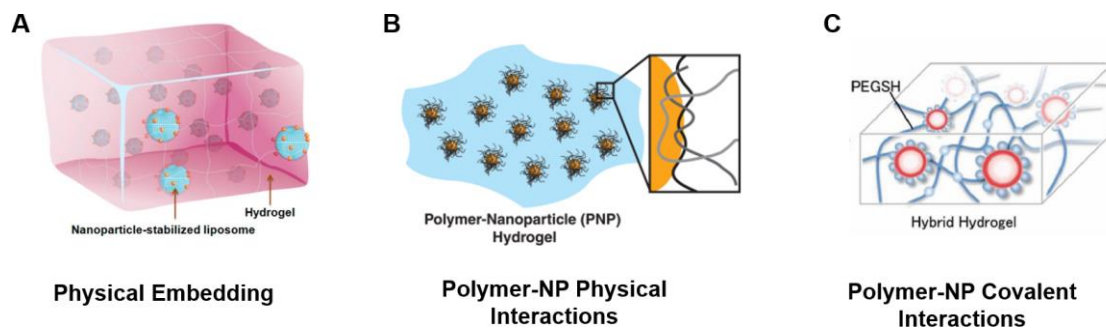


Figure 1.5 Strategies in the formation of nanoparticle-containing hydrogels. (A) Physical encapsulation of nanoparticles during hydrogel formation. (B) Fabrication of self-assembled hydrogels employing polymer-nanoparticle physical interactions (e.g. hydrophobic or electrostatic interactions). (C) Hierarchical hybrid hydrogels prepared via the use of nanoparticles as covalent crosslinkers. Reprinted with permission from (A) Ref.⁸³, copyright (2014) American Chemical Society; (B) Ref.⁸⁴, copyright (2015) Nature Publishing Group; (C) Ref.⁸⁵, copyright (2012) Wiley.

Alternatively, nanoparticle-containing hydrogels can also be constructed using nanoparticles as crosslinkers.⁸⁶⁻⁸⁸ In this approach, 3D hydrogel network can be formed through strong hydrophobic interactions or electrostatic interactions between the nanoparticles and polymers (Figure 1.5B). Recently, a series of shear-thinning injectable hybrid hydrogels have been developed based on the hydrophobic interactions between hydrophobically modified biopolymers and various nanoparticulate building blocks including liposomes, vesicles and polymeric nanoparticles.^{84, 89, 90} Similarly, Langer and co-workers⁹¹ have also leveraged electrostatic interactions to fabricate self-assembled hydrogels with shear-thinning and self-healing properties, using negatively charged biopolymers and nanoparticles enhanced with a positively charged surfactant. Additionally, nanoparticles can be covalently crosslinked with polymers to form a hydrogel network (Figure 1.5C). Akiyoshi and co-workers^{85, 92, 93} have reported nanogel-crosslinked hybrid hydrogels prepared through the Michael-type addition of

multi-arm PEG-SH and acrylate-modified pullulan nanogels. These nanoparticle-crosslinking strategies can not only integrate two material platforms into one formulation with unique physicochemical and biological properties, but also provide ample parameter space for the manipulation of delivery properties. For instance, the release rate of therapeutic molecules from these hybrid systems can be tuned by varying the size, concentration and chemical functionality of the nanoparticles.⁸⁴ Overall, nanoparticle-containing hydrogels have emerged as a versatile class of drug delivery depots for local delivery of therapeutic molecules, unleashing unique synergistic properties that are absent in both individual building blocks.

1.4 Nanoparticles for Drug Delivery

Progress in nanotechnology and materials science has recently revolutionized drug delivery with the use of nanoscale carriers.⁹⁴ Varieties of nanoparticles have been developed, including inorganic nanoparticles,⁹⁵ liposomes,⁹⁶ and polymeric nanoparticles.⁹⁷ These nanostructures of appropriate size (10–150 nm) can not only penetrate vessels and passively accumulate in specific tissues such as tumor, but also be surface functionalized with targeting ligands to actively bind to specific cells after extravasation (Figure 1.6).^{98, 99} Nanoparticle therapeutics, which are usually administered intravenously, can improve pharmacokinetic and drug tissue distribution profiles and promote intracellular delivery, providing a powerful platform for drug delivery with improved therapeutic efficacy, especially for cancer diagnosis and therapy.^{100, 101}

In recent years, a wide variety of chemically labile bonds and dynamic process have been exploited to formulate nanoparticles that are responsive to external stimuli

such as pH,¹⁰² light,¹⁰³ temperature,¹⁰⁴ and redox potential.¹⁰⁵ These stimuli-responsive nanocarriers are usually stable under circulation conditions, but can undergo rapid disassembly or degradation via protonation, (supra)molecular conformational change or cleavage reaction, allowing tailored release profiles of therapeutic molecules with excellent spatial, temporal and dosage control.¹⁰⁶⁻¹⁰⁸ For example, pH-labile linkages such as ester and hydrazone linkages have been widely incorporated into nanoparticle carriers to provide pH-selective (acid-responsive) drug release targeting at the organ level (gastrointestinal tract), tissue level (acidic extracellular tumor environment), and cellular level (endosomes), respectively.¹⁰² Various photoresponsive groups including *o*-nitrobenzyl and coumarinyl esters have been employed in the synthesis of photoresponsive block copolymer micelles.¹⁰⁹ These photo-sensitive moieties can undergo photocleavage reactions under light irradiation, shifting hydrophilic-hydrophobic balance, breaking block junctions, and disassociating crosslinks within the micelles, which subsequently offers on-demand and photocontrolled release of the payloads from these nanocarriers.¹¹⁰ Similarly, thermoresponsive polymers that exhibit lower critical solution temperature (LCST)-like behavior, such as poly(*N*-isopropylacrylamide)¹¹¹ and elastin-like polypeptides,¹¹² have been commonly used to formulate thermosensitive nanocarriers that enable facile drug encapsulation and temperature-triggered release. Reduction-sensitive disulfide linkages that can undergo cleavage in the presence of glutathione (GSH) have enabled the design of nanoparticles for targeted and intracellular delivery of therapeutic molecules.¹⁰⁵ Owing to the spatial distribution of GSH (10 mM in intracellular compartments vs. 10 μ M in circulation),¹¹³ these reduction-sensitive nanoparticles can maintain excellent stability in circulation and in extracellular fluids, and undergo rapid degradation inside cells to accomplish

efficient intracellular drug release. The wide variety of stimuli that are able to trigger drug release at the right place and time, and the diversity of the responsive materials that can be assembled into different architectures, provide great flexibility in the design of these stimuli-responsive systems and significant potential in drug delivery with improved therapeutic efficacy.

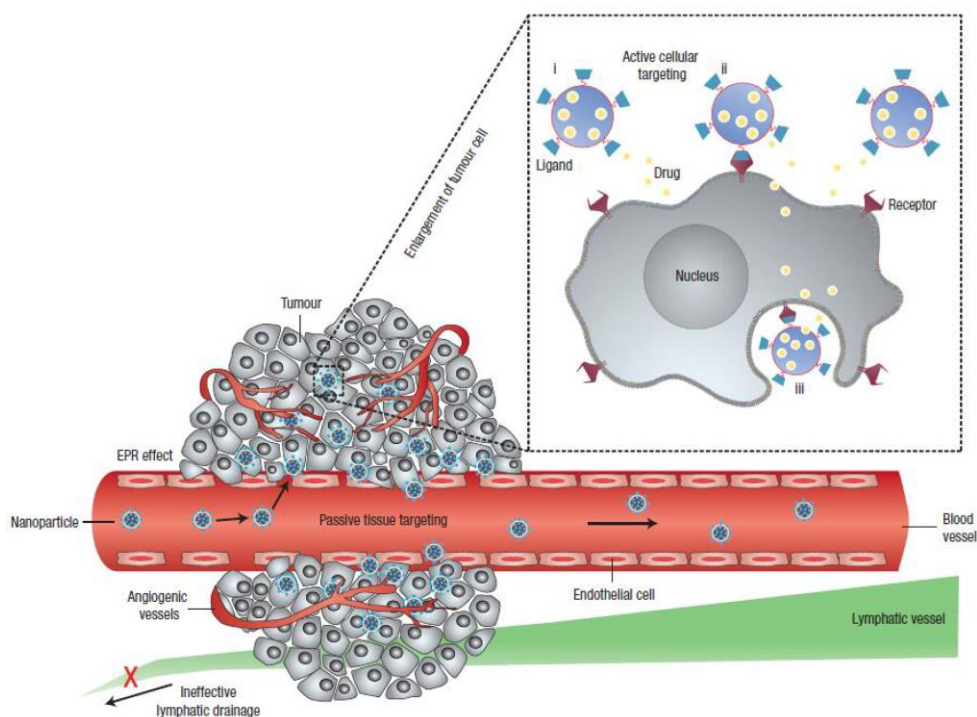


Figure 1.6 Nanoparticle agents are designed to utilize the enhanced permeability and retention (EPR) effect to exit leaky blood vessels and accumulate in the tumor, and to target tumor cells by functionalizing the surface of nanoparticles with ligands that promote cell-specific recognition and binding. The nanoparticles can (i) release their contents in close proximity to the target cells; (ii) attach to the membrane of the cell and act as an extracellular sustained-release drug depot; or (iii) internalize into the cell by endocytosis before releasing their drug payloads. Reprinted with permission from Ref.⁷⁰, copyright (2007) Nature Publishing Group.

While the technology of utilizing polymer assemblies in drug delivery is developing rapidly, many polymer nanostructures based on non-covalent interactions might be subjected to structure instability, especially when circulating in large volume of biological fluids such as the bloodstream.^{114, 115} More recently, nanogels (hydrogel nanoparticles) composed of nanoscale 3-D crosslinked network of polymer chains have emerged as promising materials for drug delivery (Figure 1.7A).^{116, 117} These nanoscale polymeric matrices can not only pass through capillary vessels and penetrate cells and tissue barriers like most nanoparticles, but also maintain high structural integrity even under dilute conditions and allow efficient encapsulation of therapeutic molecules owing to their gel-like structures.^{118, 119} Covalently crosslinked nanogels can be formed via inverse emulsion polymerization (Figure 1.7B) and nanotemplate methods (Figure 1.7C) using a wide range of chemical crosslinking strategies. As a combinatorial platform of nanoparticles and hydrogels, the versatility of nanogels can be achieved by introducing chemical functional groups, surface-active moieties and stimuli-responsive constituents, while the crosslinking density of nanogels can be tuned to tailor the swelling and pore size of the nanoscale matrices, which are responsible for the predetermined release kinetics of the entrapped drug molecules.¹²⁰⁻¹²² For instance, Anderson and co-workers have developed dextran nanogels via the alkyne-azide cycloaddition and functionalized the nanogel surface with bisphosphonate ligands for bone targeting effect.¹²³ Ravaine and co-workers, on the other hand, have synthesized well-defined hyaluronic acid (HA) nanogels with controlled cross-linking densities based on the free radical photopolymerization of methacrylate-modified HA.¹²⁴ The crosslinking densities of these nanogels could be controlled not only by the photopolymerization conditions (i.e., the duration and intensity of UV irradiation) but

also by the degree of methacrylation of HA, offering a versatile platform for the design of biocompatible, nanoparticulate drug delivery systems. Nanogels with unique physicochemical properties have thus provide a promising approach for the systemic delivery of a wide range of disease oriented therapeutics including small-molecule drugs,¹²⁵ peptides,¹²⁶ proteins,¹²⁷ and nucleic acids.¹²⁸

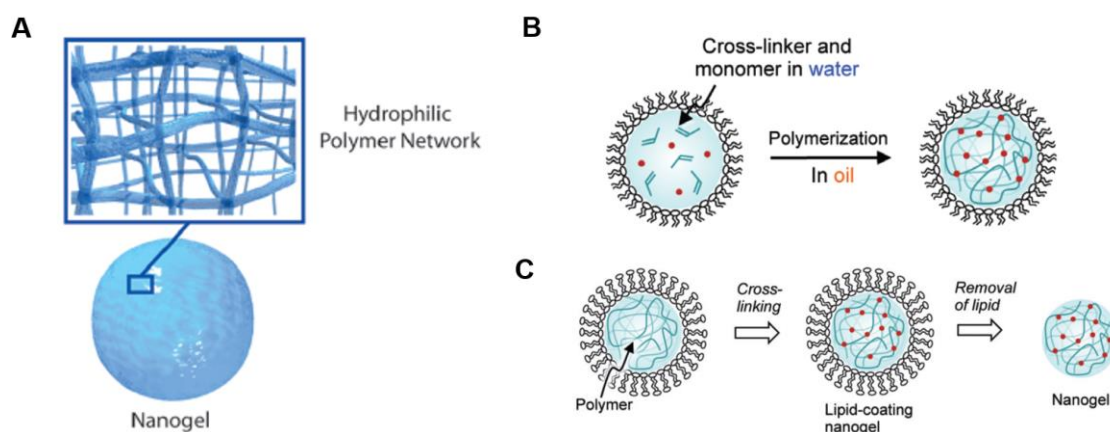


Figure 1.7 Structure and synthetic strategies of polymer nanogels. (A) Crosslinked network structure of polymer nanogels. (B) Chemical synthesis of nanogels by inverse emulsion polymerization, where each droplet of polymer solution is isolated and crosslinked into nanoparticle. (C) Preparation of nanogels using liposome templated method, where crosslinked network is formed in the aqueous lumen of the liposome. Reprinted with permission from (A) Ref.¹²⁸, copyright (2011) American Chemical Society; (B) and (C) Ref.¹¹⁷, copyright (2010) Wiley.

1.5 Dissertation Summary

Among various polymer-based drug delivery systems, materials based on polyethylene glycol (PEG) are of particular interest to biomedical researchers, especially for hydrogel-based delivery systems. PEG is an important type of hydrophilic polymers that have been approved by the FDA for biomedical application, due to its

good biocompatibility, nonimmunogenicity, and resistance to protein adsorption.¹²⁹ The hydroxyl end groups of PEG polymers can be easily functionalized with reactive functional groups for materials formation, including thiols, vinyl sulfones, maleimides, acrylates, and norbornenes.¹³⁰ PEG-based hydrogels,²² microparticles,¹³¹ and nanoparticles¹³² have been widely explored in the field of drug delivery with promising preclinical and clinical results.

This dissertation describes the investigation of PEG-based polymeric matrices from bulk to nanoscale, including polymer hydrogels, nanoparticle-crosslinked hydrogels, and nanogels for different delivery applications. Chapter 1 introduces the background and current research on polymer-based drug delivery systems including bulk hydrogels, nanoparticle-containing hydrogels and polymer nanoparticles. Chapter 2 covers the engineering of hydrophilic and hydrolytically degradable polyethylene glycol (PEG) hydrogels for the sustained delivery of an anthrax toxin-neutralizing monoclonal antibody. The release profiles of the antibody from different hydrogel formulations are studied. The biophysical properties and biological activities of the antibody after released from the hydrogels are discussed. Chapter 3 reports a novel liposome-crosslinked hybrid hydrogel system for the triggered and sequential release of multiple therapeutic molecules. Gelation and degradation of the PEG-liposome hybrid hydrogels are confirmed. Dual encapsulation and sequential release of multiple cargo molecules relevant for chemotherapies, namely doxorubicin (DOX) and cytochrome c, are performed. The release profiles of these molecules are analyzed by the mathematical fitting of relevant equations. In Chapter 4, multifunctional lipid-coated PEG nanogels crosslinked by photo-triggered Michael-type addition are developed via the use of liposome templates. The photo-sensitive gelation and temporal control of the

crosslinking reaction are discussed. The production and surface functionality of the lipid-coated nanogels are demonstrated. Chapter 5 concludes the dissertation by summarizing the major discovery of this work, the potential impact of these polymeric matrices on the field of drug delivery and future directions that could build upon these systems.

REFERENCES

1. Langer, R., New Methods of Drug Delivery. *Science* **1990**, 249, (4976), 1527-1533.
2. Allen, T. M.; Cullis, P. R., Drug delivery systems: Entering the mainstream. *Science* **2004**, 303, (5665), 1818-1822.
3. Liechty, W. B.; Kryscio, D. R.; Slaughter, B. V.; Peppas, N. A., Polymers for Drug Delivery Systems. *Annu Rev Chem Biomol* **2010**, 1, 149-173.
4. Gombotz, W. R.; Pettit, D. K., Biodegradable Polymers for Protein and Peptide Drug-Delivery. *Bioconjugate Chem.* **1995**, 6, (4), 332-351.
5. LaVan, D. A.; McGuire, T.; Langer, R., Small-scale systems for in vivo drug delivery. *Nat. Biotechnol.* **2003**, 21, (10), 1184-1191.
6. Langer, R., Drug delivery and targeting. *Nature* **1998**, 392, (6679), 5-10.
7. Tibbitt, M. W.; Dahlman, J. E.; Langer, R., Emerging Frontiers in Drug Delivery. *J. Am. Chem. Soc.* **2016**, 138, (3), 704-717.
8. Sapsford, K. E.; Algar, W. R.; Berti, L.; Gemmill, K. B.; Casey, B. J.; Oh, E.; Stewart, M. H.; Medintz, I. L., Functionalizing Nanoparticles with Biological Molecules: Developing Chemistries that Facilitate Nanotechnology. *Chem. Rev.* **2013**, 113, (3), 1904-2074.
9. Kiick, K. L., Polymer therapeutics. *Science* **2007**, 317, (5842), 1182-1183.
10. Liu, S.; Maheshwari, R.; Kiick, K. L., Polymer-Based Therapeutics. *Macromolecules* **2009**, 42, (1), 3-13.
11. Stevenson, C. L.; Santini, J. T.; Langer, R., Reservoir-based drug delivery systems utilizing microtechnology. *Adv. Drug Deliver Rev.* **2012**, 64, (14), 1590-1602.
12. Peppas, N. A.; Hilt, J. Z.; Khademhosseini, A.; Langer, R., Hydrogels in Biology and Medicine: From Molecular Principles to Bionanotechnology. *Adv. Mater.* **2006**, 18, (11), 1345-1360.

13. Slaughter, B. V.; Khurshid, S. S.; Fisher, O. Z.; Khademhosseini, A.; Peppas, N. A., Hydrogels in Regenerative Medicine. *Adv. Mater.* **2009**, 21, (32-33), 3307-3329.
14. Musyanovych, A.; Landfester, K., Polymer Micro- and Nanocapsules as Biological Carriers with Multifunctional Properties. *Macromol. Biosci.* **2014**, 14, (4), 458-477.
15. Hubbell, J. A.; Chilkoti, A., Nanomaterials for Drug Delivery. *Science* **2012**, 337, (6092), 303-305.
16. Diaz, S.; Pavez, M.; Miranda, P.; Robertson, D. N.; Sivin, I.; Croxatto, H. B., A five-year clinical trial of levonorgestrel silastic implants (Norplant TM). *Contraception* **1982**, 25, (5), 447-56.
17. Vermonden, T.; Censi, R.; Hennink, W. E., Hydrogels for Protein Delivery. *Chem. Rev.* **2012**, 112, (5), 2853-2888.
18. Kohane, D. S., Microparticles and nanoparticles for drug delivery. *Biotechnol. Bioeng.* **2007**, 96, (2), 203-209.
19. Seliktar, D., Designing Cell-Compatible Hydrogels for Biomedical Applications. *Science* **2012**, 336, (6085), 1124-1128.
20. Hoffman, A. S., Hydrogels for biomedical applications. *Adv. Drug Deliver Rev.* **2012**, 64, 18-23.
21. Buwalda, S. J.; Boere, K. W. M.; Dijkstra, P. J.; Feijen, J.; Vermonden, T.; Hennink, W. E., Hydrogels in a historical perspective: From simple networks to smart materials. *J. Controlled Release* **2014**, 190, 254-273.
22. Lin, C.-C.; Anseth, K., PEG Hydrogels for the Controlled Release of Biomolecules in Regenerative Medicine. *Pharm. Res.* **2009**, 26, (3), 631-643.
23. Censi, R.; Di Martino, P.; Vermonden, T.; Hennink, W. E., Hydrogels for protein delivery in tissue engineering. *J. Controlled Release* **2012**, 161, (2), 680-692.
24. Hoare, T. R.; Kohane, D. S., Hydrogels in drug delivery: Progress and challenges. *Polymer* **2008**, 49, (8), 1993-2007.
25. Kharkar, P. M.; Kiick, K. L.; Kloxin, A. M., Designing degradable hydrogels for orthogonal control of cell microenvironments. *Chem. Soc. Rev.* **2013**.
26. Burdick, J. A.; Murphy, W. L., Moving from static to dynamic complexity in hydrogel design. *Nat. Commun.* **2012**, 3, 1269.

27. Rodell, C. B.; Wade, R. J.; Purcell, B. P.; Dusaj, N. N.; Burdick, J. A., Selective Proteolytic Degradation of Guest-Host Assembled, Injectable Hyaluronic Acid Hydrogels. *Acs Biomater-Sci Eng* **2015**, 1, (4), 277-286.
28. Peng, K.; Tomatsu, I.; van den Broek, B.; Cui, C.; Korobko, A. V.; van Noort, J.; Meijer, A. H.; Spaink, H. P.; Kros, A., Dextran based photodegradable hydrogels formed via a Michael addition. *Soft Matter* **2011**, 7, (10), 4881-4887.
29. Baldwin, A. D.; Kiick, K. L., Reversible maleimide-thiol adducts yield glutathione-sensitive poly(ethylene glycol)-heparin hydrogels. *Polym. Chem.* **2013**, 4, (1), 133-143.
30. Sahoo, S.; Chung, C.; Khetan, S.; Burdick, J. A., Hydrolytically degradable hyaluronic acid hydrogels with controlled temporal structures. *Biomacromolecules* **2008**, 9, (4), 1088-1092.
31. Chung, C.; Beecham, M.; Mauck, R. L.; Burdick, J. A., The influence of degradation characteristics of hyaluronic acid hydrogels on in vitro neocartilage formation by mesenchymal stem cells. *Biomaterials* **2009**, 30, (26), 4287-4296.
32. Kim, I. L.; Mauck, R. L.; Burdick, J. A., Hydrogel design for cartilage tissue engineering: A case study with hyaluronic acid. *Biomaterials* **2011**, 32, (34), 8771-8782.
33. Lutolf, M. P.; Lauer-Fields, J. L.; Schmoekel, H. G.; Metters, A. T.; Weber, F. E.; Fields, G. B.; Hubbell, J. A., Synthetic matrix metalloproteinase-sensitive hydrogels for the conduction of tissue regeneration: Engineering cell-invasion characteristics. *P Natl Acad Sci USA* **2003**, 100, (9), 5413-5418.
34. Lutolf, M. P.; Hubbell, J. A., Synthesis and Physicochemical Characterization of End-Linked Poly(ethylene glycol)-co-peptide Hydrogels Formed by Michael-Type Addition. *Biomacromolecules* **2003**, 4, (3), 713-722.
35. Lutolf, M. P.; Hubbell, J. A., Synthetic biomaterials as instructive extracellular microenvironments for morphogenesis in tissue engineering. *Nat Biotech* **2005**, 23, (1), 47-55.
36. Kloxin, A. M.; Kasko, A. M.; Salinas, C. N.; Anseth, K. S., Photodegradable Hydrogels for Dynamic Tuning of Physical and Chemical Properties. *Science* **2009**, 324, (5923), 59-63.
37. DeForest, C. A.; Anseth, K. S., Cytocompatible click-based hydrogels with dynamically tunable properties through orthogonal photoconjugation and photocleavage reactions. *Nat. Chem.* **2011**, 3, (12), 925-931.

38. Kloxin, A. M.; Tibbitt, M. W.; Kasko, A. M.; Fairbairn, J. A.; Anseth, K. S., Tunable Hydrogels for External Manipulation of Cellular Microenvironments through Controlled Photodegradation. *Adv. Mater.* **2010**, 22, (1), 61-+.
39. Griffin, D. R.; Kasko, A. M., Photodegradable Macromers and Hydrogels for Live Cell Encapsulation and Release (vol 134, pg 13103, 2012). *J. Am. Chem. Soc.* **2012**, 134, (42), 17833-17833.
40. Griffin, D. R.; Kasko, A. M., Photoselective Delivery of Model Therapeutics from Hydrogels. *ACS Macro Lett.* **2012**, 1, (11), 1330-1334.
41. Griffin, D. R.; Schlosser, J. L.; Lam, S. F.; Nguyen, T. H.; Maynard, H. D.; Kasko, A. M., Synthesis of Photodegradable Macromers for Conjugation and Release of Bioactive Molecules. *Biomacromolecules* **2013**, 14, (4), 1199-1207.
42. Ejaz, M.; Yu, H. N.; Yan, Y.; Blake, D. A.; Ayyala, R. S.; Grayson, S. M., Evaluation of redox-responsive disulfide cross-linked poly(hydroxyethyl methacrylate) hydrogels. *Polymer* **2011**, 52, (23), 5262-5270.
43. Wu, Z. M.; Zhang, X. G.; Zheng, C.; Li, C. X.; Zhang, S. M.; Dong, R. N.; Yu, D. M., Disulfide-crosslinked chitosan hydrogel for cell viability and controlled protein release. *Eur. J. Pharm. Sci.* **2009**, 37, (3-4), 198-206.
44. Singh, S.; Topuz, F.; Hahn, K.; Albrecht, K.; Groll, J., Embedding of Active Proteins and Living Cells in Redox-Sensitive Hydrogels and Nanogels through Enzymatic Cross-Linking. *Angew. Chem. Int. Ed.* **2013**, 52, (10), 3000-3003.
45. Baldwin, A. D.; Kiick, K. L., Tunable degradation of maleimide-thiol adducts in reducing environments. *Bioconjug Chem* **2011**, 22, (10), 1946-53.
46. Traverso, N.; Ricciarelli, R.; Nitti, M.; Marengo, B.; Furfaro, A. L.; Pronzato, M. A.; Marinari, U. M.; Domenicotti, C., Role of glutathione in cancer progression and chemoresistance. *Oxid Med Cell Longev* **2013**, 2013, 972913.
47. Choh, S. Y.; Cross, D.; Wang, C., Facile Synthesis and Characterization of Disulfide-Cross-Linked Hyaluronic Acid Hydrogels for Protein Delivery and Cell Encapsulation. *Biomacromolecules* **2011**, 12, (4), 1126-1136.
48. Ossipov, D.; Kootala, S.; Yi, Z. Y.; Yang, X.; Hilborn, J., Orthogonal Chemoselective Assembly of Hyaluronic Acid Networks and Nanogels for Drug Delivery. *Macromolecules* **2013**, 46, (10), 4105-4113.

49. Kharkar, P. M.; Kloxin, A. M.; Kiick, K. L., Dually degradable click hydrogels for controlled degradation and protein release. *J. Mater. Chem. B* **2014**, 2, (34), 5511-5521.
50. Yu, L.; Ding, J. D., Injectable hydrogels as unique biomedical materials. *Chem. Soc. Rev.* **2008**, 37, (8), 1473-1481.
51. Minh, K. N.; Lee, D. S., Injectable Biodegradable Hydrogels. *Macromol. Biosci.* **2010**, 10, (6), 563-579.
52. Li, Y. L.; Rodrigues, J.; Tomas, H., Injectable and biodegradable hydrogels: gelation, biodegradation and biomedical applications. *Chem. Soc. Rev.* **2012**, 41, (6), 2193-2221.
53. Appel, E. A.; del Barrio, J.; Loh, X. J.; Scherman, O. A., Supramolecular polymeric hydrogels. *Chem. Soc. Rev.* **2012**, 41, (18), 6195-6214.
54. Webber, M. J.; Appel, E. A.; Meijer, E. W.; Langer, R., Supramolecular biomaterials. *Nat. Mater.* **2016**, 15, (1), 13-26.
55. Mather, B. D.; Viswanathan, K.; Miller, K. M.; Long, T. E., Michael addition reactions in macromolecular design for emerging technologies. *Prog. Polym. Sci.* **2006**, 31, (5), 487-531.
56. Nair, D. P.; Podgórski, M.; Chatani, S.; Gong, T.; Xi, W.; Fenoli, C. R.; Bowman, C. N., The Thiol-Michael Addition Click Reaction: A Powerful and Widely Used Tool in Materials Chemistry. *Chem. Mater.* **2014**, 26, (1), 724-744.
57. Pritchard, C. D.; O'Shea, T. M.; Siegwart, D. J.; Calo, E.; Anderson, D. G.; Reynolds, F. M.; Thomas, J. A.; Slotkin, J. R.; Woodard, E. J.; Langer, R., An injectable thiol-acrylate poly(ethylene glycol) hydrogel for sustained release of methylprednisolone sodium succinate. *Biomaterials* **2011**, 32, (2), 587-597.
58. Bakaic, E.; Smeets, N. M. B.; Hoare, T., Injectable hydrogels based on poly(ethylene glycol) and derivatives as functional biomaterials. *Rsc Adv* **2015**, 5, (45), 35469-35486.
59. Metters, A.; Hubbell, J., Network Formation and Degradation Behavior of Hydrogels Formed by Michael-Type Addition Reactions. *Biomacromolecules* **2004**, 6, (1), 290-301.
60. Zustiak, S. P.; Leach, J. B., Hydrolytically Degradable Poly(Ethylene Glycol) Hydrogel Scaffolds with Tunable Degradation and Mechanical Properties. *Biomacromolecules* **2010**, 11, (5), 1348-1357.

61. Zustiak, S. P.; Leach, J. B., Characterization of Protein Release From Hydrolytically Degradable Poly(Ethylene Glycol) Hydrogels. *Biotechnol. Bioeng.* **2011**, 108, (1), 197-206.
62. Buwalda, S. J.; Dijkstra, P. J.; Feijen, J., In Situ Forming Poly(ethylene glycol)-Poly(L-lactide) Hydrogels via Michael Addition: Mechanical Properties, Degradation, and Protein Release. *Macromol. Chem. Phys.* **2012**, 213, (7), 766-775.
63. Nie, T.; Baldwin, A.; Yamaguchi, N.; Kiick, K. L., Production of heparin-functionalized hydrogels for the development of responsive and controlled growth factor delivery systems. *J. Controlled Release* **2007**, 122, (3), 287-296.
64. Nie, T.; Akins, R. E.; Kiick, K. L., Production of heparin-containing hydrogels for modulating cell responses. *Acta Biomater.* **2009**, 5, (3), 865-875.
65. McGann, C. L.; Levenson, E. A.; Kiick, K. L., Resilin-Based Hybrid Hydrogels for Cardiovascular Tissue Engineering. *Macromol. Chem. Phys.* **2013**, 214, (2), 203-213.
66. McGann, C. L.; Akins, R. E.; Kiick, K. L., Resilin-PEG Hybrid Hydrogels Yield Degradable Elastomeric Scaffolds with Heterogeneous Microstructure. *Biomacromolecules* **2016**, 17, (1), 128-140.
67. Elbert, D. L.; Pratt, A. B.; Lutolf, M. P.; Halstenberg, S.; Hubbell, J. A., Protein delivery from materials formed by self-selective conjugate addition reactions. *J. Controlled Release* **2001**, 76, (1-2), 11-25.
68. Lutolf, M. P.; Raeber, G. P.; Zisch, A. H.; Tirelli, N.; Hubbell, J. A., Cell-Responsive Synthetic Hydrogels. *Adv. Mater.* **2003**, 15, (11), 888-892.
69. Baldwin, A. D.; Robinson, K. G.; Militar, J. L.; Derby, C. D.; Kiick, K. L.; Akins, R. E., In situ crosslinkable heparin-containing poly(ethylene glycol) hydrogels for sustained anticoagulant release. *J. Biomed. Mater. Res. A* **2012**, 100A, (8), 2106-2118.
70. Peer, D.; Karp, J. M.; Hong, S.; Farokhzad, O. C.; Margalit, R.; Langer, R., Nanocarriers as an emerging platform for cancer therapy. *Nat. Nanotechnol.* **2007**, 2, (12), 751-760.
71. Gaharwar, A. K.; Peppas, N. A.; Khademhosseini, A., Nanocomposite Hydrogels for Biomedical Applications. *Biotechnol. Bioeng.* **2014**, 111, (3), 441-453.
72. Thoniyot, P.; Tan, M. J.; Karim, A. A.; Young, D. J.; Loh, X. J., Nanoparticle-Hydrogel Composites: Concept, Design, and Applications of These Promising, Multi-Functional Materials. *Adv. Sci.* **2015**, 2, (1-2), 140010.

73. Merino, S.; Martín, C.; Kostarelos, K.; Prato, M.; Vázquez, E., Nanocomposite Hydrogels: 3D Polymer–Nanoparticle Synergies for On-Demand Drug Delivery. *ACS Nano* **2015**, 9, (5), 4686-4697.
74. Sershen, S. R.; Westcott, S. L.; Halas, N. J.; West, J. L., Independent optically addressable nanoparticle-polymer optomechanical composites. *Appl. Phys. Lett.* **2002**, 80, (24), 4609-4611.
75. Wang, C.; Flynn, N. T.; Langer, R., Controlled structure and properties of thermoresponsive nanoparticle-hydrogel composites. *Adv. Mater.* **2004**, 16, (13), 1074-1079.
76. Saravanan, P.; Raju, M. P.; Alam, S., A study on synthesis and properties of Ag nanoparticles immobilized polyacrylamide hydrogel composites. *Mater. Chem. Phys.* **2007**, 103, (2-3), 278-282.
77. Marcelo, G.; Lopez-Gonzalez, M.; Mendicuti, F.; Tarazona, M. P.; Valiente, M., Poly(N-isopropylacrylamide)/Gold Hybrid Hydrogels Prepared by Catechol Redox Chemistry. Characterization and Smart Tunable Catalytic Activity. *Macromolecules* **2014**, 47, (17), 6028-6036.
78. Xiang, Y. Q.; Chen, D. J., Preparation of a novel pH-responsive silver nanoparticle/poly (HEMA-PEGMA-MAA) composite hydrogel. *Eur. Polym. J.* **2007**, 43, (10), 4178-4187.
79. Popescu, M. T.; Mourtas, S.; Pampalakis, G.; Antimisiaris, S. G.; Tsitsilianis, C., pH-Responsive Hydrogel/Liposome Soft Nanocomposites For Tuning Drug Release. *Biomacromolecules* **2011**, 12, (8), 3023-3030.
80. Lopez-Noriega, A.; Hastings, C. L.; Ozbakir, B.; O'Donnell, K. E.; O'Brien, F. J.; Storm, G.; Hennink, W. E.; Duffy, G. P.; Ruiz-Hernandez, E., Hyperthermia-Induced Drug Delivery from Thermosensitive Liposomes Encapsulated in an Injectable Hydrogel for Local Chemotherapy. *Adv. Healthcare Mater.* **2014**, 3, (6), 854-859.
81. Chung, Y. I.; Ahn, K. M.; Jeon, S. H.; Lee, S. Y.; Lee, J. H.; Tae, G., Enhanced bone regeneration with BMP-2 loaded functional nanoparticle-hydrogel complex. *J. Controlled Release* **2007**, 121, (1-2), 91-99.
82. Stanwick, J. C.; Baumann, M. D.; Shoichet, M. S., Enhanced neurotrophin-3 bioactivity and release from a nanoparticle-loaded composite hydrogel. *J. Controlled Release* **2012**, 160, (3), 666-675.

83. Gao, W. W.; Vecchio, D.; Li, J. M.; Zhu, J. Y.; Zhang, Q. Z.; Fu, V.; Li, J. Y.; Thamphiwatana, S.; Lu, D. N.; Zhang, L. F., Hydrogel Containing Nanoparticle-Stabilized Liposomes for Topical Antimicrobial Delivery. *ACS Nano* **2014**, 8, (3), 2900-2907.
84. Appel, E. A.; Tibbitt, M. W.; Webber, M. J.; Mattix, B. A.; Veiseh, O.; Langer, R., Self-assembled hydrogels utilizing polymer-nanoparticle interactions. *Nat. Commun.* **2015**, 6:6295.
85. Sekine, Y.; Moritani, Y.; Ikeda-Fukazawa, T.; Sasaki, Y.; Akiyoshi, K., A Hybrid Hydrogel Biomaterial by Nanogel Engineering: Bottom-Up Design with Nanogel and Liposome Building Blocks to Develop a Multidrug Delivery System. *Adv. Healthcare Mater.* **2012**, 1, (6), 722-728.
86. Skardal, A.; Zhang, J. X.; McCoard, L.; Oottamasathien, S.; Prestwich, G. D., Dynamically Crosslinked Gold Nanoparticle - Hyaluronan Hydrogels. *Adv. Mater.* **2010**, 22, (42), 4736-4740.
87. Garcia-Astrain, C.; Chen, C.; Buron, M.; Palomares, T.; Eceiza, A.; Fruk, L.; Corcuera, M. A.; Gabilondo, N., Biocompatible Hydrogel Nanocomposite with Covalently Embedded Silver Nanoparticles. *Biomacromolecules* **2015**, 16, (4), 1301-1310.
88. Xiao, L. X.; Tong, Z. X.; Chen, Y. C.; Pochan, D. J.; Sabanayagam, C. R.; Jia, X. Q., Hyaluronic Acid-Based Hydrogels Containing Covalently Integrated Drug Depots: Implication for Controlling Inflammation in Mechanically Stressed Tissues. *Biomacromolecules* **2013**, 14, (11), 3808-3819.
89. Lee, J. H.; Oh, H.; Baxa, U.; Raghavan, S. R.; Blumenthal, R., Biopolymer-Connected Liposome Networks as Injectable Biomaterials Capable of Sustained Local Drug Delivery. *Biomacromolecules* **2012**, 13, (10), 3388-3394.
90. Chen, Y. J.; Javvaji, V.; MacIntire, I. C.; Raghavan, S. R., Gelation of Vesicles and Nanoparticles Using Water-Soluble Hydrophobically Modified Chitosan. *Langmuir* **2013**, 29, (49), 15302-15308.
91. Appel, E. A.; Tibbitt, M. W.; Greer, J. M.; Fenton, O. S.; Kreuels, K.; Anderson, D. G.; Langer, R., Exploiting Electrostatic Interactions in Polymer-Nanoparticle Hydrogels. *ACS Macro Lett.* **2015**, 4, (8), 848-852.
92. Hashimoto, Y.; Mukai, S.; Sawada, S.; Sasaki, Y.; Akiyoshi, K., Nanogel tectonic porous gel loading biologics, nanocarriers, and cells for advanced scaffold. *Biomaterials* **2015**, 37, 107-115.

93. Hashimoto, Y.; Mukai, S.; Sawada, S.; Sasaki, Y.; Akiyoshi, K., Advanced Artificial Extracellular Matrices Using Amphiphilic Nanogel-Cross-Linked Thin Films To Anchor Adhesion Proteins and Cytokines. *Acs Biomater-Sci Eng* **2016**, 2, (3), 375-384.
94. Ferrari, M., Cancer nanotechnology: Opportunities and challenges. *Nat. Rev. Cancer* **2005**, 5, (3), 161-171.
95. Rana, S.; Bajaj, A.; Mout, R.; Rotello, V. M., Monolayer coated gold nanoparticles for delivery applications. *Adv. Drug Deliver Rev.* **2012**, 64, (2), 200-216.
96. Gao, W. W.; Hu, C. M. J.; Fang, R. H.; Zhang, L. F., Liposome-like nanostructures for drug delivery. *J. Mater. Chem. B* **2013**, 1, (48), 6569-6585.
97. Chan, J. M.; Valencia, P. M.; Zhang, L. F.; Langer, R.; Farokhzad, O. C., Polymeric Nanoparticles for Drug Delivery. *Methods Mol Biol* **2010**, 624, 163-175.
98. Petros, R. A.; DeSimone, J. M., Strategies in the design of nanoparticles for therapeutic applications. *Nat. Rev. Drug Discov.* **2010**, 9, (8), 615-627.
99. Yoo, J. W.; Irvine, D. J.; Discher, D. E.; Mitragotri, S., Bio-inspired, bioengineered and biomimetic drug delivery carriers. *Nat. Rev. Drug Discov.* **2011**, 10, (7), 521-535.
100. Davis, M. E.; Chen, Z.; Shin, D. M., Nanoparticle therapeutics: an emerging treatment modality for cancer. *Nat. Rev. Drug Discov.* **2008**, 7, (9), 771-782.
101. Blanco, E.; Shen, H.; Ferrari, M., Principles of nanoparticle design for overcoming biological barriers to drug delivery. *Nat. Biotechnol.* **2015**, 33, (9), 941-951.
102. Gao, W. W.; Chan, J. M.; Farokhzad, O. C., pH-Responsive Nanoparticles for Drug Delivery. *Mol. Pharmaceut.* **2010**, 7, (6), 1913-1920.
103. Rwei, A. Y.; Wang, W. P.; Kohane, D. S., Photoresponsive nanoparticles for drug delivery. *Nano Today* **2015**, 10, (4), 451-467.
104. Rahikkala, A.; Aseyev, V.; Tenhu, H.; Kauppinen, E. I.; Raula, J., Thermoresponsive Nanoparticles of Self-Assembled Block Copolymers as Potential Carriers for Drug Delivery and Diagnostics. *Biomacromolecules* **2015**, 16, (9), 2750-2756.
105. Cheng, R.; Feng, F.; Meng, F.; Deng, C.; Feijen, J.; Zhong, Z., Glutathione-responsive nano-vehicles as a promising platform for targeted intracellular drug and gene delivery. *J. Controlled Release* **2011**, 152, (1), 2-12.

106. Colson, Y. L.; Grinstaff, M. W., Biologically Responsive Polymeric Nanoparticles for Drug Delivery. *Adv. Mater.* **2012**, 24, (28), 3878-3886.
107. Delplace, V.; Nicolas, J., Degradable vinyl polymers for biomedical applications. *Nat. Chem.* **2015**, 7, (10), 771-784.
108. Mura, S.; Nicolas, J.; Couvreur, P., Stimuli-responsive nanocarriers for drug delivery. *Nat. Mater.* **2013**, 12, (11), 991-1003.
109. Gohy, J. F.; Zhao, Y., Photo-responsive block copolymer micelles: design and behavior. *Chem. Soc. Rev.* **2013**, 42, (17), 7117-7129.
110. Zhao, Y., Light-Responsive Block Copolymer Micelles. *Macromolecules* **2012**, 45, (9), 3647-3657.
111. Ward, M. A.; Georgiou, T. K., Thermoresponsive Polymers for Biomedical Applications. *Polymers-Basel* **2011**, 3, (3), 1215-1242.
112. McDaniel, J. R.; Callahan, D. J.; Chilkoti, A., Drug delivery to solid tumors by elastin-like polypeptides. *Adv. Drug Deliver Rev.* **2010**, 62, (15), 1456-1467.
113. Meng, F. H.; Hennink, W. E.; Zhong, Z., Reduction-sensitive polymers and bioconjugates for biomedical applications. *Biomaterials* **2009**, 30, (12), 2180-2198.
114. Bae, Y. H.; Yin, H., Stability issues of polymeric micelles. *J. Controlled Release* **2008**, 131, (1), 2-4.
115. Kim, S.; Shi, Y. Z.; Kim, J. Y.; Park, K.; Cheng, J. X., Overcoming the barriers in micellar drug delivery: loading efficiency, in vivo stability, and micelle-cell interaction. *Expert Opin. Drug Del.* **2010**, 7, (1), 49-62.
116. Nayak, S.; Lyon, L. A., Soft Nanotechnology with Soft Nanoparticles. *Angew. Chem. Int. Ed.* **2005**, 44, (47), 7686-7708.
117. Sasaki, Y.; Akiyoshi, K., Nanogel engineering for new nanobiomaterials: from chaperoning engineering to biomedical applications. *The Chemical Record* **2010**, 10, (6), 366-376.
118. Kabanov, A. V.; Vinogradov, S. V., Nanogels as Pharmaceutical Carriers: Finite Networks of Infinite Capabilities. *Angew. Chem. Int. Ed.* **2009**, 48, (30), 5418-5429.
119. Raemdonck, K.; Demeester, J.; De Smedt, S., Advanced nanogel engineering for drug delivery. *Soft Matter* **2009**, 5, (4), 707-715.

120. Eckmann, D. M.; Composto, R. J.; Tsourkas, A.; Muzykantov, V. R., Nanogel carrier design for targeted drug delivery. *J. Mater. Chem. B* **2014**, 2, (46), 8085-8097.
121. Chacko, R. T.; Ventura, J.; Zhuang, J. M.; Thayumanavan, S., Polymer nanogels: A versatile nanoscopic drug delivery platform. *Adv. Drug Deliver Rev.* **2012**, 64, (9), 836-851.
122. Zha, L. S.; Banik, B.; Alexis, F., Stimulus responsive nanogels for drug delivery. *Soft Matter* **2011**, 7, (13), 5908-5916.
123. Heller, D. A.; Levi, Y.; Pelet, J. M.; Doloff, J. C.; Wallas, J.; Pratt, G. W.; Jiang, S.; Sahay, G.; Schroeder, A.; Schroeder, J. E.; Chyan, Y.; Zurenko, C.; Querbes, W.; Manzano, M.; Kohane, D. S.; Langer, R.; Anderson, D. G., Modular 'Click-in-Emulsion' Bone-Targeted Nanogels. *Adv. Mater.* **2013**, 25, (10), 1449-1454.
124. Messenger, L.; Portecop, N.; Hachet, E.; Lapeyre, V.; Pignot-Paintrand, I.; Catargi, B.; Auzely-Velty, R.; Ravaine, V., Photochemical crosslinking of hyaluronic acid confined in nanoemulsions: towards nanogels with a controlled structure. *J. Mater. Chem. B* **2013**, 1, (27), 3369-3379.
125. Li, M. Q.; Tang, Z. H.; Sun, H.; Ding, J. X.; Song, W. T.; Chen, X. S., pH and reduction dual-responsive nanogel cross-linked by quaternization reaction for enhanced cellular internalization and intracellular drug delivery. *Polym. Chem.* **2013**, 4, (4), 1199-1207.
126. Alles, N.; Soysa, N. S.; Hussain, M. D. A.; Tomomatsu, N.; Saito, H.; Baron, R.; Morimoto, N.; Aoki, K.; Akiyoshi, K.; Ohya, K., Polysaccharide nanogel delivery of a TNF-alpha and RANKL antagonist peptide allows systemic prevention of bone loss. *Eur. J. Pharm. Sci.* **2009**, 37, (2), 83-88.
127. Chen, W.; Zheng, M.; Meng, F. H.; Cheng, R.; Deng, C.; Jan, F. J.; Zhong, Z. Y., In Situ Forming Reduction-Sensitive Degradable Nanogels for Facile Loading and Triggered Intracellular Release of Proteins. *Biomacromolecules* **2013**, 14, (4), 1214-1222.
128. Smith, M. H.; Lyon, L. A., Multifunctional Nanogels for siRNA Delivery. *Acc. Chem. Res.* **2012**, 45, (7), 985-993.
129. Knop, K.; Hoogenboom, R.; Fischer, D.; Schubert, U. S., Poly(ethylene glycol) in Drug Delivery: Pros and Cons as Well as Potential Alternatives. *Angew. Chem. Int. Ed.* **2010**, 49, (36), 6288-6308.
130. Zhu, J., Bioactive modification of poly(ethylene glycol) hydrogels for tissue engineering. *Biomaterials* **2010**, 31, (17), 4639-4656.

131. Flake, M. M.; Nguyen, P. K.; Scott, R. A.; Vandiver, L. R.; Willits, R. K.; Elbert, D. L., Poly(ethylene glycol) Microparticles Produced by Precipitation Polymerization in Aqueous Solution. *Biomacromolecules* **2011**, 12, (3), 844-850.
132. Murayama, S.; Jo, J.; Shibata, Y.; Liang, K.; Santa, T.; Saga, T.; Aoki, I.; Kato, M., The simple preparation of polyethylene glycol-based soft nanoparticles containing dual imaging probes. *J. Mater. Chem. B* **2013**, 1, (38), 4932-4938.

Chapter 2

CONTROLLED RELEASE OF AN ANTHRAX TOXIN-NEUTRALIZING ANTIBODY FROM HYDROLYTICALLY DEGRADABLE POLYETHYLENE GLYCOL HYDROGELS

2.1 Introduction

Anthrax is caused by *Bacillus anthracis*, a Gram-positive, rod-shaped, spore-forming bacterium that primarily affects livestock but can spread to humans.^{1,2} Due to the ability of the pathogen to form endospores that can be easily concealed, transported, and released, *B. anthracis* poses a great threat as a bioterrorism agent, highlighted by the anthrax postal attack in 2001.^{3,4} The pathogenesis of *B. anthracis* is mediated by a tripartite toxin. This exotoxin consists of protective antigen (PA) and two enzymatically active proteins: lethal factor (LF) and edema factor (EF). PA functions as a cell-binding receptor for LF and EF to form lethal toxin (LeTx) and edema toxin, respectively, making it an ideal target for vaccine and countermeasure development. The development of biotechnology and genetic engineering methodologies has enabled monoclonal antibody (mAb) therapy to be developed as an effective countermeasure for protection against anthrax.^{5,6} The utilization of mAbs that target specific cells or proteins permits anthrax toxin neutralization by a variety of mechanisms, including neutralizing pathogen growth, limiting its spread from infected to adjacent cells, or by inhibiting the toxin's biological activity.⁷ During the past 10 years, several human antibodies against anthrax protective antigen (PA) have been demonstrated to provide passive protection in variety of animal models including rats, rabbits, guinea pigs and

non-human primates.⁸⁻¹⁰ One such mAb was developed by Fraunhofer USA Center for Molecular Biotechnology (FhCMB) and shown to provide full protection against an inhalation anthrax spore challenge in non-human primates.^{11, 12} FhCMB engineered this mAb in their plant-based production platform to be a non-glycosylated (NG) version of a mAb against PA, termed PANG. This NG variant was shown to have superior half-life and protective efficacy compared to a glycosylated counterpart. Therefore, PANG was selected as the mAb of interest for the work described below.

Similar to most protein therapeutics, antibodies can suffer from poor stability due to chemical degradation as well as physical aggregation.¹³ Also, repetitive dosing may be required to achieve a therapeutic effect, which compromises patient's comfort, convenience, and compliance.¹⁴⁻¹⁶ Water-swollen polymeric hydrogels have been extensively investigated as vehicles for the delivery of a variety of small and large molecules, including proteins.¹⁷⁻²¹ By encapsulation in the network, proteins can be protected against degradation and released from the hydrogel matrix in a controlled manner over an extended period of time, either in blood circulation or in the surrounding tissues.²²⁻²⁴ Degradable hydrogels are particularly desirable for protein delivery, since the release rate of the therapeutic proteins can be manipulated by the degradation of the matrix, and clearance of the device from the body can be achieved when the release is completed.²⁵⁻²⁸ Recently, several hydrogels based on synthetic polymers, natural polymers, and peptides have been formulated to offer local and sustained release of antibodies including immunoglobulin (IgG), Herceptin (a breast cancer antibody), and Bevacizumab (an anti-VEGF antibody), with enhanced therapeutic efficacy that reduces the number of injections and lowers the administered dose.²⁹⁻³⁴

In this study, we present hydrolytically degradable polyethylene glycol (PEG) hydrogels as a reservoir system for the controlled delivery of PANG, an anthrax LeTx neutralizing antibody. Degradable PEG hydrogels were formed via Michael-type addition using multi-arm PEG thiols (-SH) and linear PEG acrylates (-Ac). These hydrogels were rendered hydrolytically degradable via the acrylate ester linkages (see polymer structures in Scheme 1). We characterized the swelling properties of these hydrogels and demonstrated that the release rate of PANG can be adjusted by varying the molecular structures of the hydrogel precursors. Post-release and in-gel characterizations including polyacrylamide gel electrophoresis (SDS-PAGE), size-exclusion chromatography (SEC), circular dichroism (CD), and fluorescence indicated that PANG remained stable when encapsulated and released from the gel. A toxin neutralization assay showed that the released PANG remained biologically active and exhibited toxin-neutralizing activity in a concentration-dependent manner.

2.2 Materials and Methods

2.2.1 Materials

Four-arm, thiol-functionalized PEG (PEG-4SH, $M_n = 5000, 10000, \text{ and } 20000$ g/mol), eight-arm, thiol-functionalized PEG (PEG-8SH, $M_n = 10000 \text{ and } 20000$ g/mol) and linear diacrylated PEG (PEG-2Ac, $M_n = 2000, 3500, 5000 \text{ and } 7500$ g/mol) were purchased from JenKem Technology USA Inc. (Allen, TX, USA). Low molecular weight, diacrylated PEG (PEG-2Ac, $M_n = 700$) was purchased from Sigma-Aldrich (St. Louis, MO, USA). The non-glycosylated mAb (PANG) was produced by Fraunhofer

USA (Newark, DE, USA). All other reagents and materials were purchased from Fisher Scientific (Pittsburgh, PA, USA) unless otherwise noted.

2.2.2 Purification of Plant-Produced mAb PANG

Engineering, expression, and purification of PANG followed methods previously described with minor modifications.¹² Briefly, *Agrobacterium tumefaciens* transformed with the plasmid pGR-D4, carrying either the heavy chain or light chain, were used for agroinfiltration of *Nicotiana benthamiana*. Infiltrated plant material was blended in 1 volume of Tris based extraction buffer and centrifuged at 16,000 x g for 15 minutes at 4°C. The supernatant was collected and the pH adjusted to 5.3, mixed for 15 minutes at room temperature, and centrifuged a second time. The pH of the supernatant was then raised to 7.5, followed by filtration through a 0.45/0.2µm Sartopore filter and loading onto a 10 ml HiTrap MAb Select resin (GE Healthcare, Piscataway, NJ, USA). The column was washed with 15 column volumes of 50 mM Tris, pH7.5 buffer before elution with 100 mM citrate buffer (pH 3.0). Eluted PANG was buffered to neutral with pH 9 Tris buffer. The protein was concentrated using a Centricon Plus-70 (3000 MWCO) and dialyzed into PBS.

2.2.3 Formation of Degradable PEG Hydrogels

The hydrogels were formed by a Michael-type addition between multi-arm PEG-SH and hydrolytically degradable crosslinkers of linear PEG-diacrylate. The molar ratio of thiols/acrylates was 1:1 for all hydrogels. Each polymer precursor was dissolved in a phosphate-buffered saline (PBS) solution (pH=7.4). The identities of the polymer precursors for various hydrogel formulations are summarized in Table 1. The convention for naming the hydrogel samples is based on the number of arms and

molecular weight of the multi-functional PEG and the molecular weight of the linear PEG ‘crosslinker’. For example, the notation “8-arm 10/2K” indicates a hydrogel comprising a 10 kDa, 8-arm PEG-SH mixed with a 2 kDa linear PEG-diacrylate. Immediately after mixing, the solution was quickly vortexed, and then transferred to a scintillation vial and allowed to gel at 37°C. Gelation occurred in several minutes, but the hydrogels were left in the incubator overnight to achieve maximum cross-linking. For protein encapsulation, a solution of PANG (15.7 mg/mL) was used to dissolve the polymer precursor to achieve a final protein concentration of 5 mg/mL or 2.5 mg/mL.

2.2.4 Rheological Characterization of PEG Hydrogels

Oscillatory rheology experiments conducted on a stress-controlled AR-G2 rheometer (TA Instruments, New Castle, DE, USA) were used to characterize the gelation time of the PEG hydrogels. Experiments were conducted at 37°C using a 20 mm-diameter, cone and plate geometry with a 25 μm gap distance, with oscillatory time, frequency, and strain sweeps performed. Strain sweeps were performed on samples from 0.1% to a maximum strain of 1000% to determine the limit of the linear viscoelastic region. Dynamic oscillatory time sweeps were performed to monitor the *in situ* gelation of different PEG hydrogel solutions at angular frequencies of 6 rad/s and 1% strain chosen from the linear viscoelastic region. The PEG-SH and PEG-Ac precursors were dissolved in PBS separately with a final polymer concentration of 20wt%. The precursors were then combined, vortexed, and loaded onto the rheometer stage. The temporal evolution of G' (storage modulus) and G'' (loss modulus) was recorded throughout the crosslinking experiments.

2.2.5 Swelling Experiments

Hydrogels (100 μL) were incubated at 37°C in water. Hydrogel samples were collected at regular intervals of swelling, excess water removed by blotting, and their mass after swelling was measured. The hydrogels were then dried under vacuum overnight, and their dry mass was measured. The equilibrium mass swelling ratio q was experimentally obtained by the following equation:

$$q = \frac{W_{swollen}}{W_{dry}}$$

where $W_{swollen}$ and W_{dry} are the weights of the polymer at swollen and dried states, respectively.

2.2.6 *In Vitro* Protein Release Experiments

The protein release experiments were performed at 37°C in a glass vial with PBS buffer. Hydrogels (400 μL) were placed on the bottom of the vial and 5 mL of PBS was added over the gel. One mL of PBS was sampled from the vial at predetermined time points and replaced with 1 mL of fresh PBS. The final time point of the release experiments was defined as the time point when the buffer solutions above the gels became too viscous for sampling (which was prior to 100% hydrogel degradation). The resulting release samples were distributed into several aliquots and stored at -80°C to avoid potential damage to the PANG before characterization. Samples were reserved for determination of concentration and determination of cumulative release. (Samples were also reserved for characterization of protein conformation and activity; see below.) Protein samples were concentrated by centrifugation using Amicon Ultra-0.5 mL Centrifugal Filters (3KDa, Billerica, MA, USA), and protein concentration was

characterized via UV-Vis spectrometry with detection at 280 nm. Protein stability was confirmed by SDS-PAGE electrophoresis.

The cumulative protein release (given as a percentage of encapsulated protein, (P_r)) was calculated using the following equation:

$$P_r(\%) = \frac{V_e \sum_{i=1}^{n-1} C_i + V_0 C_n}{m_{PANG}} \times 100\%$$

Where m_{PANG} represents the amount of protein encapsulated in the hydrogel, V_0 is the whole volume of the release media (5 mL), V_e is the volume of each sample that is being taken out at each time point (1 mL), and C_i represents the concentration of the PANG protein measured by UV-Vis in the i^{th} sample (C_n represents the n^{th} sample).

2.2.7 Size Exclusion Chromatography

Size exclusion chromatography (SEC) studies were performed on an Agilent 1260 HPLC with PANG resolved over a ZENIX SEC-300 7.8×300 mm column (Sepax Technologies, Newark, DE, USA) with PBS as the mobile phase. All samples were analyzed at a flow rate of 1.0 mL per minute, with UV detection at 280 nm.

2.2.8 Circular Dichroism Spectroscopy

Circular dichroic spectra were recorded on a Jasco J-810 spectropolarimeter (Jasco Inc, Easton, MD, USA) equipped with a Jasco PTC-424S temperature controller. Background scans of PBS were recorded and subtracted automatically from the sample scans. For in-gel experiments, the samples (50 μ L) were loaded into a 0.20 mm path length demountable cuvette. For solution-phase experiments, the samples were loaded into a 1mm path length quartz cuvette. Data points for the wavelength-dependent CD spectra were recorded at every nanometer with a 1 nm bandwidth and an averaging time

of 10s for each data point from 190 to 250 nm, at room temperature. The mean residue ellipticity $[\theta]_{\text{MRE}}$ (degrees $\text{cm}^2 \text{dmol}^{-1}$), was calculated via use of the concentration, molecular weight of the samples, number of residues, and cell path length.

2.2.9 Fluorescence Emission Spectroscopy

Fluorescence emission of released PANG and PANG control was measured by using a HORIBA Jobin Yvon SPEX FluoroMax-4 spectrofluorometer (HORIBA Scientific, Edison, NJ, USA) at room temperature with quartz cuvettes of 1 cm path length. Emission spectra were recorded between 310 and 400 nm after excitation at 300 nm. In-gel experiments were carried out using a QuantaMaster spectrofluorometer (Photon Technologies International, Edison, NJ, USA) at room temperature with quartz cuvettes of 1.0 mm path length. Emission spectra were recorded between 310 nm and 400 nm on excitation at 295 nm. The excitation and emission slit widths were set at 5.0 and 2.5 nm, respectively. All spectra were corrected for the background emission of PBS.

2.2.10 Anthrax Lethal Toxin Neutralization Assay

Samples collected after release were characterized for toxin-binding activity via an anthrax lethal toxin (LeTx) neutralization assay that was performed using decreasing amounts of the released samples. Specifically, the biological activity of PANG was measured using a LeTx neutralization assay as described previously with modifications.³⁵ J774A.1 (ATCC TIB-67, Manassas, VA, USA) cells were plated in 96-well flat-bottomed tissue culture plates at 2.5×10^4 cells/well in 50 μL and incubated for 16-19 h at 37°C with 5% CO_2 . Test samples were diluted and titrated on the plated cells in the presence or absence of LeTx (List Biological Laboratories, Campbell, CA,

USA). After a 4 h incubation at 37°C with 5% CO₂, cell viability was assessed by the addition of WST-1 (Roche Applied Sciences, Indianapolis, IN, USA), a proliferation reagent, followed by a spectrophotometric measurement at 450 nm. A four-parameter logistic-log regression model was used to analyze data plotted as OD versus the reciprocal of the sample dilution. The inflection point for each curve from this model is reported as the dilution of the sample that provides 50% inhibition of LeTx; termed effective dilution 50 (ED₅₀).

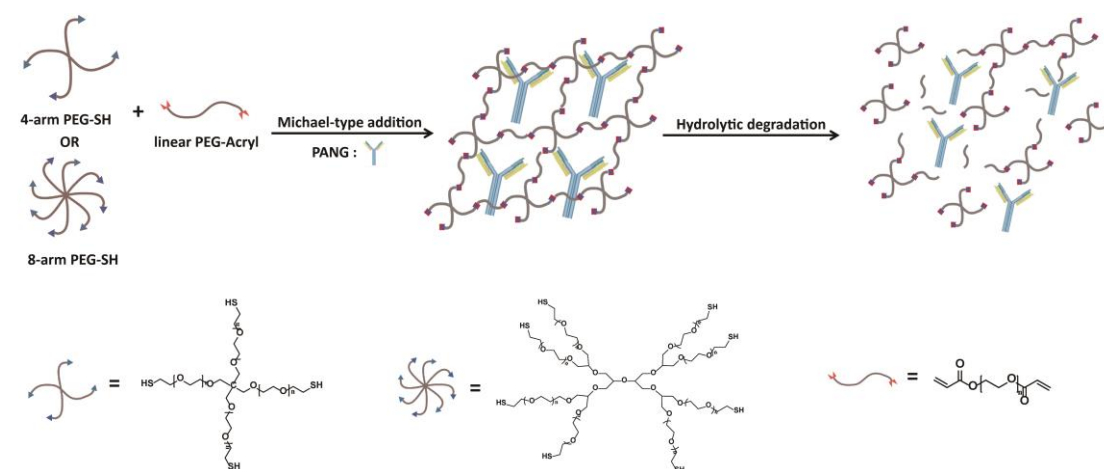


Figure 2.1 Schematic representation of the formation and degradation of PANG-loaded PEG hydrogels.

2.3 Results

2.3.1 Hydrogel Compositions and Formation

The Michael-type addition reaction has long been used as a versatile crosslinking strategy for the development of injectable biomaterials, owing to its rapid

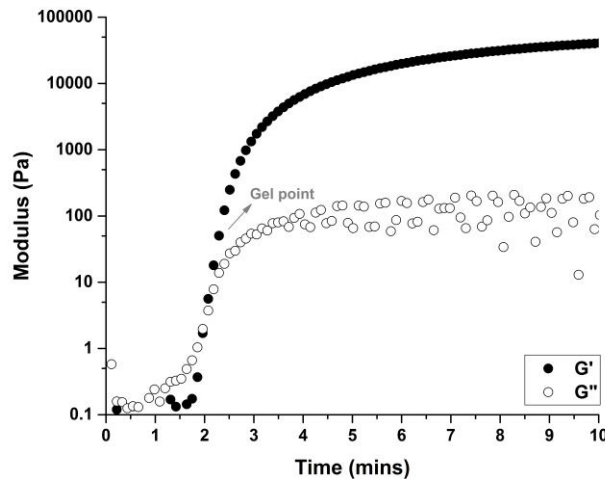


Figure 2.2 *In situ* gelation of 20wt% 8-arm 10/2K hydrogel, as characterized by oscillatory rheology. The evolution of G' (storage modulus) and G'' (loss modulus) was monitored as a function of time.

kinetics and mild reaction conditions.³⁶ Hydrogels were formed *in situ* from multi-arm PEG-SH precursors with linear PEG diacrylate crosslinkers via Michael-type addition (Figure 2.1) in PBS buffer. Gelation occurred within 1-3.5 minutes depending on the molecular structures of the precursors, as characterized by oscillatory rheology time sweeps (Figure 2.2). Figure 1 shows the time sweep profile of the evolution of G' and G'' for the 20wt% 8-arm 10/2K hydrogel. (The convention 8-arm 10/2K indicates a hydrogel comprising a 10 kDa, 8-arm PEG-SH mixed with a 2 kDa linear PEG-diacrylate; this convention is used throughout the manuscript to indicate the compositions of the various hydrogels studied.) A rapid increase of G' was observed after mixing, with a crossover point (where G' becomes larger than G'') at approximately 2 minutes.³⁷ Although the apparent gelation times estimated by a tube inversion method were greater (ca. 2-5 minutes) compared to those observed in the

rheological profiles, they were proportionate for all PEG hydrogels studied (i.e., longer inversion times correlated with longer rheological crossover times). The composition of hydrogels was varied by using polymers with different functionalities, molecular weights, and concentrations (Table 1), in order to tune the rate of release of the antibody.

Table 2.1 Formulations of different PEG hydrogels

| Sample | Polymers employed | Polymer concentration (wt%) | PANG loading concentration (mg/mL) |
|---------------|------------------------------|-----------------------------|------------------------------------|
| 4-arm 10/5K | 10K PEG-4SH / 5K PEG-2Ac | 10, 20, 30 | 5, 2.5 |
| 4-arm 5/2K | 5K PEG-4SH / 2K PEG-2Ac | 20 | 2.5 |
| 4-arm 5/3.5K | 5K PEG-4SH / 3.5K PEG-2Ac | 20 | 2.5 |
| 8-arm 20/5K | 20K PEG-8SH / 5K PEG-2Ac | 20 | 2.5 |
| 8-arm 10/2K | 10K PEG-8SH / 2K PEG-2Ac | 20 | 2.5 |
| 8-arm 10K/700 | 10K PEG-8SH / 700 PEG-2Ac | 20 | 2.5 |

2.3.2 Swelling Experiments

Swelling is a critical parameter for hydrogels employed in biomedical and pharmaceutical applications as the equilibrium swelling ratio is inversely correlated with the hydrogel crosslinking density, which in turn influences solute diffusion in and release from the hydrogel.³⁸ In Figure 2.3, the relationship between network composition and hydrogel crosslinking density was explored by evaluating the equilibrium swelling ratio. The data in Figure 2.3a show the equilibrium swelling ratios (q) of 4-arm 10/5K gels at various polymer concentrations. It was observed that the q

value of 4-arm 10/5K hydrogels decreased from 13.8 ± 0.5 to 11.8 ± 0.7 and then further to 8.8 ± 0.2 as the precursor concentration increased from 10wt% to 20wt% to 30wt%, which can be attributed to the lower degrees of intramolecular reactions at higher monomer concentrations in step-growth polymerizations, resulting in an increased overall crosslinking density.³⁹⁻⁴²

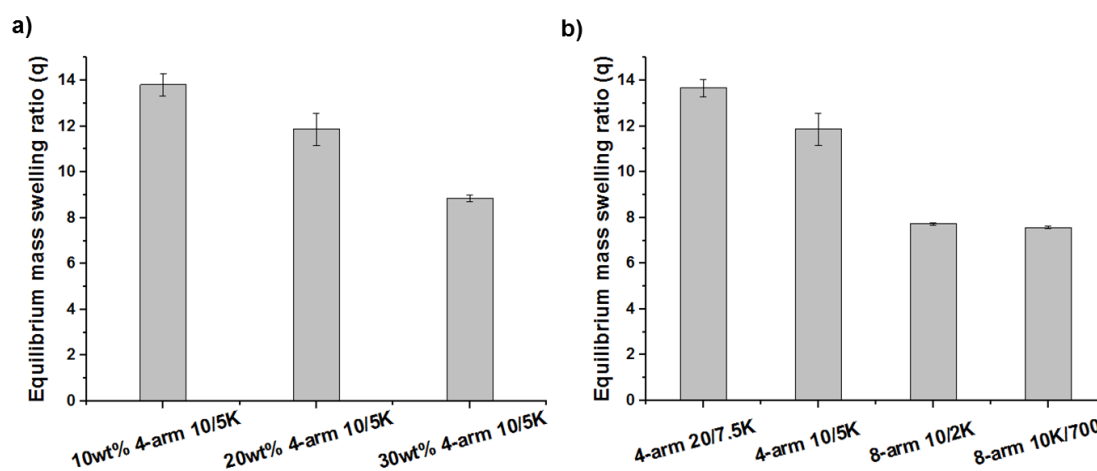


Figure 2.3 Equilibrium swelling properties of various PEG hydrogels. (a) 4-arm 10/5K gels at different concentration; (b) 20wt% hydrogels prepared from polymer precursors with different functionalities and molecular weights.

The equilibrium swelling ratios (q) of hydrogels synthesized from precursors with different functionalities and molecular weights were also investigated. The data in Figure 2.3b demonstrate that hydrogels polymerized from 4-arm PEG-SH precursors have significantly higher swelling ratios than those of the hydrogels polymerized from 8-arm PEG-SH precursors (*ca.* 12 vs 7.5), as expected given the increased crosslinking density of the 8-arm precursors. The data in Figure 2.3b also confirm that the equilibrium swelling ratio of the 4-arm 20/7.5K hydrogel is greater than that of the 4-

arm 10/5K hydrogel (13.6 vs 11.8), consistent with the increased molecular weight between crosslinks (\overline{M}_c) for the 4-arm 20/7.5K hydrogels and as would be expected according to Flory-Rehner theory.^{41,43} The changes in the hydrogels formed from 8-arm precursors are not as significant as those for the hydrogels formed from 4-arm precursors, as the extent of crosslinking for the 8-arm hydrogels is already high. Comparable swelling ratio data from PEG hydrogels with similar architectures were reported by Metters and Hubbell,³⁹ in which such dependence of swelling ratio on precursor concentration, functionality, and molecular weight was also observed. These results confirm that the network density and physical swelling of these hydrogels can be easily tuned, which provides insights in the design of hydrogels that meet the performance criteria demanded by a specific biomedical application.

2.3.3 *In Vitro* Studies of PANG Release from PEG-Based Hydrogels

The PEG hydrogels formed by Michael-type addition were employed as the delivery vehicles for PANG, a plant-produced non-glycosylated mAb against the protective antigen of anthrax, which is able to neutralize anthrax lethal toxin activity *in vivo* and *in vitro*.¹² The release of PANG from various PEG hydrogels was measured every 24h for the first 10 days and then monitored every week until the buffer solutions above the gels became too viscous for sampling (as a result of matrix degradation). The 20wt% hydrogel formulation was chosen for expanded studies of PANG release, given the steady release kinetics of PANG and the injection-friendly viscosity of precursor solutions. Interestingly, precipitation of the antibody was observed within most of the hydrogel formulations, consistent with previously observed PEG-induced protein precipitation⁴⁴ that is generally attributed to volume exclusion effects. The steric exclusion of PEG chains from the solvent space between protein molecules results in

increased local concentration of proteins and ultimately leads to protein precipitation when the solubility is exceeded.⁴⁵⁻⁴⁷ Therefore, a lower initial loading concentration of PANG (2.5 mg/mL) was adopted in these studies in order to minimize the influence of protein precipitation on the release properties of different hydrogel compositions.

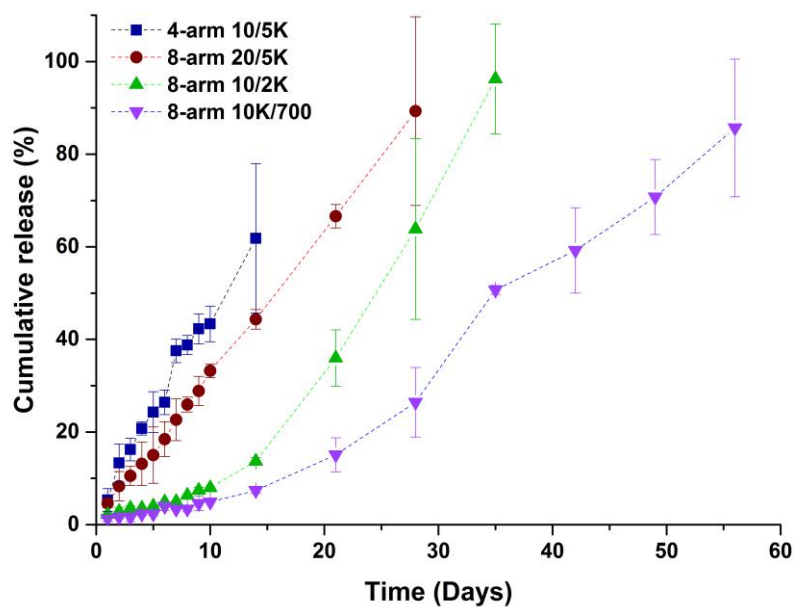


Figure 2.4 *In vitro* cumulative release of PANG from various PEG hydrogels at a precursor concentration of 20wt%, with an initial loading concentration of 2.5 mg/mL, as a function of time. The release of protein was monitored by measuring the absorbance, at 280 nm, of the buffer solution above the gel at the indicated time intervals.

A series of 20wt% PEG hydrogels prepared from 4-arm and 8-arm PEGs with various linear PEG crosslinkers were targeted to manipulate antibody delivery rates; results are presented in Figure 2.4. Controlled release of the antibody without initial

burst was observed from most of these hydrogels. The timespan of the release of the antibody varied from 14 days up to 56 days depending on the polymer architectures and molecular weights of the precursors, which is consistent with results reported in similar systems for protein release.^{22, 40, 48} For 4-arm 10/5K hydrogels, the antibody was released in a sustained fashion for approximately two weeks, with approximately 60% of PANG released at day 14. For 8-arm 20/5K hydrogels, approximately 90% of the antibody was released with zero-order kinetics over 28 days, with release of 3-4% of the antibody each day. For 8-arm 10/2K and 10K/700 hydrogels, following a slow initial release of approximately 10% of the antibody for the first 14 days, an increased rate of antibody release was observed, achieving a release of approximately 95% at day 35 and 85% at day 56, respectively.

In agreement with previous swelling experiments, release of PANG from 8-arm hydrogels was slower than that from 4-arm hydrogels due to the increase in crosslinking density. While approximately 60% of PANG was released on day 14 from the 4-arm 10/5K hydrogels, the amount of PANG released at the same time from 8-arm hydrogels was only 44%, 13% and 7% for the 8-arm 20/5K, 10/2K and 10K/700 hydrogels, respectively, and, the release of PANG could be extended from 28 days to 56 days. These observed trends are in accordance with theory⁴⁹ as well as with other existing reports.^{39, 43, 50} However, the release kinetics of PANG were unexpectedly similar for almost all of the 4-arm hydrogels, despite the variation in the molecular weight of the precursors (Figure 2.5). During the first week of the experiment, the cumulative release curves of 4-arm 5/2K, 5/3.5K and 10/5K almost overlap, with approximately 43%, 38% and 37% of PANG released at day 7, respectively. This discrepancy might be explained by the effect of the PEG molecular weight on the precipitation of PANG. PEGs with

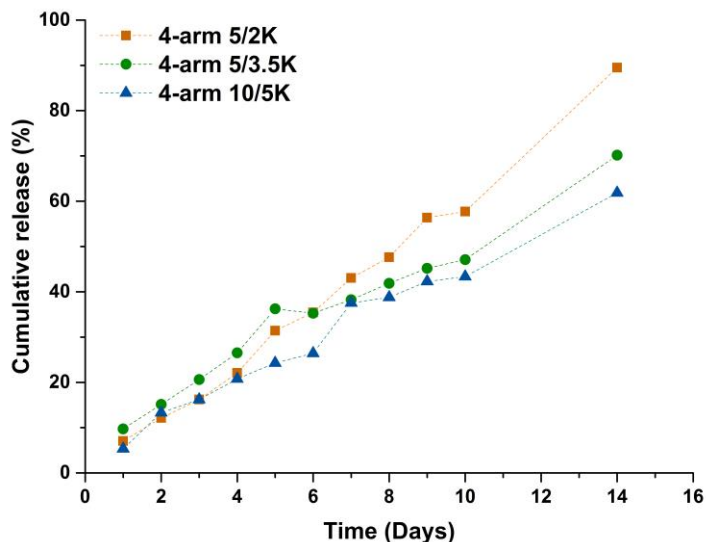


Figure 2.5 *In vitro* cumulative release of PANG from various 20wt% 4-arm hydrogels with different precursor molecular weights, with an initial loading concentration of 2.5 mg/mL, as a function of time. The release of protein was monitored by measuring the absorbance, at 280 nm, of the buffer solution above the gel at the indicated time intervals.

lower molecular weights produce smaller aggregating interactions between protein molecules, owing to the reduction in steric exclusion for the smaller macromolecules.^{51, 52} The solubility of PANG thus would be expected to increase as the molecular weight of the linear PEG decreases, which would facilitate the release of PANG from the 4-arm 5/2K and 5/3.5K hydrogels and might subsequently offset the expected reduction in release rate from the gels with decreased \overline{M}_C .

2.3.4 In-Gel and Post-Release Characterization of PANG

To characterize PANG after its release from the hydrogels, SEC and SDS-PAGE were used to examine aggregation and possible degradation of the released protein. To

obtain further insight into the conformational properties of PANG during encapsulation and after release, CD and fluorescence spectroscopy in both hydrogel and solution were used to examine the secondary and tertiary structures of the protein, respectively.

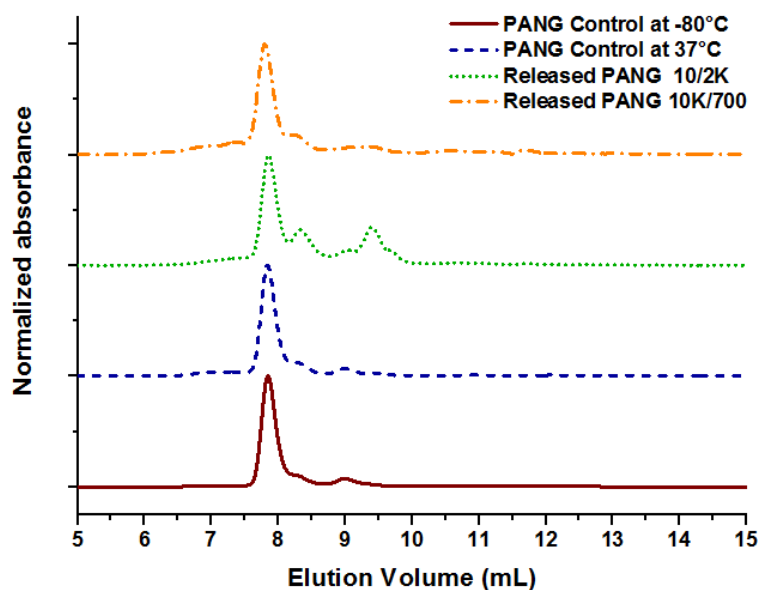


Figure 2.6 Normalized SEC trace of PANG controls and PANG released from the hydrogels after 28 days in PBS. Elution was monitored by UV absorbance at 280 nm.

For characterization of protein stability, samples of PANG released from 8-arm 10/2K and 10K/700 hydrogels were selected as a more stringent test owing to the longer duration of retention of PANG in these networks. PANG samples collected after 28 days of release were examined by SEC, as shown in Figure 2.6. Peaks of monomeric PANG, from all the samples, were observed at an elution volume of 7.8 mL. A soluble PANG control incubated at 37°C (without hydrogel) showed a similar elution profile to that observed for the PANG solution stored at -80°C, indicating that PANG was stable over

the test period. Quantitative analysis of the amount of monomeric PANG in these samples is also shown in Table 2.2. The PANG released from both type of hydrogels contained approximately 90-92% monomer, which is very close to that of a control solution of PANG dissolved directly (ca. 92-97% monomer), indicating that PANG released from both types of hydrogels was mainly in a monomeric state and showed no significant aggregation. In a similar report,⁴⁰ Leach and coworkers also confirmed that bovine serum albumin (BSA) was mostly maintained as monomer (more than 90%) after its release from PEG hydrogels. The small peak at about 9.5 mL in the elution profile of the PANG released from the 10/2K hydrogel is possibly due to the presence of PEG fragments caused by hydrogel degradation (visible in the UV owing to the ester linkage at the termini). The lack of these fragments from the 10/700 hydrogel is likely a result of the slower rate of degradation of the 10/700 hydrogel.

Table 2.2 SEC analysis of the physical state of released PANG

| Sample type | Time (day) | % monomer |
|---------------------------------------|-------------------|------------------|
| PANG control at -80°C | | 97.7% |
| PANG control at 37°C | 28 | 91.5% |
| PANG released from 10/2K gel | 28 | 92.0% |
| PANG released from 10K/700 gel | 28 | 89.3% |

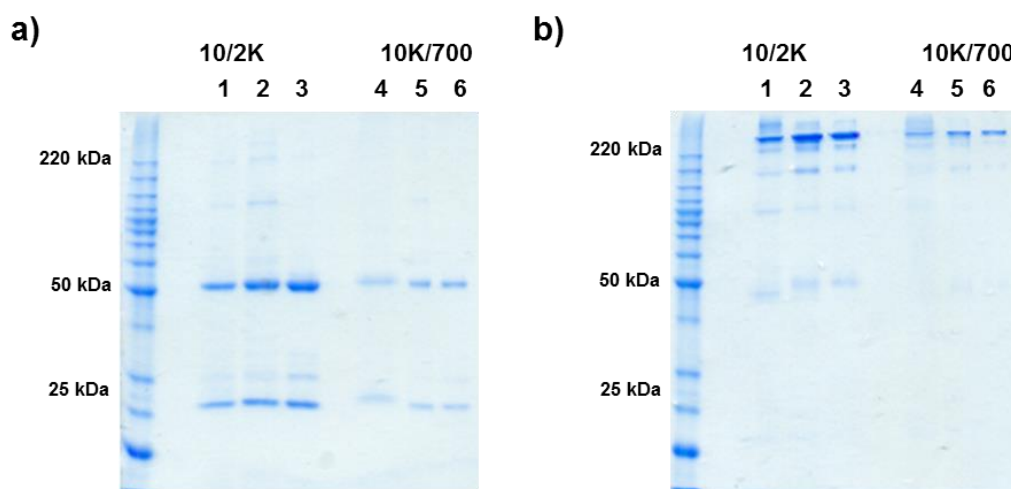


Figure 2.7 SDS-PAGE electrophoresis depicting protein release under (a) reducing and (b) non-reducing conditions. Lane 1: D35 sample from 10/2K; Lane 2: D35 PANG Control at 37°C; Lane 3: PANG Standard at -80°C; Lane 4: D56 sample from 10K/700; Lane 5: D56 PANG Control at 37°C; Lane 6: PANG Standard at -80°C.

Protein samples collected at later time points, when almost all of the PANG had been released (day 35 and day 56, respectively), were also characterized via SDS-PAGE (Figure 2.7). Similar to most antibodies, PANG comprises two heavy chains (50 kDa) and two light chains (25 kDa) connected by disulfide bonds. Therefore, electrophoresis under reducing (with DTT) and non-reducing (without DTT) conditions was used to examine the structural integrity of the antibody. Generally, separate heavy chains and light chains are observed in SDS-PAGE under reducing conditions while the intact antibody is observed under non-reducing condition. PANG released from 8-arm 10/2K and 10K/700 hydrogels was loaded in Lane 1 and Lane 4, respectively. PANG controls stored at either 37°C or -80°C were loaded in Lane 2-3 and Lane 5-6, respectively, for parallel comparison with the release samples. In Figure 2.7a, two bands representing the heavy chains (50kDa) and light chains (25kDa) of the antibody were observed as

expected in each lane. In Figure 2.7b, bands indicative of the intact antibody were observed at approximately 220kDa, significantly greater than the expected molecular weight (~145kDa), likely due to incomplete linearization and unfolding of the antibody under these conditions. Some fragmentation products were observed for the higher concentration PANG samples (Lane 1-3) under non-reducing conditions, which might be a result of disulfide-bond scrambling catalyzed by free sulfhydryl groups in the antibody itself.⁵³⁻⁵⁵ Nevertheless, these data demonstrate that the majority of PANG released from the hydrogels, even after extended periods, showed an electrophoretic profile comparable to the PANG controls.

The conformational properties of PANG after its release from the matrices were investigated by CD and fluorescence emission spectroscopy respectively, as shown in Figure 2.8. Figure 2.8a illustrates CD confirmation of the secondary structure of PANG after its release. Negative peaks were observed at 218 nm for both of the release samples as well as for the antibody control, which is consistent with the presence of β -sheet conformations in the protein.⁵⁶ More importantly, the CD spectra of the released PANG closely resembled that of the PANG control. The low signal-to-noise ratio observed in some spectra, especially in the PANG solution collected from the 10K/700 hydrogel after 56 days, may be attributed to the relatively low concentration (even after concentration via centrifugal filtration) of released PANG in these samples, along with the possible presence of detached PEG fragments from the hydrogel matrix.⁵⁷ Figure 2.8b shows the data from fluorescence emission spectroscopy, which was used to detect changes in the tertiary structure of the PANG after its release from the hydrogel, as the emission spectrum is sensitive to the tryptophan microenvironment within the 3D structure of the protein. The data in Figure 2.8b show an emission maximum of

tryptophan at 340 nm; the emission spectra of the released PANG were similar to those of the PANG control with respect to both the emission maximum and fluorescence intensity normalized for concentration. These results suggest that PANG maintained its structural conformation after undergoing the precipitation and re-dissolution process, as well as release from the PEG hydrogels.

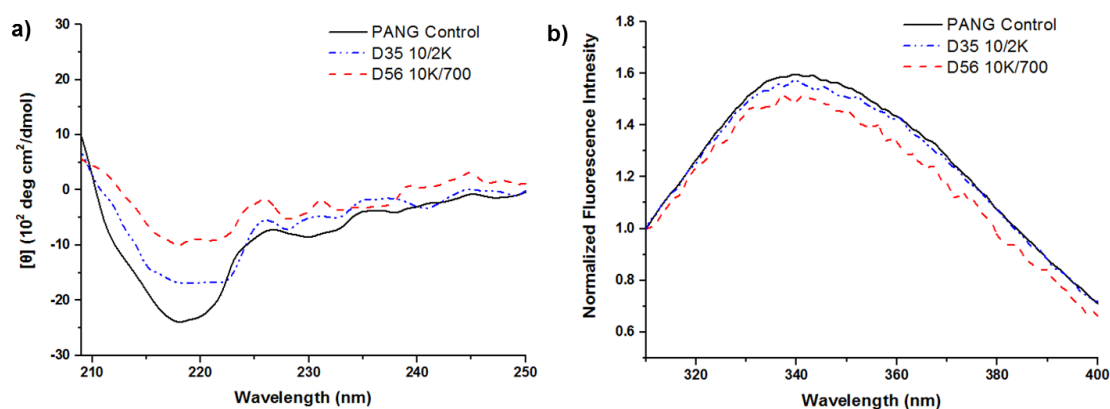


Figure 2.8 Conformational characterization of PANG control solutions and of PANG released from the hydrogels. (a) CD spectra of solutions of PANG control and PANG released from hydrogels; (b) Normalized fluorescence emission spectra of PANG control and PANG released from hydrogels.

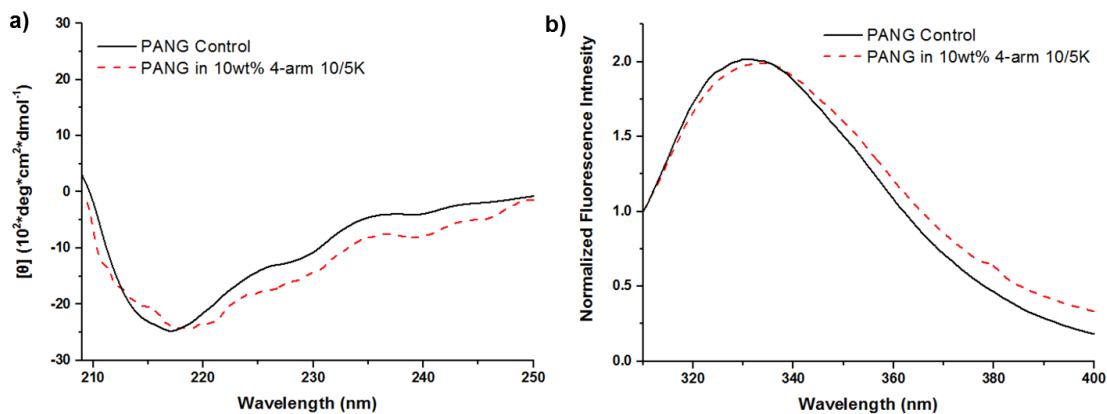


Figure 2.9 Conformational characterizations of PANG (5 mg/mL) when encapsulated within the hydrogels. (a) CD spectra of PANG control and encapsulated PANG; (b) Normalized fluorescence emission spectra of PANG control and encapsulated PANG.

Although hydrogel strategies have been widely used to protect proteins from degradation and denaturation, the conformational properties of proteins during *in situ* gelation and encapsulation have rarely been studied. In order to understand the conformation of PANG when incorporated within the hydrogel, PANG-loaded PEG hydrogels were also studied via CD and fluorescence spectroscopy (Figure 2.9). In this case, a relatively low polymer concentration (10wt% hydrogel) was employed to alleviate the opacity caused by PEG-induced precipitation. Similar to the data in Figure 6, the characteristic negative peak at approximately 218 nm of β -sheet conformations were observed (Figure 2.9a) while the expected fluorescence emission maximum of PANG was observed at 331-334 nm (Figure 2.9b). The data in Figure 2.9 confirm that soluble PANG encapsulated in the polymer network exhibited similar secondary and tertiary structures as those of the antibody control. The slight red shift of the emission maximum of the in-gel PANG (334 nm) compared to that of the PANG control (331 nm) in Figure 2.9b might be attributed to a slightly more hydrophilic local environment

within the hydrogel.⁵⁸ These data indicate that the processes involved during the *in situ* gelation in the presence of PANG did not adversely affect the antibody conformation.

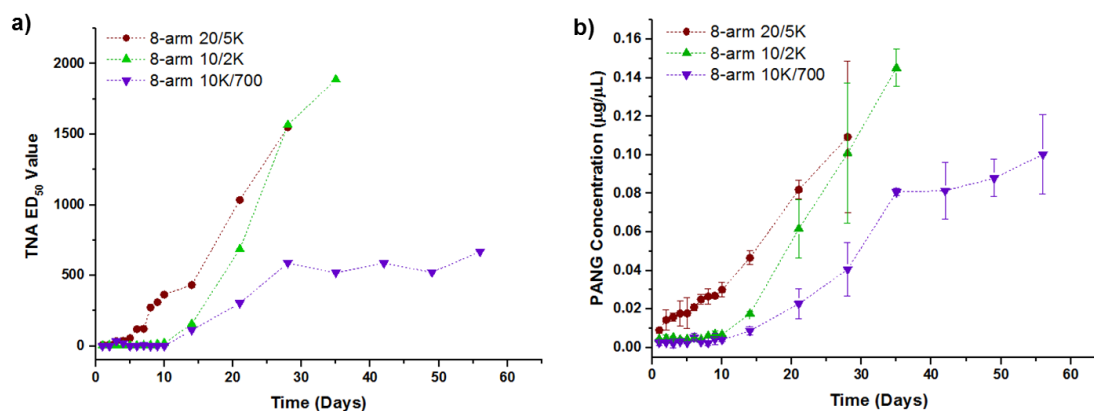


Figure 2.10 *In vitro* characterization of PANG released from PEG hydrogels. (a) Toxin-neutralizing activity of released PANG on J774A.1 cells incubated with LeTx; (b) Concentration profile of the *in vitro* released protein samples as characterized by UV-Vis at 280 nm.

2.3.5 Biological Activity of Released PANG

To examine the biological activity of the antibody released from the hydrogels, an anthrax lethal toxin neutralization assay (TNA) was employed to assess the ability of PANG to neutralize anthrax lethal toxin (LeTx). Test samples were applied to cells in the presence of LeTx, and the dilution of the sample at which 50% of the cells are protected from LeTx was determined to be the effective dilution 50 (ED₅₀).¹² ED₅₀ values establish a quantitative criterion to a dose response curve that allows for the comparison of the biological activity of PANG in each test sample. Higher ED₅₀ values indicate that a higher sample dilution yields 50% protection, and thus indicate a sample with greater neutralizing activity (which is related to the concentration of functional PANG in the sample). As shown in Figure 2.10a, the ED₅₀ values of these release

samples gradually increased over time, after an initial lag period. For 8-arm 20/5K hydrogels, little toxin neutralizing activity was observed for the first 5 days. After that, the release samples exhibited a significant increase in activity, reaching an ED₅₀ value of 1550 at day 28. Similarly, following an initial delay in biological activity over the first 10 days, samples from 8-arm 10/2K and 10K/700 hydrogels showed increased activity, achieving an ED₅₀ value of 1890 at day 35 and 670 at day 56, respectively. The PANG released from the hydrogel matrix clearly retained its ability to neutralize anthrax LeTx *in vitro* up to 56 days. The initial delay in toxin-neutralization might be attributed to the slow initial release of PANG from the hydrogels. Furthermore, the toxin-neutralizing profile of the released proteins closely mirrored the concentration profile determined via UV-Vis (Figure 2.10b), further confirming that the functionality of the antibody was not affected by its extended encapsulation in the PEG hydrogels.

2.4 Discussion

In contrast to many other existing antibody release vehicles, PANG release from these PEG hydrogels exhibited zero-order kinetics without any significant burst effect during the initial release stage, likely a result of the PEG-induced precipitation of the antibodies. At an early stage of the experiment, PANG release from the hydrogel is hindered due to the fact that only a minor, non-precipitated fraction of the incorporated antibody is available for diffusion out of the matrix, resulting in a lack of burst release. (Opacity associated with the precipitation of PANG was observed within the hydrogel for most formulations until approximately 40% of the antibody was released.) In most hydrogel delivery systems, swelling of the polymer network and release of protein result in a decreasing protein concentration gradient, leading to a decrease in release rate.^{59, 60}

The consistent release rate observed for our experiments, in contrast, may be a result of a balance between hydrogel degradation and dissolution of the antibody precipitate throughout the course of the experiment. As the gels swell/degrade, the soluble antibody concentration within the network decreases (decreased concentration gradient), and the dissolution of antibody precipitate increases (increased concentration gradient). These two limiting factors of antibody release counteract each other, which might yield a more consistent concentration gradient and lead to an almost constant release rate of PANG over prolonged periods of time.²² This proposed mechanism, which still requires hydrogel degradation for the release of antibody from the hydrogels, is further evidenced by the release profiles of the 8-arm 10/2K and 10K/700 hydrogels with high network density. The swelling and degradation of these hydrogels was observed to be very limited during initial time points, which would be expected to retard protein release. Consistent with this expectation, only minimal protein release (ca. 10%) was observed over the first 10 days of the experiment, and zero-order release was observed only once hydrogel swelling and degradation became significant, leading to increased dissolution and subsequent release of the precipitated antibody.

The observation of these release profiles for PANG, in conjunction with the precipitation of the protein, is consistent with results reported by others. For example, Hubbell and coworkers took advantage of the precipitation of human growth hormone (hGH) by linear PEG (or complexation of zinc) to protect the protein during *in situ* gelation and dramatically decrease the rate of protein release from PEG hydrogels.⁵⁰ Hennink and coworkers also confirmed the effect of protein precipitation by NaCl or concentrated dextran on prolonging the release of hGH from dextran hydrogel microspheres.⁶¹ Additionally, Herrmann *et al.* demonstrated that PEG-containing lipidic

implants significantly reduced the burst release of rh-interferon α -2a (IFN- α), due to the PEG-induced, reversible precipitation of protein.⁶² Similar to these reports, our results suggest that the precipitation and subsequent dissolution of PANG have contributed significantly to its prolonged release from the hydrogel network.

Altogether, our studies illustrate the facile use of hydrogel based methods to control the delivery of an antibody that is active for the neutralization of the LeTx of anthrax. The data presented here for PANG suggest more general applications for the controlled release of therapeutic proteins/antibodies by PEG-induced precipitation methods. Although the ability of PEG to precipitate proteins has been extensively studied and widely used in the field of protein separation and purification,^{44,45} only few studies have explored the precipitation of protein within PEG hydrogel-based controlled release systems and its potential benefit in controlling delivery profiles.^{50, 61-63} The *in situ*, reversible precipitation of the protein induced by PEG in this report may not only provide protein stabilization during the gelation process without the addition of any exogenous precipitants, but also offer a useful strategy to prevent burst release and prolong the release of protein over an extended period of time. Additionally, the in-gel characterization of the protein provides insight about the conformational properties of proteins during *in situ* gelation and encapsulation, potentially relevant to the clinical translation and approval of such protein delivery systems.

2.5 Conclusions

In this study, hydrolytically degradable PEG hydrogels have been synthesized and used as injectable local delivery materials for sustained release of the antibody PANG. The delivery properties of the hydrogels can be easily adjusted by varying the

chemical composition of the precursors. PANG was released from the hydrogel matrix in a controlled manner ranging from 14 to 56 days *in vitro*. Burst release of the antibody was prevented by PEG-induced protein precipitation. The secondary and tertiary structures of the hydrogel released antibodies as well as their biological activities were not affected by encapsulation and release from the hydrogel. These results suggest that the injectable PEG hydrogels, combined with PEG-induced protein precipitation, hold significant potential in the sustained and long-term delivery of therapeutic antibodies.

REFERENCES

1. Ross, J. M., The Pathogenesis of Anthrax Following the Administration of Spores by the Respiratory Route. *J Pathol Bacteriol* **1957**, 73, (2), 485-494.
2. Vanness, G. B., Ecology of Anthrax. *Science* **1971**, 172, (3990), 1303-1307.
3. Inglesby, T. V.; Henderson, D. A.; Bartlett, J. G.; Ascher, M. S.; Eitzen, E.; Friedlander, A. M.; Hauer, J.; McDade, J.; Osterholm, M. T.; O'Toole, T.; Parker, G.; Perl, T. M.; Russell, P. K.; Tonat, K.; Biodefense, W. G. C., Anthrax as a biological weapon - Medical and public health management. *Jama-J Am Med Assoc* **1999**, 281, (18), 1735-1745.
4. Jernigan, J. A.; Stephens, D. S.; Ashford, D. A.; Omenaca, C.; Topiel, M. S.; Galbraith, M.; Tapper, M.; Fisk, T. L.; Zaki, S.; Popovic, T.; Meyer, R. F.; Quinn, C. P.; Harper, S. A.; Fridkin, S. K.; Sejvar, J. J.; Shepard, C. W.; McConnell, M.; Guarner, J.; Shieh, W. J.; Malecki, J. M.; Gerberding, J. L.; Hughes, J. M.; Perkins, B. A.; Investigation, A. B., Bioterrorism-related inhalational anthrax: The first 10 cases reported in the United States. *Emerg Infect Dis* **2001**, 7, (6), 933-944.
5. Chen, Z. C.; Moayeri, M.; Purcell, R., Monoclonal Antibody Therapies against Anthrax. *Toxins* **2011**, 3, (8), 1004-1019.
6. Ding, G. P.; Chen, X. M.; Zhu, J.; Duesbery, N. S.; Cheng, X. J.; Cao, B. A., A Human/Murine Chimeric Fab Antibody Neutralizes Anthrax Lethal Toxin In Vitro. *Clin Dev Immunol* **2013**.
7. Park, J. W.; Smolen, J., Monoclonal antibody therapy. *Adv Protein Chem* **2001**, 56, 369-421.
8. Mohamed, N.; Clagett, M.; Li, J.; Jones, S.; Pincus, S.; D'Alia, G.; Nardone, L.; Babin, M.; Spitalny, G.; Casey, L., A high-affinity monoclonal antibody to anthrax protective antigen passively protects rabbits before and after aerosolized *Bacillus anthracis* spore challenge. *Infect Immun* **2005**, 73, (2), 795-802.
9. Peterson, J. W.; Comer, J. E.; Noffsinger, D. M.; Wenglikowski, A.; Walberg, K. G.; Chatuev, B. M.; Chopra, A. K.; Stanberry, L. R.; Kang, A. S.; Scholz, W. W.; Sircar, J., Human monoclonal anti-protective antigen antibody completely protects rabbits and is synergistic with ciprofloxacin in protecting mice and guinea pigs against inhalation anthrax. *Infect Immun* **2006**, 74, (2), 1016-1024.
10. Peterson, J. W.; Comer, J. E.; Baze, W. B.; Noffsinger, D. M.; Wenglikowski, A.; Walberg, K. G.; Hardcastle, J.; Pawlik, J.; Bush, K.; Taormina, J.; Moen, S.; Thomas, J.; Chatuev, B. M.; Sower, L.; Chopra, A. K.; Stanberry, L. R.; Sawada, R.; Schotz, W. W.; Sircar, J., Human monoclonal antibody AVP-21D9 to protective antigen reduces dissemination of the *Bacillus anthracis* ames strain from the lungs in a rabbit model. *Infect Immun* **2007**, 75, (7), 3414-3424.

11. Chichester, J. A.; Manceva, S. D.; Rhee, A.; Coffin, M. V.; Musiychuk, K.; Mett, V.; Shamloul, M.; Norikane, J.; Streatfield, S. J.; Yusibov, V., A plant-produced protective antigen vaccine confers protection in rabbits against a lethal aerosolized challenge with *Bacillus anthracis* Ames spores. *Hum Vacc Immunother* **2013**, 9, (3), 544-552.
12. Mett, V.; Chichester, J. A.; Stewart, M. L.; Musiychuk, K.; Bi, H.; Reifsnyder, C. J.; Hull, A. K.; Albrecht, M. T.; Goldman, S.; Baillie, L. W. J.; Yusibov, V., A non-glycosylated, plant-produced human monoclonal antibody against anthrax protective antigen protects mice and non-human primates from *B. anthracis* spore challenge. *Hum Vaccines* **2011**, 7, 183-190.
13. Daugherty, A. L.; Mrsny, R. J., Formulation and delivery issues for monoclonal antibody therapeutics. *Adv. Drug Deliver Rev.* **2006**, 58, (5-6), 686-706.
14. Szlachcic, A.; Zakrzewska, M.; Otlewski, J., Longer action means better drug: Tuning up protein therapeutics. *Biotechnol. Adv.* **2011**, 29, (4), 436-441.
15. Harris, J. M.; Chess, R. B., Effect of pegylation on pharmaceuticals. *Nat. Rev. Drug Discov.* **2003**, 2, (3), 214-221.
16. Tang, L.; Persky, A. M.; Hochhaus, G.; Meibohm, B., Pharmacokinetic aspects of biotechnology products. *J. Pharm. Sci.* **2004**, 93, (9), 2184-2204.
17. Li, Y. L.; Rodrigues, J.; Tomas, H., Injectable and biodegradable hydrogels: gelation, biodegradation and biomedical applications. *Chem. Soc. Rev.* **2012**, 41, (6), 2193-2221.
18. Lin, C.-C.; Anseth, K., PEG Hydrogels for the Controlled Release of Biomolecules in Regenerative Medicine. *Pharm. Res.* **2009**, 26, (3), 631-643.
19. Vermonden, T.; Censi, R.; Hennink, W. E., Hydrogels for Protein Delivery. *Chem. Rev.* **2012**, 112, (5), 2853-2888.
20. Censi, R.; Di Martino, P.; Vermonden, T.; Hennink, W. E., Hydrogels for protein delivery in tissue engineering. *J. Controlled Release* **2012**, 161, (2), 680-692.
21. Bhattarai, N.; Gunn, J.; Zhang, M., Chitosan-based hydrogels for controlled, localized drug delivery. *Adv. Drug Deliver Rev.* **2010**, 62, (1), 83-99.
22. Elbert, D. L.; Pratt, A. B.; Lutolf, M. P.; Halstenberg, S.; Hubbell, J. A., Protein delivery from materials formed by self-selective conjugate addition reactions. *J. Controlled Release* **2001**, 76, (1-2), 11-25.
23. Yamaguchi, N.; Zhang, L.; Chae, B. S.; Palla, C. S.; Furst, E. M.; Kiick, K. L., Growth factor mediated assembly of cell receptor-responsive hydrogels. *J. Am. Chem. Soc.* **2007**, 129, (11), 3040-3041.
24. Freudenberg, U.; Hermann, A.; Welzel, P. B.; Stirl, K.; Schwarz, S. C.; Grimmer, M.; Zieris, A.; Panyanuwat, W.; Zschoche, S.; Meinhold, D.; Storch, A.; Werner, C., A star-PEG-heparin hydrogel platform to aid cell replacement therapies for neurodegenerative diseases. *Biomaterials* **2009**, 30, (28), 5049-5060.
25. Kraehenbuehl, T. P.; Ferreira, L. S.; Zammaretti, P.; Hubbell, J. A.; Langer, R., Cell-responsive hydrogel for encapsulation of vascular cells. *Biomaterials* **2009**, 30, (26), 4318-4324.

26. Kharkar, P. M.; Kloxin, A. M.; Kiick, K. L., Dually degradable click hydrogels for controlled degradation and protein release. *J. Mater. Chem. B* **2014**, 2, (34), 5511-5521.
27. Sahoo, S.; Chung, C.; Khetan, S.; Burdick, J. A., Hydrolytically degradable hyaluronic acid hydrogels with controlled temporal structures. *Biomacromolecules* **2008**, 9, (4), 1088-1092.
28. Griffin, D. R.; Schlosser, J. L.; Lam, S. F.; Nguyen, T. H.; Maynard, H. D.; Kasko, A. M., Synthesis of Photodegradable Macromers for Conjugation and Release of Bioactive Molecules. *Biomacromolecules* **2013**, 14, (4), 1199-1207.
29. Licciardi, M.; Grassi, M.; Di Stefano, M.; Feruglio, L.; Giuliani, G.; Valenti, S.; Cappelli, A.; Giammona, G., PEG-benzofulvene copolymer hydrogels for antibody delivery. *Int. J. Pharm.* **2010**, 390, (2), 183-190.
30. Lee, A. L. Z.; Ng, V. W. L.; Gao, S. J.; Hedrick, J. L.; Yang, Y. Y., Injectable Hydrogels from Triblock Copolymers of Vitamin E- Functionalized Polycarbonate and Poly(ethylene glycol) for Subcutaneous Delivery of Antibodies for Cancer Therapy. *Adv. Funct. Mater.* **2014**, 24, (11), 1538-1550.
31. Hu, C. C.; Chaw, J. R.; Chen, C. F.; Liu, H. W., Controlled release bevacizumab in thermoresponsive hydrogel found to inhibit angiogenesis. *Bio-Med. Mater. Eng.* **2014**, 24, (6), 1941-1950.
32. Tian, W. M.; Zhang, C. L.; Hou, S. P.; Yu, X.; Cui, F. Z.; Xu, Q. Y.; Sheng, S. L.; Cui, H.; Li, H. D., Hyaluronic acid hydrogel as Nogo-66 receptor antibody delivery system for the repairing of injured rat brain: in vitro. *J. Controlled Release* **2005**, 102, (1), 13-22.
33. Guziewicz, N.; Best, A.; Perez-Ramirez, B.; Kaplan, D. L., Lyophilized silk fibroin hydrogels for the sustained local delivery of therapeutic monoclonal antibodies. *Biomaterials* **2011**, 32, (10), 2642-2650.
34. Koutsopoulos, S.; Zhang, S. G., Two-layered injectable self-assembling peptide scaffold hydrogels for long-term sustained release of human antibodies. *J. Controlled Release* **2012**, 160, (3), 451-458.
35. Hull, A. K.; Criscuolo, C. J.; Mett, V.; Groen, H.; Steeman, W.; Westra, H.; Chapman, G.; Legutki, B.; Baillie, L.; Yusibov, V., Human-derived, plant-produced monoclonal antibody for the treatment of anthrax. *Vaccine* **2005**, 23, (17-18), 2082-2086.
36. Mather, B. D.; Viswanathan, K.; Miller, K. M.; Long, T. E., Michael addition reactions in macromolecular design for emerging technologies. *Prog. Polym. Sci.* **2006**, 31, (5), 487-531.
37. Ghosh, K.; Shu, X. Z.; Mou, R.; Lombardi, J.; Prestwich, G. D.; Rafailovich, M. H.; Clark, R. A. F., Rheological characterization of in situ cross-linkable hyaluronan hydrogels. *Biomacromolecules* **2005**, 6, (5), 2857-2865.
38. Weber, L. M.; Lopez, C. G.; Anseth, K. S., Effects of PEG hydrogel crosslinking density on protein diffusion and encapsulated islet survival and function. *J. Biomed. Mater. Res. A* **2009**, 90A, (3), 720-729.

39. Metters, A.; Hubbell, J., Network Formation and Degradation Behavior of Hydrogels Formed by Michael-Type Addition Reactions. *Biomacromolecules* **2004**, *6*, (1), 290-301.
40. Zustiak, S. P.; Leach, J. B., Characterization of Protein Release From Hydrolytically Degradable Poly(Ethylene Glycol) Hydrogels. *Biotechnol. Bioeng.* **2011**, *108*, (1), 197-206.
41. Shih, H.; Lin, C.-C., Cross-Linking and Degradation of Step-Growth Hydrogels Formed by Thiol–Ene Photoclick Chemistry. *Biomacromolecules* **2012**, *13*, (7), 2003-2012.
42. Elliott, J. E.; Anseth, J. W.; Bowman, C. N., Kinetic modeling of the effect of solvent concentration on primary cyclization during polymerization of multifunctional monomers. *Chem. Eng. Sci.* **2001**, *56*, (10), 3173-3184.
43. Zustiak, S. P.; Leach, J. B., Hydrolytically Degradable Poly(Ethylene Glycol) Hydrogel Scaffolds with Tunable Degradation and Mechanical Properties. *Biomacromolecules* **2010**, *11*, (5), 1348-1357.
44. Annunziata, O.; Asherie, N.; Lomakin, A.; Pande, J.; Ogun, O.; Benedek, G. B., Effect of polyethylene glycol on the liquid-liquid phase transition in aqueous protein solutions. *P Natl Acad Sci USA* **2002**, *99*, (22), 14165-14170.
45. Wang, Y.; Lomakin, A.; Latypov, R. F.; Laubach, J. P.; Hideshima, T.; Richardson, P. G.; Munshi, N. C.; Anderson, K. C.; Benedek, G. B., Phase transitions in human IgG solutions. *J. Chem. Phys.* **2013**, *139*, (12).
46. Ellis, R. J., Macromolecular crowding: obvious but underappreciated. *Trends Biochem. Sci* **2001**, *26*, (10), 597-604.
47. Sharma, V. K.; Kalonia, D. S., Polyethylene glycol-induced precipitation of interferon alpha-2a followed by vacuum drying: Development of a novel process for obtaining a dry, stable powder. *Aaps Pharmsci* **2004**, *6*, (1).
48. Buwalda, S. J.; Dijkstra, P. J.; Feijen, J., In Situ Forming Poly(ethylene glycol)-Poly(L-lactide) Hydrogels via Michael Addition: Mechanical Properties, Degradation, and Protein Release. *Macromol. Chem. Phys.* **2012**, *213*, (7), 766-775.
49. Slaughter, B. V.; Khurshid, S. S.; Fisher, O. Z.; Khademhosseini, A.; Peppas, N. A., Hydrogels in Regenerative Medicine. *Adv. Mater.* **2009**, *21*, (32-33), 3307-3329.
50. van de Wetering, P.; Metters, A. T.; Schoenmakers, R. G.; Hubbell, J. A., Poly(ethylene glycol) hydrogels formed by conjugate addition with controllable swelling, degradation, and release of pharmaceutically active proteins. *J. Controlled Release* **2005**, *102*, (3), 619-627.
51. Bhat, R.; Timasheff, S. N., Steric Exclusion Is the Principal Source of the Preferential Hydration of Proteins in the Presence of Polyethylene Glycols. *Protein Sci.* **1992**, *1*, (9), 1133-1143.
52. Wang, Y.; Latypov, R. F.; Lomakin, A.; Meyer, J. A.; Kerwin, B. A.; Vunnum, S.; Benedek, G. B., Quantitative Evaluation of Colloidal Stability of Antibody Solutions using PEG-Induced Liquid-Liquid Phase Separation. *Mol. Pharmaceut.* **2014**, *11*, (5), 1391-1402.

53. Liu, H.; Gaza-Bulseco, G.; Chumsae, C.; Newby-Kew, A., Characterization of lower molecular weight artifact bands of recombinant monoclonal IgG1 antibodies on non-reducing SDS-PAGE. *Biotechnol. Lett* **2007**, 29, (11), 1611-1622.
54. Taylor, F. R.; Prentice, H. L.; Garber, E. A.; Fajardo, H. A.; Vasilyeva, E.; Blake Pepinsky, R., Suppression of sodium dodecyl sulfate–polyacrylamide gel electrophoresis sample preparation artifacts for analysis of IgG4 half-antibody. *Anal. Biochem.* **2006**, 353, (2), 204-208.
55. Zhu, Z. C.; Chen, Y.; Ackerman, M. S.; Wang, B.; Wu, W.; Li, B.; Obenauer-Kutner, L.; Zhao, R.; Tao, L.; Ihnat, P. M.; Liu, J.; Gandhi, R. B.; Qiu, B., Investigation of monoclonal antibody fragmentation artifacts in non-reducing SDS-PAGE. *J. Pharm. Biomed. Anal.* **2013**, 83, (0), 89-95.
56. Greenfield, N. J., Using circular dichroism spectra to estimate protein secondary structure. *Nat. Protocols* **2007**, 1, (6), 2876-2890.
57. Koutsopoulos, S.; Unsworth, L. D.; Nagaia, Y.; Zhang, S. G., Controlled release of functional proteins through designer self-assembling peptide nanofiber hydrogel scaffold. *P Natl Acad Sci USA* **2009**, 106, (12), 4623-4628.
58. Varlan, A.; Hillebrand, M., Bovine and Human Serum Albumin Interactions with 3-Carboxyphenoxathiin Studied by Fluorescence and Circular Dichroism Spectroscopy. *Molecules* **2010**, 15, (6), 3905-3919.
59. van Dijk-Wolthuis, W. N. E.; Hoogeboom, J. A. M.; van Steenbergen, M. J.; Tsang, S. K. Y.; Hennink, W. E., Degradation and Release Behavior of Dextran-Based Hydrogels. *Macromolecules* **1997**, 30, (16), 4639-4645.
60. Huang, X.; Brazel, C. S., On the importance and mechanisms of burst release in matrix-controlled drug delivery systems. *J. Controlled Release* **2001**, 73, (2–3), 121-136.
61. Vlugt-Wensink, K. D. F.; Meijer, Y. J.; van Steenbergen, M. J.; Verrijk, R.; Jiskoot, W.; Crommelin, D. J. A.; Hennink, W. E., Effect of excipients on the encapsulation efficiency and release of human growth hormone from dextran microspheres. *Eur J Pharm Biopharm* **2007**, 67, (3), 589-596.
62. Herrmann, S.; Mohl, S.; Siepmann, F.; Siepmann, J.; Winter, G., New insight into the role of polyethylene glycol acting as protein release modifier in lipidic implants. *Pharm. Res.* **2007**, 24, (8), 1527-1537.
63. Johnson, O. L.; Cleland, J. L.; Lee, H. J.; Charnis, M.; Duenas, E.; Jaworowicz, W.; Shepard, D.; Shahzamani, A.; Jones, A. J. S.; Putney, S. D., A month-long effect from a single injection of microencapsulated human growth hormone. *Nat. Med.* **1996**, 2, (7), 795-799.

Chapter 3

LIPOSOME-CROSSLINKED HYBRID HYDROGELS FOR GLUTATHIONE-TRIGGERED DELIVERY OF MULTIPLE CARGO MOLECULES

3.1 Introduction

Advances in nanotechnology have contributed significantly to the development of novel nanoscale carriers in the field of drug delivery.¹⁻⁵ A wide variety of nanoparticles has been developed over the past few decades, including inorganic nanoparticles,⁶⁻⁸ liposomes,⁹⁻¹¹ polymeric micelles,¹²⁻¹⁴ and nanogels.¹⁵⁻¹⁷ These nanoparticles are of appropriate size (10–150 nm) both to penetrate vessels and accumulate in specific tissues (e.g., tumors) and also for their surfaces to be functionalized with specific ligands for targeting effects, providing a promising platform for drug delivery with enhanced therapeutic efficacy.¹⁸⁻²⁰ In particular, various liposomal formulations including both classical and stealth liposomes have been widely used in pre-clinical and clinical studies, with a number of drug-encapsulated liposomal products such as AmBisome[®] and Doxil[®] on the market and many more under clinical development.^{21, 22} Parallel to the development of nanotechnology approaches in drug delivery, hydrogels have also been a focus of continued study as an important class of materials for the delivery of a variety of bioactive molecules including nutrients, drugs, and proteins.²³⁻²⁵ Composed of hydrophilic three-dimensional polymer networks, hydrogels have several advantageous properties including high water content, tunable viscoelasticity, and biocompatibility, which allow bioactive molecules to be protected against degradation and released from the hydrogel matrix in a controlled manner over

an extended period of time.^{26,27} Among various kinds of polymeric hydrogels, hydrogels synthesized from polyethylene glycol (PEG), an FDA-approved polymer, have been extensively studied in the field of drug delivery and tissue engineering with encouraging pre-clinical and clinical results.^{26, 28, 29} Additionally, several PEG hydrogel-based medical devices composed of reactive PEG polymers including thiol-modified PEG and acrylate-modified PEG have received approval for use as sealants (CoSeal™)³⁰ and wound healing matrices (Premvia™).³¹

In recent years, there has been an increasing interest in the incorporation of nanoparticles into hydrogels for improved therapeutic efficacy.³²⁻³⁴ Such hybrid systems not only preserve the structural integrity and functionalities of the incorporated nanoparticles, but also combine the advantageous properties of two distinct drug delivery platforms, offering unique benefits such as improved tissue localization, minimized burst release, and controlled sequential delivery. A common approach for the preparation of these hybrid hydrogels is to trigger gelation of hydrogel-forming monomer solutions in nanoparticle suspensions. Varieties of nanoparticles including metallic nanoparticles,³⁵ carbon-based nanomaterials³⁶ and polymeric nanoparticles³⁷ have been physically embedded within the hydrogel network to create reinforced polymeric hydrogels, developing nanocomposites with tailored physical properties and custom-made functionalities. Particularly, owing to their well-known advantages in drug delivery,³⁸ drug-loaded liposomes and modified liposome nanoparticles have been incorporated into a wide range of hydrogels based on synthetic polymers,^{39, 40} natural polymers,^{41, 42} and peptides^{43, 44} to provide prolonged release of the therapeutic molecules and significantly enhance therapeutic efficacy. Nevertheless, in these above cases, there is no specific interaction between the polymer matrix and the nanoparticle.

More recently, other strategies involving the use of nanoparticles as crosslinkers for hydrogel formation have been exploited,⁴⁵⁻⁴⁸ introducing additional engineering flexibility and structural diversity to these hybrid systems. For example, hydrophobic interactions between polymers and nanoparticles have been utilized to engineer self-assembled hydrogels with shear-thinning and self-healing properties. Raghavan and co-workers⁴⁹⁻⁵¹ developed a series of injectable hybrid hydrogels based on the interactions between hydrophobically modified chitosan and various bilayer-structured building blocks (liposomes, vesicles, and cells). The hydrophobes from chitosan embedded in the hydrophobic interiors of the vesicle/cell bilayer membranes, forming hydrogels with shear-thinning behavior. Similarly, Langer and co-workers⁵² designed shear-thinning injectable hydrogels via the polymer-nanoparticle interactions between hydrophobically modified cellulose derivatives and hydrophobic nanoparticle surfaces. Additionally, polymer-nanoparticle hybrid hydrogels have also been fabricated via the covalent interactions between polymer chains and nanoparticle surfaces. Akiyoshi and co-workers^{53, 54} reported biodegradable hybrid hydrogels based on the Michael-type addition between thiolated 4-arm polyethylene glycol (PEG) and acryloyl-modified pullulan nanogels. The PEG polymer chains covalently crosslinked the pullulan nanogels into a three-dimensional crosslinked network, with the nanogels serving as structural components. These multicomponent hybrid hydrogels offer great opportunities for the sequential delivery of multiple drugs/growth factors, which improves therapeutic efficacy by synergistic effects that aid in overcoming drug resistance in cancer therapy^{11, 55-58} and better mimic the temporal profile of the healing process *in vivo* in tissue regeneration.^{59, 60} Despite the promise of these methods,

nanoparticle-crosslinked hydrogels with chemo-responsiveness that is based on specific polymer-nanoparticle interactions have not been widely developed.^{48, 61}

Inspired by these elegant approaches, we report an advanced, responsive drug delivery system that integrates liposome nanoparticles and PEG polymers into a unifying hydrogel construct for the controlled sequential delivery of multiple therapeutic molecules. Specifically, we have developed glutathione-sensitive, liposome-crosslinked hybrid hydrogels based on the reversible Michael-type addition between arylthiol-functionalized 4-arm PEG and maleimide-functionalized liposomes. The successful formation of the liposomes and liposome-crosslinked hydrogels was confirmed via dynamic light scattering and oscillatory rheology. Mass loss and *in vitro* drug delivery experiments also confirmed that the selective capacity of certain thioether succinimides to undergo retro-Michael reaction and thiol exchanges⁶²⁻⁶⁵ serves as the basis of crosslink scission between the PEG polymers and liposomes in thiol-containing microenvironments, resulting in matrix degradation and subsequent release of therapeutic molecules. The hierarchical structure of the gel enables dual encapsulation and differential release of multiple therapeutic cargos from one robust hybrid system with unique physical and chemical properties that are absent in the individual building blocks.

3.2 Materials and Methods

3.2.1 Materials

Four-arm, alkylthiol-functionalized PEG (PEG-SH, M_n 20,000 g/mol) and four-arm, hydroxyl-functionalized PEG (M_n 20,000 g/mol) were purchased from JenKem

Technology USA Inc. (Allen, TX, USA). All lipids were purchased from Avanti Polar Lipids (Alabaster, AL, USA), including: 1,2-dioleoyl-*sn*-glycero-3-phosphocholine (DOPC), anionic 1,2-dioleoyl-*sn*-glycero-3-phospho-(1'-*rac*-glycerol) (DOPG), the anionic maleimide-functionalized lipid 1,2-dioleoyl-*sn*-glycero-3-phosphoethanolamine-N-[4-(*p*-maleimidophenyl) butyramide (MPB-PE), and the fluorescent labeled lipid 1-Oleoyl-2-[12-[(7-nitro-2-1,3-benzoxadiazol-4-yl)amino]dodecanoyl]-*sn*-Glycero-3-Phosphocholine (NBD-PC). 4-mercaptophenylpropionic acid (4-mercaptohydrocinnamic acid) was purchased from TCI America (Portland, OR, USA). Doxorubicin hydrochloride (DOX) was purchased from Alfa Aesar (Ward Hill, MA, USA). Glutathione (GSH) and cytochrome *c* from equine heart were purchased from Sigma-Aldrich (Saint Louis, MO, USA). All other reagents and materials were purchased from Fisher Scientific (Pittsburgh, PA, USA) unless otherwise noted. ¹H NMR spectra were acquired under standard quantitative conditions at ambient temperature on a Bruker AV400 NMR spectrometer (Billerica, MA, USA). All samples were dissolved in CDCl₃ (D, 99.8%) +0.05% V/V TMS.

3.2.2 Synthesis of Arylthiol End-Functionalized 4-Arm PEG

The synthesis of arylthiolated four-arm PEG was performed by modifying PEG with 4-mercaptohydrocinnamic acid based on a modified protocol from previous reports.⁶³ Briefly, 20K 4-arm PEG (2g, 0.4 mmol OH groups), 4-mercaptophenylpropionic acid (0.36g, 2mmol), *p*-toluenesulfonic acid (*p*-TSA, 27.55mg, 0.16 mmol) and DTT (30.8 mg, 0.2 mmol) were dissolved in toluene (30mL). The reaction mixture was refluxed at 155°C with stirring for 48h. Water was collected by using a Dean Stark trap. The reaction mixture was precipitated in cold ether and white polymer powder was collected after filtration. The polymer product was stored

under N₂ at -20°C for future use. ¹H NMR (400 MHz, CDCl₃): δ 7.22 (d, 2H), 7.10 (d, 2H), 4.27 – 4.21 (m, 2H), 3.67 (s, 449H), 2.92 (t, 2H), 2.65 (t, 2H).

3.2.3 Preparation of Maleimide-Functionalized Liposomes

The liposomes were prepared based on the conventional dehydration-rehydration method as previously reported.⁹⁻¹¹ 10 μmol of lipids in chloroform (a lipid composition of DOPC:DOPG:MPB = 4:1:5 molar ratio was typically used), were dispensed into small round bottom flasks, and the organic solvents were evaporated under nitrogen overnight to prepare dried thin lipid films. The lipid films were rehydrated at room temperature in 1 mL 0.2M bis-tris buffer at pH 7.0 for 1 h with rigorous vortexing for 30 s every 5 min, and then sonicated in alternating power cycles of 8% amplitude (~30W) in 30 s intervals for 5 min on ice. The resulting liposomes were extruded 21 times through a 0.2 μm polycarbonate membrane (Whatman, Piscataway, NJ, USA) using an Avanti Mini-Extruder (Avanti Polar Lipids Inc., Alabaster, AL, USA). The liposome solutions were freshly made and used shortly after preparation to avoid the ring-opening (hydrolysis) reactions of the maleimide moieties, which might prevent them from further reactions.⁶⁶ The average size of the monodisperse liposomes was analyzed via dynamic light scattering (DLS) at 25°C on a Malvern Zetasizer Nano ZS apparatus with Malvern Instruments DTS software (v.6.01) using the cumulants fit (Malvern Instruments, Malvern, Worcestershire, UK).

3.2.4 Preparation of Liposome-Crosslinked Hybrid Hydrogels

The liposomal hybrid hydrogels were prepared by Michael-type addition between arylthiol end-functionalized 4-arm PEG and the maleimide-functionalized liposomes. Briefly, 20K 4-arm PEG arylthiol was dissolved directly in 10 mM liposome

solutions (50 μ L, in 0.2M bis-tris buffer at pH 7.0) at room temperature and the mixture was vortexed for approximately 30 s to completely dissolve the solid polymers. The mixture was then purged with nitrogen and incubated quiescently at 37°C overnight to achieve complete crosslinking, although rheological experiments (below) confirm that gelation occurs within several minutes. The molar ratios of the maleimide groups from liposomes to the –SH groups from PEG were approximately 1:1, 1:2, and 1:4, which was altered by altering the amount of PEG-SH precursors added during preparation (3wt%, 6wt%, and 12wt% respectively). Thiol-insensitive hybrid hydrogels (control) were prepared by using 20K 4-arm, alkylthiol-functionalized PEG based on the same procedure. Detailed chemical structures of these thiolated PEG polymer precursors are included in Scheme 1. A PEG hydrogel-only control (without liposomes) was also prepared by dissolving 20K 4-arm PEG arylthiol and 10K 4-arm PEG maleimide in PBS separately and then mixing the two precursor solutions together.

3.2.5 Rheological Studies

Oscillatory rheological characterization of the hybrid hydrogels was performed on a stress-controlled AR-G2 rheometer (TA Instruments, New Castle, DE, USA) equipped with a Peltier plate. *In situ* gelation experiments were conducted at 37°C using a 20 mm-diameter, 1° cone and plate geometry with a 25 μ m gap distance, with oscillatory time, frequency, and strain sweeps performed. Strain sweeps were performed on samples from 0.1% to a maximum strain of 1000% to determine the limit of the linear viscoelastic region. Dynamic oscillatory time sweeps were performed to monitor the *in situ* gelation and mechanical properties of different hybrid hydrogel compositions at angular frequencies of 6 rad/s and 1% strain amplitude chosen from the linear viscoelastic region. Dynamic oscillatory frequency sweeps were conducted from 0.1 to

100 rad/s at 1% strain amplitude. Thiolated PEG polymer precursors were dissolved in the liposome suspension (~40 μ L). The mixture was then quickly vortexed and loaded onto the rheometer stage.

The results for PEG alkylthiol hydrogels instead of PEG arylthiol are shown for these *in situ* rheological experiments as the arylthiol-based hydrogels showed frequency-responsive behaviors (likely resulting from the hydrophobic interaction between the aromatic moieties of PEG arylthiol and lipid bilayers) that complicated comparisons. For experiments to confirm the role of the liposomes in the mechanical integrity of the hydrogels, the hybrid hydrogels (~65 μ L) were formed in a 3mL syringe prior to loading onto the rheometer stage, and then incubated *in situ* with 10% Triton™ X-100 in water at 37°C. Dynamic oscillatory time sweeps were conducted at angular frequencies of 6 rad/s and 1% strain amplitude using an 8 mm-diameter, parallel plate geometry with a 200 μ m gap distance to monitor the changes in storage modulus when the hydrogels were immersed in 10% Triton™ X-100.

3.2.6 Scanning Electron Microscopy

The liposome-crosslinked hybrid hydrogels (~25 μ L) were dehydrated in a series of ethanol/water solutions (1 mL) progressing from 30% ethanol to 50%, and 70% for 4h respectively, and eventually to 100% ethanol for 12h at room temperature. The dehydrated gels were dried at the critical point of CO₂ for 1 h using an Autosamdri-815B critical point dryer (Tousimis, Rockville, MD, USA). Samples were sputter coated with a thin layer of gold-palladium to provide a more conductive surface and imaged using scanning electron microscopy (SEM) at an accelerating voltage of 3.0 kV (Zeiss Auriga 60, Oberkochen, Germany).

3.2.7 Fluorescent Labeling and Confocal Microscopy

Fluorescent labeled liposomes were prepared as described above by incorporating 0.5% (molar ratio) of the fluorescent labeled lipid NBD-PC during the lipid thin film formation process (total lipid composition NBD-PC:DOPC:DOPG:MPB = 0.05:3.95:1:5 molar ratio). The liposome-crosslinked hydrogels were formed using the resulting fluorescent liposome solutions in a 35 mm MatTek (Ashland, MA, USA) cell culture dishes ((7 mm glass bottom) and incubated overnight at 37°C with 85% humidity. The hydrogels were washed three times with PBS and then immersed in PBS for confocal imaging using a Zeiss 710 Confocal Microscope (Oberkochen, Germany) at 488nm. For confocal imaging of NBD-labeled liposomes, fluorescently labeled hydrogels were formed as mentioned above and incubated in 10 mM GSH at 37°C to triggered degradation. Gel supernatant was collected at day 6 and used for imaging. The NBD-labeled liposome stock solutions were diluted 10 times and used as a control. Samples were transferred to an 8-Chamber Lab-Tek Coverglass (Rochester, NY, USA) and imaged on a Zeiss 710 Confocal Microscope.

3.2.8 Mass Loss Studies

Hydrogel samples were formed as described above by directly dissolving PEG-SH polymers (~3 mg) in liposome suspensions (~50 μ L, in 0.2M bis-tris buffer at pH 7.0) in 1.5 mL Eppendorf tubes and then incubating the mixture at 37°C overnight. After being placed in phosphate buffer saline (PBS) for 24h to achieve equilibrium swelling, the hydrogel samples were immersed in 1mL 10 mM GSH solutions in PBS, or PBS alone, at 37°C. At predetermined time points (every 48 h for the first 4 days and every 24 h after that until day 7), the mass of hydrogels after incubation was measured after

blotting off excess water. The percentage of mass remaining from a hydrogel sample was calculated as $\frac{\text{mass after incubation}}{\text{swollen mass}} \times 100\%$.

3.2.9 *In Vitro* DOX Encapsulation and Release

To prepare DOX-loaded liposomes, doxorubicin hydrochloride (DOX) was dissolved in a minimum amount of DMSO (ca. 10% of the total volume of liposome solutions, which were approximately 1mL in volume) and added dropwise to the liposome suspensions (in 0.2M bis-tris buffer at pH 7.0) while stirring, at a drug-to-lipid ratio of approximately 1:3. The mixture was stirred overnight at room temperature. The resulting DOX-loaded liposomes (usually in ~150 μ L aliquots for each experiment), were used without further purification due to the small volume of the samples and the limited amount of unencapsulated DOX present (which was confirmed in DOX release experiments, see below). The encapsulation efficiency of DOX was indicated to be approximately 92%, and was determined by washing the DOX-loaded liposomes three times with PBS and then extracting the encapsulated DOX with 10% Triton™ X-100 treatment. A calibration curve for DOX was developed by measuring the fluorescence intensity of DOX solutions at a concentration range of 0.25-10 μ g/mL (excitation 485 nm, emission 590 nm) using a Perkin Elmer Fusion microplate reader (Waltham, MA, USA).

DOX-loaded liposome-crosslinked hydrogels were prepared by dissolving either the aryl or alkylthiolated PEG polymers in DOX-loaded liposome suspensions. The resulting hydrogels (~50 μ L) were then directly immersed in 1mL 10 mM GSH in PBS solutions or PBS alone at 37°C. A volume of 0.5 mL of the supernatant was removed and replenished every day, and the release of DOX was monitored by

measuring the fluorescence intensity (excitation 485 nm, emission 590 nm) of the removed buffer as described above.

3.2.10 Co-Delivery of DOX and Cytochrome c *In Vitro*

DOX-loaded liposomes were prepared as described above, and the liposome suspensions (in 0.2M bis-tris buffer at pH 7.0) were used to prepare hybrid hydrogels at 37°C as above except with cytochrome c dissolved along with the arylthiol PEG polymers (potential side reactions including disulfide exchange between the protein and polymers are slow and thus expected to be insignificant within the timescale of the rapid crosslinking reaction),⁶⁷ with a total of 1 mg cytochrome c in 50 µL of hydrogel to ensure detection upon release and to measure release at a high concentration gradient. The hydrogels were placed in 1.5 mL Eppendorf tubes and 10 mM GSH in PBS (1 mL) was added to immerse the hydrogels. The hydrogels were incubated at 37°C, and 0.5 mL of the supernatant was removed and replaced with fresh buffer every 24h. The amount of cytochrome c was determined using a Pierce™ Microplate BCA Protein Assay Kit - Reducing Agent Compatible (Thermo Scientific, Rockford, IL, USA). The amount of DOX released was measured by fluorescence intensity using a microplate reader.

3.2.11 Data Fitting of the Release Profiles of DOX and Cytochrome c

The release constant k of DOX from the aryl lipogel in 10 mM GSH was calculated based on the linear fitting of the release data based on the Ritger–Peppas equation:

$$\frac{M_t}{M_\infty} = kt^n, \text{ where } n=1 \text{ for zero-order release. (3.1)}$$

The release constant k of DOX from the lipogels with first order release (lacking network degradation) was calculated based on the early-time approximation of Fickian diffusion (Higuchi model, $0 \leq \frac{M_t}{M_\infty} \leq 0.6$):

$$\frac{M_t}{M_\infty} = 4 \left(\frac{Dt}{\pi h^2} \right)^{1/2}, k = 4 \left(\frac{D}{\pi h^2} \right)^{1/2}; \quad (3.2)$$

The release constant k of cytochrome c was calculated based on the late-time approximation of Fickian diffusion ($0.4 \leq \frac{M_t}{M_\infty} \leq 1$):

$$\frac{M_t}{M_\infty} = 1 - \left(\frac{8}{\pi^2} \right) \exp[(-\pi^2 Dt)/h^2], k = (-\pi^2 D)/h^2; \quad (3.3)$$

M_t is the amount of drug released at time t , M_∞ is the total mass of drug loaded into the hydrogel, D is the diffusion coefficient of the drug within the polymer matrix, π is 3.14, and h is the thickness of the hydrogel.

3.2.12 Data Analysis

Statistical analysis was performed using a two-tailed Student's t -test. A p value of <0.05 was considered to be statistically different.

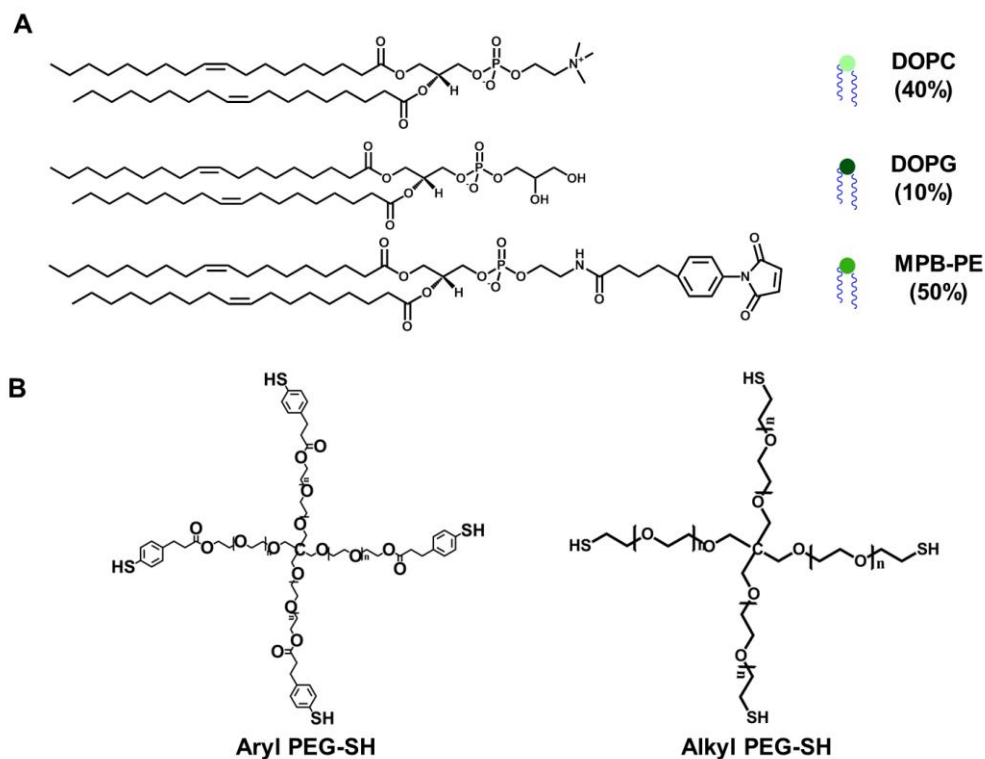


Figure 3.1 Chemical structures of the lipids used for liposome formulation (A) and the PEG-SH polymers employed for hybrid hydrogel formation (B). DOPC: 1,2-dioleoyl-sn-glycero-3-phosphocholine; DOPG: 1,2-dioleoyl-sn-glycero-3-phospho-(1'-rac-glycerol); MPB-PE: 1,2-dioleoyl-sn-glycero-3-phosphoethanolamine-N-[4-(p-maleimidophenyl) butyramide].

3.3 Results and Discussion

3.3.1 Hydrogel Design

Maleimide-functionalized liposomes (10 mM, $D_H \sim 100\text{nm}$ according to DLS measurements) were prepared by the conventional hydration of dried lipid thin films (the total lipids comprised 50% by mole of a maleimide-functionalized lipid, MPB-PE, as well as 40% DOPC and 10% DOPG, Figure 3.1A). Previous work reported by our group demonstrates that arylthiol-maleimide adducts and hydrogels (owing to the low

pK_a of the aryl thiol) can undergo a retro Michael-type reaction and thiol-exchange in the presence of thiol-containing molecules (which leads to crosslink scission in the case of hydrogels), while alkylthiol-maleimide adducts and hydrogels exhibit limited activity in the retro reaction under the same conditions.⁶²⁻⁶⁵ More detailed investigations of the reactivity of various thiol compounds in retro Michael-type reaction and thiol-exchange are underway and will be the subject of future reports. Therefore, 4-arm PEG polymers functionalized with arylthiols (GSH-sensitive) or alkylthiols (GSH-insensitive) were utilized during hydrogel formation to selectively control network degradation (Figure 3.1B).

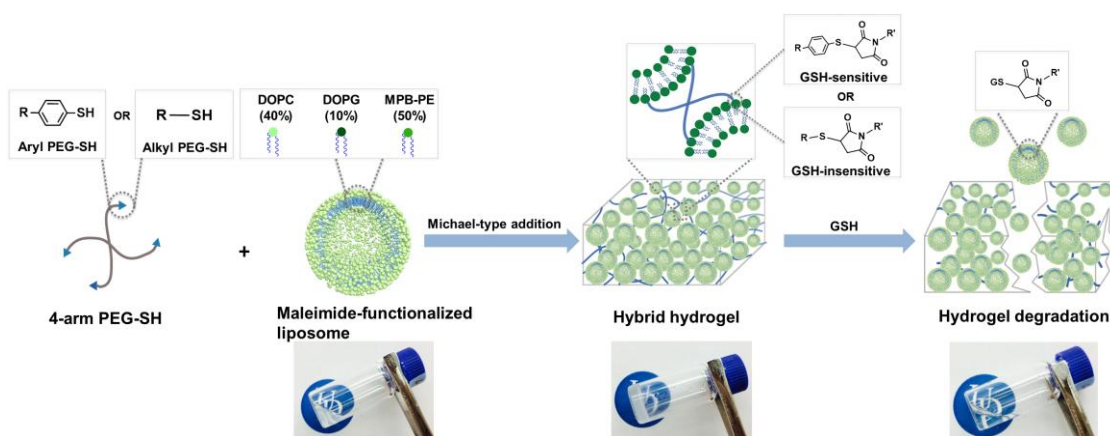


Figure 3.2 Schematic representation of the formation and degradation of the liposome-crosslinked hybrid hydrogels. The UD logos are used with permission from the University of Delaware.

The liposome-crosslinked hybrid hydrogels (lipogels) were prepared subsequently by thiol-maleimide Michael-type addition between the thiol groups of the PEG polymers and the maleimide groups on the liposome surface, where the liposomes

serve as structural elements (crosslinks) within the polymer gel network (Figure 3.2). As shown in the images, mixtures of solutions of the liposomes and thiol-functionalized PEG formed self-supporting hydrogels. Although it is possible that the 4-arm PEG-SH would also form disulfide-based crosslinks, the reaction kinetics of thiol oxidation (ca. $15.2 \text{ M}^{-1} \text{ s}^{-1}$)⁶⁸ are several orders of magnitude slower than those of the Michael-type additions (ca. $1.3 \times 10^3 \text{ M}^{-1} \text{ s}^{-1}$),⁶⁹ so significant amounts of crosslinking due to disulfide bond formation were not expected. A key feature of the hydrogel design is that the thioether succinimide crosslinks formed by the reaction of arylthiol moieties and maleimide groups are degradable via a thiol-exchange reaction (enabled by retro-Michael-type addition reaction) in the presence of glutathione,⁶²⁻⁶⁵ which results in the degradation of the hydrogel to yield a viscous liquid (Figure 3.2). We postulated that this would result in the release of the liposomes along with any encapsulated molecules in the hydrogels. These hydrogel compositions should therefore permit the triggered release of multiple compounds via passive diffusion from the hydrogel network and/or via thiol-triggered release of drug-containing liposomes.

3.3.2 Rheological Characterization

The ability of the maleimide-functionalized liposomes to form a percolated hydrogel network upon reaction with thiol-functionalized PEG was confirmed in a series of rheological experiments. Initial observations indicated that hydrogel formation required the presence of both maleimide-functionalized liposomes and 4-arm PEG-SH; the liposome and PEG polymer solutions alone remained low-viscosity liquids over the timescales at which gelation occurred (Figure 3.2). Oscillatory time sweep and frequency sweep measurements were also performed to quantitatively monitor the *in situ* gelation and examine the stability of the three-dimensional crosslinked networks.

Oscillatory frequency sweeps of the arylthiol-based hybrid hydrogels indicated the frequency dependence of both moduli, suggesting contributions from hydrophobic interactions between the liposomes and the PEG-arylthiol polymers (data not shown),^{49, 50} which complicated comparisons of mechanical properties between hydrogels of different polymer compositions. Therefore, *in situ* rheological results of the alkylthiol-based hydrogels are shown to simplify these comparisons.

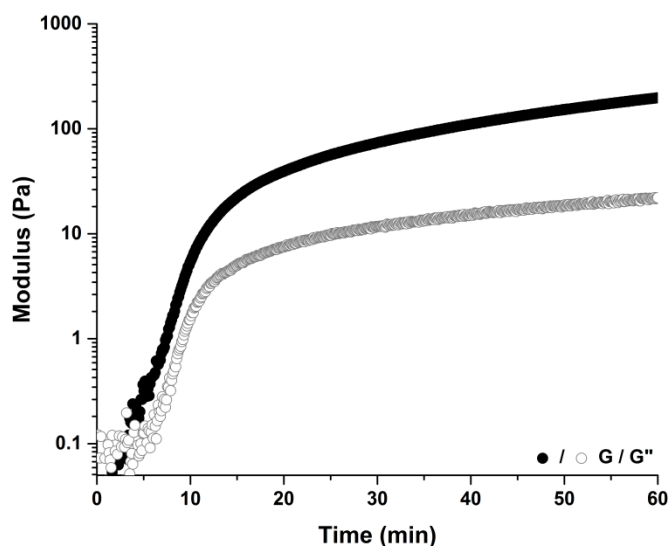


Figure 3.3 Representative oscillatory time sweep of the liposome-crosslinked hydrogels (1:2 Mal:SH ratio) in pH=7.0 bis-tris buffer at 37°C.

Rapid gelation of the materials (indicated here by the crossover point where G' (~0.40 Pa) becomes larger than G'' (~0.14 Pa), Figure 3.3) usually occurred within 5 minutes which, owing to the rapid kinetics, excludes the possibility of gelation based on disulfide bonds and suggests that hydrogel formation is driven mainly by thiol-

maleimide Michael-type addition reactions. Compared to other thiol-maleimide hydrogel systems,^{63, 64, 70, 71} the gelation kinetics observed from the hybrid hydrogels were not as rapid, possibly due to steric hindrance and limited chemical accessibility of the maleimide groups on the liposome surface. The hydrogels were subsequently cured for 7 hours to achieve maximum crosslinking. To further confirm that there was not significant crosslinking based on disulfide bonds, oscillatory time sweep experiments were performed on hydrogels comprising only 4-arm alkyl PEG-SH, where the lack of a significant increase in storage modulus suggested that disulfide crosslinking did not contribute significantly to the mechanical properties of the hydrogels (data not shown).

Confirmation of the impact of the thiol-maleimide reaction on hydrogel properties was assessed by changing the ratio of maleimide groups (Mal) on the liposome surface to thiol groups (SH) on the PEG polymer strands. Initial experiments in which the liposome concentration was varied from 0.5mM to 10 mM indicated that stable hydrogels could be formed reproducibly with liposome concentrations of at least 10 mM (data not shown). Owing to the ease with which the maleimide:thiol ratio could be reproducibly changed by varying thiol content (rather than by altering the amount of maleimide in the liposomes), liposome-containing precursor solutions were mixed with increasing fractions of alkylthiol PEG polymers (10 mM liposome solutions were mixed with 3wt%, 6wt%, and 12wt% PEG, corresponding to Mal:SH ratios of 1:1, 1:2 and 1:4 respectively).

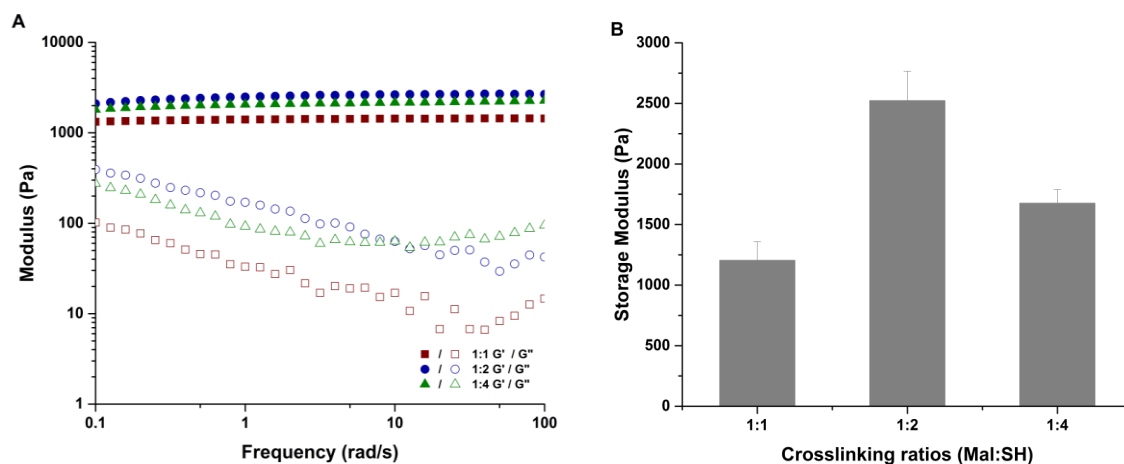


Figure 3.4 Rheological characterization of liposome-crosslinked hybrid hydrogels at various crosslinking ratios (1:1, 1:2, and 1:4 Mal:SH ratios). A) Oscillatory frequency sweep of the hydrogels from 0.1 to 100 rad/s at 1% strain amplitude. B) Summary of storage moduli (G') of hydrogels prepared at different crosslinking ratios.

The storage and loss moduli (G' and G'' , respectively) of these hydrogels were measured as a function of frequency; representative data are presented in Figure 3.4A. The frequency independence of G' indicated the formation of a stable, crosslinked network with G' dominating in the entire frequency range of 0.1-100 rad/s. The data in Figure 3.4B more clearly highlight that the storage moduli of the liposome-crosslinked hydrogels increased from 1200 Pa to 2500 Pa when the crosslinking ratios were varied from 1:1 (Mal:SH) to 1:2 (Mal:SH), a result in part due to the higher polymer concentration but also likely due to a reduction in the number of elastically inactive loops and unreacted chain ends when the stoichiometric ratio is 1:2. Other reports have shown that a 1:1 stoichiometric ratio rarely results in the highest storage modulus, owing to a reduced mobility of the crosslinker chains with increasing gel viscosity, which leads

to incomplete reaction.⁷²⁻⁷⁴ However, when the amount of thiol was further increased (1:4 Mal:SH), the storage modulus of the hydrogels decreased to 1600 Pa despite the high concentration of polymer. The low degree of crosslinking at higher polymer concentration likely results both from steric hindrance and consumption of functional groups on the liposomes, thus reducing the extent of polymer bridging between liposomes.⁵² Owing to the more efficient crosslinking in the 1:2 Mal:SH hydrogel, this composition was employed in all further studies of the hydrogels. Taken together, these rheological results illustrate the relatively rapid formation of a stable, viscoelastic hydrogel network, indicative of network crosslinking based on the Michael-type addition (ca. $1.3 \times 10^3 \text{ M}^{-1} \text{ s}^{-1}$)⁶⁹ rather than disulfide formation (ca. $15.2 \text{ M}^{-1} \text{ s}^{-1}$).⁶⁸ Given the rapid gelation, mild preparation conditions, and biocompatibility of the thiol-maleimide crosslinking chemistry demonstrated by others in cell encapsulation⁷⁵⁻⁷⁷ and *in vivo* delivery,⁷¹ these hydrogels have significant potential for minimally invasive, direct injection applications.

3.3.3 Morphology of the Liposome-Crosslinked Hydrogels

To visualize the liposomes in the hydrogel matrix, scanning electron microscopy (SEM) was performed on the hybrid hydrogels after critical point drying. The representative SEM images in Figure 3.5 show that liposomes with a diameter of $105 \pm 25 \text{ nm}$ (calculated from analysis via ImageJ of over 200 particles and consistent with DLS characterization of liposomes liberated from the hydrogel (below)) are well distributed on the hydrogel surface; the apparently low number of liposomes detectable in these images is a result of the evaluation of strictly the surface of the hydrogels.

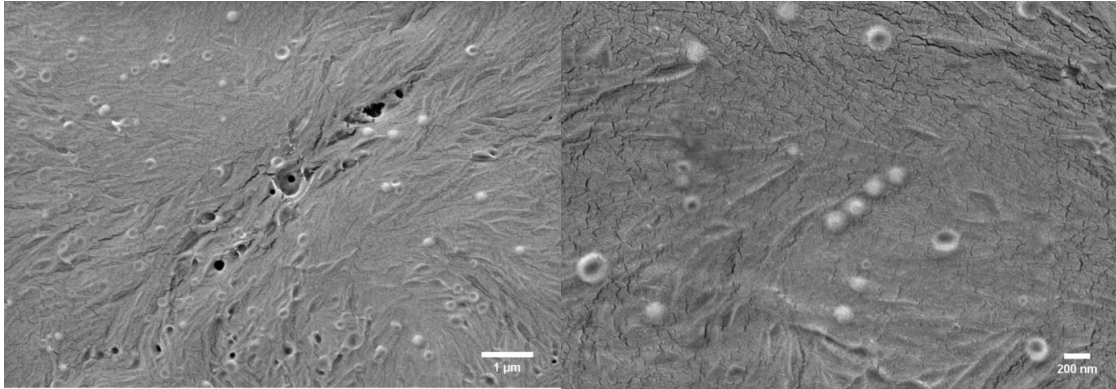


Figure 3.5 Scanning electron microscopy (SEM) images of the liposome-crosslinked hybrid hydrogels after critical point drying.

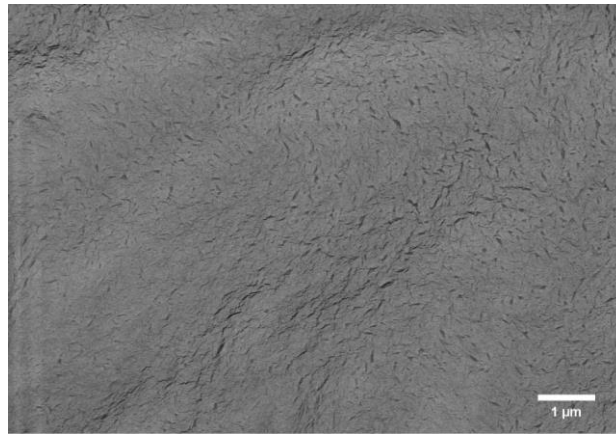


Figure 3.6 Scanning electron microscopy (SEM) images of 6wt% PEG hydrogel control lacking liposomes.

The number of intact liposomes in the bulk of the hydrogel cannot be probed directly in the SEM experiment, but is indicated to be significantly greater than the density observed on the surface, given the robust mechanical properties of the liposome-crosslinked hydrogels (above) and the poor mechanical properties of a mixture of non-maleimide liposomes and PEG-SH polymers (data not shown). Although some ruptured

liposomes can be observed in the SEM images above, possibly due to the drying process during sample preparation, the liposomes mainly retain their size and thus are indicated to remain intact throughout the crosslinking and degradation processes as indicated by the DLS characterization below. In contrast, no such nanostructure was observed in SEM images of a PEG hydrogel control lacking liposomes under the same conditions (Figure 3.6). These data are consistent with previous reports^{43, 49, 53} and confirm the structural integrity of the liposomes during the crosslinking reactions.

3.3.4 Fluorescence Imaging of the Liposome-Crosslinked Hydrogels

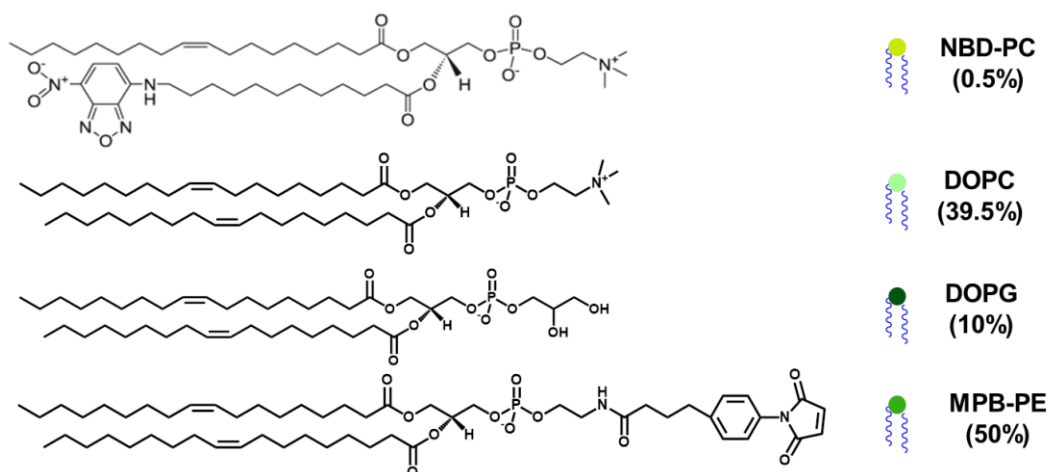


Figure 3.7 Chemical structures of the lipids used for fluorescent labeled liposome formulation. NBD-PC: 1-Oleoyl-2-[12-[(7-nitro-2-1,3-benzoxadiazol-4-yl)amino]dodecanoyl]-sn-Glycero-3-Phosphocholine; DOPC: 1,2-dioleoyl-sn-glycero-3-phosphocholine; DOPG: 1,2-dioleoyl-sn-glycero-3-phospho-(1'-rac-glycerol); MPB-PE: 1,2-dioleoyl-sn-glycero-3-phosphoethanolamine-N-[4-(p-maleimidophenyl) butyramide].

To further explore the distribution of liposomes in the bulk and the network structure of the hybrid hydrogels in hydrated state, fluorescent labeled hydrogels were

formulated using NBD-labeled liposomes and observed via confocal laser scanning microscopy (CLSM). The NBD-labeled liposomes were prepared by incorporating 0.5% (molar ratio) of NBD-PC during the lipid thin film formation process (total lipid composition NBD-PC:DOPC:DOPG:MPB = 0.05:3.95:1:5 molar ratio, Figure 3.7). The representative confocal images of the resulting hydrogels in PBS are shown in Figure 3.8, where the liposomes appear as bright green particles on the dark background. The high population and density of liposomes throughout the hydrogels is generally consistent with the robust mechanical properties of the liposome-crosslinked hydrogels as measured by rheological experiments. As shown in Figure 3.8A, the liposomes are well distributed throughout the matrix, forming an interconnected network.⁵⁴ Interestingly, slight clustering and aggregation of liposomes is also observed (Figure 3.8B), owing to reduced mobility of the liposomes with increasing gel viscosity during crosslinking and slight evaporation of the solution during incubation.⁷⁴ Nevertheless, the overall Z-Stack image (Figure 3.8C) illustrates that the majority of the hybrid hydrogels is composed of a dense network of interconnected liposomes, confirming the high population of liposomes in the bulk that is in good agreement with the mechanical strength of the hydrogels, as well as the unique and complex network structure of these nanoparticle-crosslinked hybrid systems comparing to other existing crosslinked polymer network.

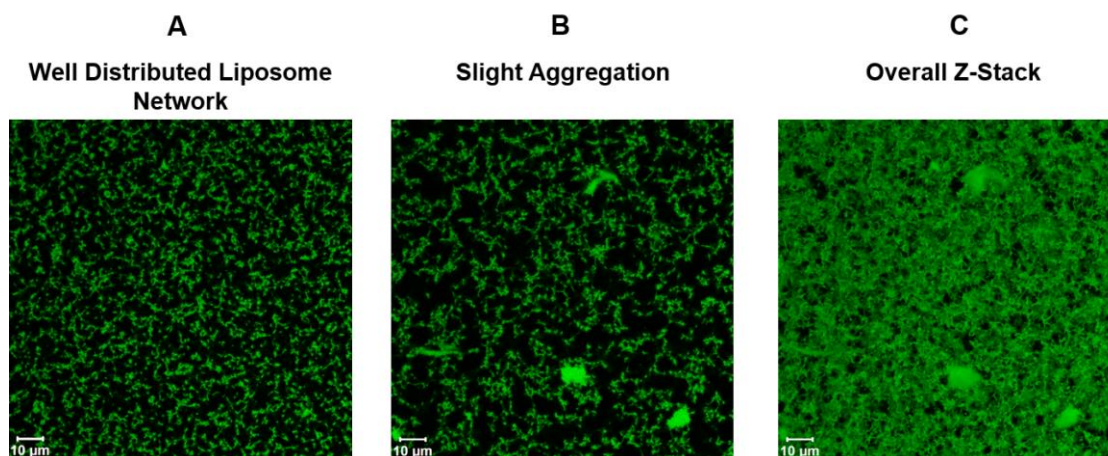


Figure 3.8 Confocal images of fluorescent labeled liposome-crosslinked hydrogels. A) Liposomes are well distributed throughout the majority of the matrix, forming an interconnected network. B) Slight aggregation of liposomes during gelation is observed within the matrix due to increased viscosity and evaporation of the solution during crosslinking. C) Overall Z-Stack of the fluorescent liposome distribution within the hydrogel to a depth of $\sim 15 \mu\text{m}$.

3.3.5 Hydrogel Stability

To verify the role of liposomes as crosslinkers in the polymer matrix, the liposome-crosslinked hydrogels were incubated with 10% Triton™ X-100 in water, a nonionic detergent that solubilizes lipid bilayers.⁷⁸ Visual inspection and rheological characterization of the liposome-crosslinked hydrogels upon treatment with the Triton™ solution are shown in Figure 3.9. Images of the samples illustrate that opacity associated with the presence of liposome nanoparticles in the hydrogels was significantly reduced after incubation with Triton™, suggesting the solubilization of liposomes within the network. The evolution of the storage modulus of the hydrogels during the incubation with Triton™ was also monitored via oscillatory rheology, where the initial modulus of the hydrogels prior to Triton™ addition was normalized to 1 to facilitate comparison. As expected, the Triton™-treated hydrogels exhibited a rapid decrease in storage modulus

to approximately 30% of its initial value within 3 hours, whereas no significant change in normalized modulus was observed in the PEG hydrogel control under the same conditions. The rapid decrease in storage modulus of the hydrogels indicates a substantial decrease in the number of crosslinks within the network as a result of the disruption of liposome bilayer structure by Triton™ X-100. Taken together, these results confirm that the maleimide-functionalized liposomes serve as crosslinks within the hybrid hydrogels.

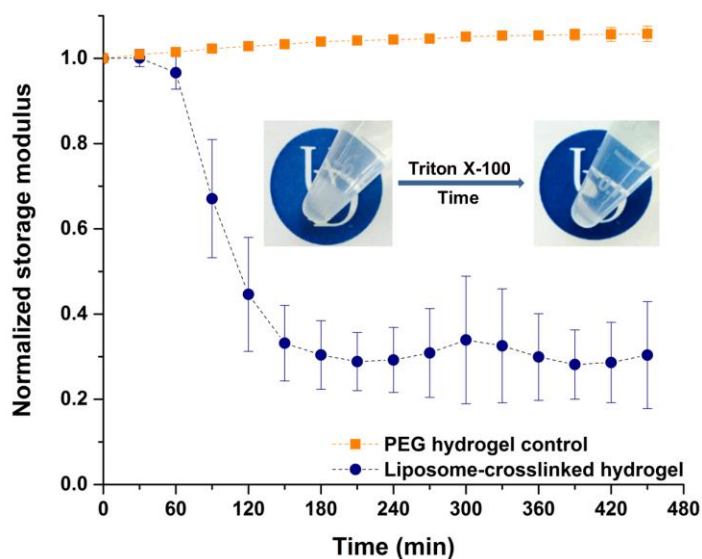


Figure 3.9 Evolution of storage modulus of the liposome-crosslinked hydrogel, as well as a PEG hydrogel control, when incubated with 10% Triton™ X-100 in water at 37°C, as monitored by oscillatory rheology. Mean and S.D. are shown ($n = 3$). Inset: visual inspection of the liposome-crosslinked hydrogel immersed in 10% Triton™ X-100 at 37°C over time. Both hydrogel images were taken with 10% Triton™ X-100 in the supernatant to mimic the conditions in the rheological measurements and to provide parallel comparisons. The UD logos are used with permission from the University of Delaware.

Thioether succinimide crosslinks of maleimide–arylthiol hydrogels are known to undergo a retro Michael-type reaction and thiol-exchange, which leads to thiol-mediated network degradation.⁶³⁻⁶⁵ Although the kinetics of the retro-Michael addition and thiol exchange were independent of the use of GSSG or GSH as demonstrated in our previous report,⁶² suggesting that GSH in either of its forms will be competent for the thiol exchange, we specifically used GSH throughout this study (as opposed to other thiol-containing molecules such as GSSG and DTT) for hydrogel degradation due to the presence of GSH under physiologically/pathologically relevant conditions *in vivo*.

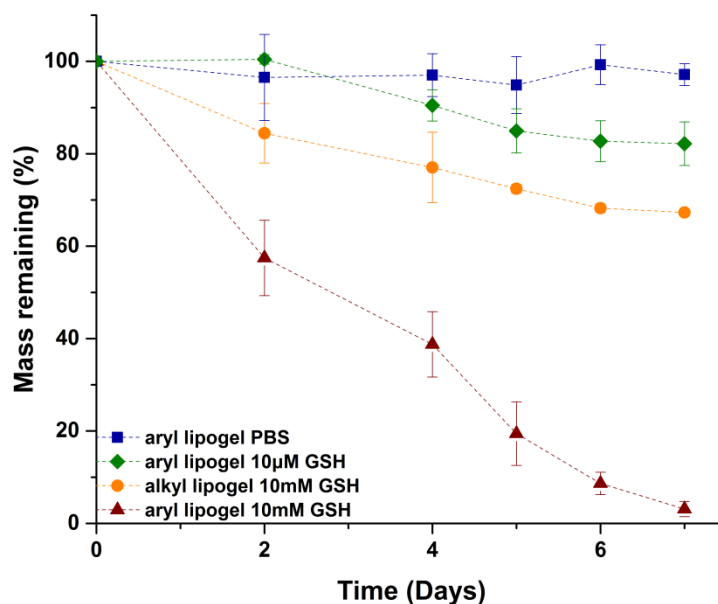


Figure 3.10 Mass loss studies of the liposome-crosslinked hybrid hydrogels in incubation with PBS and GSH in various concentrations at 37°C after initial equilibrium swelling in PBS for 24h. Mean and S.D. are shown (n = 3).

GSH, a thiol-containing tripeptide localized in intracellular compartments,^{79, 80} is found at elevated levels (ca. 0.5-10 mM) in various types of tumors (versus ca. 10 μ M in circulation), likely associated with increased cellular proliferation and metastatic activity.⁸¹ Therefore, the stability of these liposome-crosslinked hybrid hydrogels in the presence of GSH was evaluated by a series of mass loss studies in physiologically relevant buffer conditions (PBS) with GSH concentrations that are analogous to those of extracellular environments (ca. 10 μ M GSH) as well as intracellular compartments and carcinoma tissues (ca. 10 mM GSH).^{79, 80} Figure 3.10 displays results from experiments in which the mass of the liposome-crosslinked hydrogels (synthesized from the PEG arylthiol (aryl lipogel) and from the alkyl PEG-SH (alkyl lipogel)) was monitored as a function of time. No significant loss of mass was observed for the aryl lipogel when it was incubated in PBS (~97% of the hydrogel remained intact at day 7), indicating the stability of such liposome-crosslinked hydrogels under physiologically relevant buffer conditions. Similarly, only slow and moderate degradation of the aryl lipogel was observed for GSH concentrations of 10 μ M (with approximately 85% of the hydrogel remaining intact at day 7), demonstrating the stability of the hydrogels under conditions consistent with those in extracellular environments. Under low GSH concentration, the hydrogel degradation rate is dependent on both the number of crosslinks and the concentration of GSH. The degradation kinetics were thus calculated as second-order reactions, with an apparent rate constant of $k_{app} = 1.9 \times 10^{-3} \text{ mM}^{-1} \text{ h}^{-1}$ (Figure 3.11A). In contrast, a rapid decrease of mass was observed for the aryl lipogel in 10 mM GSH solutions, where almost complete hydrogel dissolution was observed within a week (~3% of the hydrogel remained intact at day 7), indicating that the liposome-crosslinked hydrogels undergo significant matrix degradation in GSH-

abundant environments. Given the linearity of the degradation curve, the hydrogel degradation in 10 mM GSH was fit to zero-order kinetics, showing an apparent rate constant of $k_{app} = 4.8 \times 10^{-3} \text{ mM h}^{-1}$ (Figure 3.11B). It should be noted that these liposome-crosslinked hydrogels show slower GSH-mediated degradation than that observed in the bulk arylthiol-maleimide hydrogels we have previously reported,^{63, 64} in these previous experiments, complete network

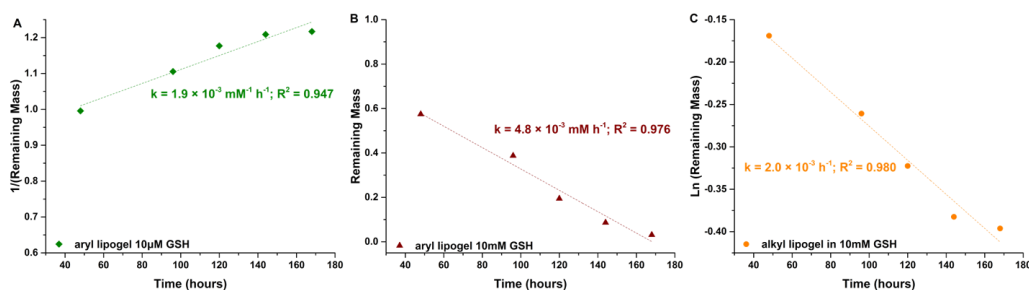


Figure 3.11 Fitting of the degradation profiles from liposome-crosslinked hybrid hydrogels synthesized from arylthiol-PEG and alkylthiol-PEG respectively. A) Degradation kinetics of the aryl lipogel in 10 μM GSH; fitting is performed based on the rate law for second order kinetics ($-\frac{d[M]}{dt} = k[M][GSH] \approx k[M]^2$) considering the comparable concentration of GSH and crosslinks. B) Degradation kinetics of the aryl lipogel in 10 mM GSH; fitting is performed based on zero-order kinetics ($-\frac{d[M]}{dt} = k$) given the almost linear release observed. C) Degradation kinetics of the alkyl lipogel in 10 mM GSH; fitting is performed based on first-order kinetics ($-\frac{d[M]}{dt} = k[M]$) because of the excess amount of GSH, which renders its concentration unchanged over the course of the experiment.

degradation was observed in approximately 4 days in 10 mM GSH and 8 days in 10 μ M GSH. The increased stability of the polymer-nanoparticle hybrid hydrogels here likely results from steric hindrance of the arylthioether succinimide crosslinks at the polymer-liposome interface and from the fact that they reside in a more hydrophobic local environment as opposed to the homogeneous distribution of the crosslinks in the previously reported bulk hydrophilic network.

Interestingly, the alkyl lipogel, a thiol-insensitive hydrogel control, also exhibited a slight decrease in mass in the presence of 10 mM GSH, reaching a mass-retention plateau of approximately 70% at day 7. Due to the excess amount of GSH, the degradation kinetics were calculated according to first-order kinetics, with an apparent rate constant of $k_{app} = 2.0 \times 10^{-3} \text{ h}^{-1}$ (Figure 3.11C). The observed degradation may be attributable to the degradation of any disulfide linkages present in the network as a result of the excess stoichiometry of the thiol employed during gelation. The reduction in mass (ca. 30%) is generally consistent with what would be expected based on the 1:2 Mal:SH stoichiometric ratio employed during gelation and the disulfide bond formation that consequently could occur after long incubation times.⁸² Under these conditions approximately 50% of the PEG-SH could be available to form disulfide bonds. Regardless, these data demonstrate that the liposome-crosslinked hybrid hydrogels can undergo network degradation in a responsive manner to GSH owing to the presence of arylthioether succinimide linkages, offering significant opportunities in the design of such polymer-nanoparticle hybrid hydrogels for controlled and triggered drug delivery.

3.3.6 Liposome Stability

The structural integrity of the liposomes incorporated in and released from the hybrid hydrogel was further examined by dynamic light scattering (DLS); results are

shown in Figure 3.12. The maleimide-functionalized liposomes showed a diameter of 105 ± 2 nm in solution before crosslinking. Following hydrogel formation, the liposome-crosslinked hydrogels were incubated in 10 mM GSH in PBS at 37°C to trigger degradation. Analysis of the hydrogel supernatant after complete hydrogel dissolution demonstrated that the released liposomes exhibited an average diameter of 109 ± 2 nm, essentially unchanged from that of the liposomes before crosslinking. These results confirm the stability of the liposomes, without rupture or apparent changes in morphology, during crosslinking and network disassociation, in accordance with the SEM observations of the liposome-crosslinked hydrogels above and consistent with

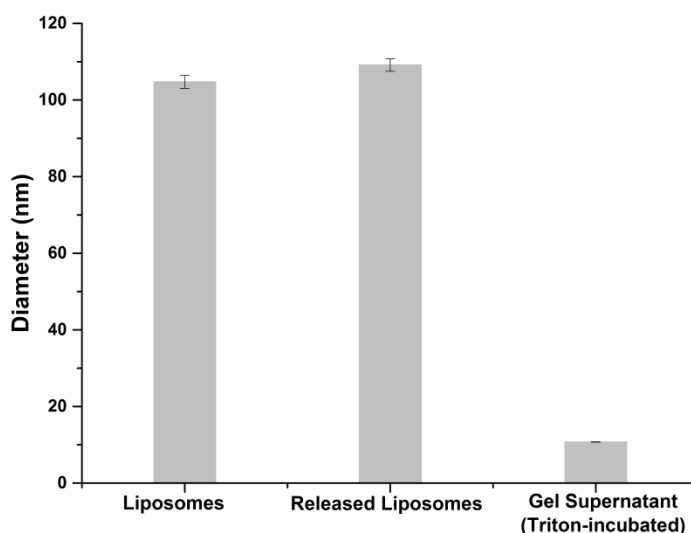


Figure 3.12 Hydrodynamic diameter of liposomes prior to hydrogel formation, released liposomes after complete network degradation in 10 mM GSH, and any particles in the gel supernatant after 10% TritonTM X-100 incubation at 37°C , as determined by dynamic light scattering (DLS).

results previously reported for a liposome-containing polyacrylamide gel system.⁴⁰ Analysis of the supernatant after treatment with Triton™ indicated the presence of much smaller nanoparticles with diameters of approximately 10 nm, consistent with the size of Triton™-containing mixed micelles⁸³ and confirming the liposomal nature of the nanoparticles released from the hydrogel after treatment with GSH.

The stability of the liposomes after network degradation was also confirmed by confocal microscopy using NBD-labeled liposomes to formulate the hybrid hydrogels. Gel supernatant was collected for imaging analysis after dissolution of the fluorescently labeled hydrogels in 10 mM GSH. As shown in Figure 3.13, the liposomes released after network degradation appear as individual green dots without any significant aggregation, closely resembling the liposomes prior to hydrogel formation. These results, combined with DLS and SEM data above, demonstrate that intact liposomes are released upon network degradation, providing opportunities to independently control and extend the release of drug encapsulated in the liposomes after dissolution of the hydrogels.

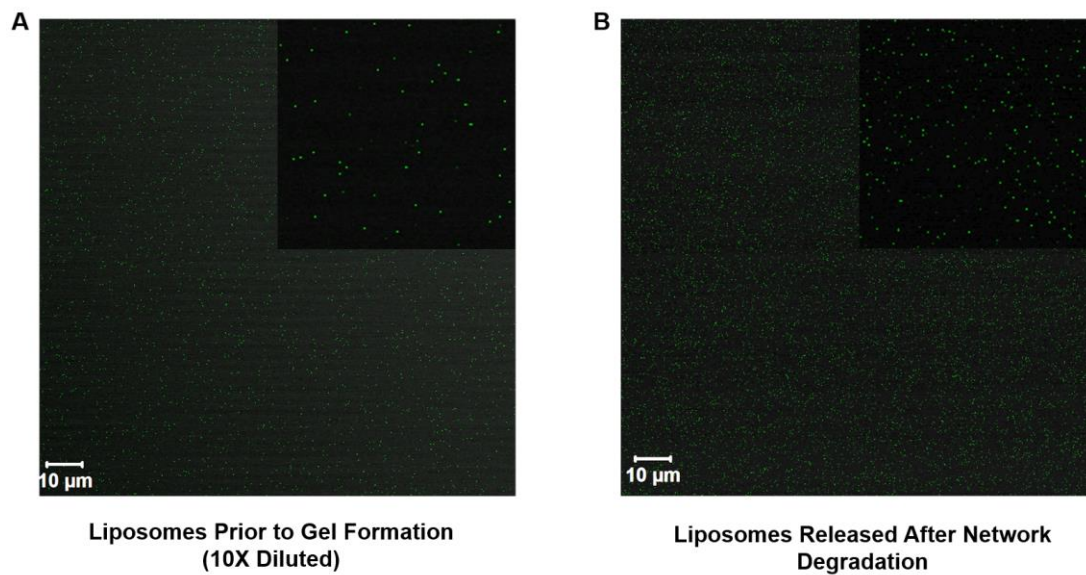


Figure 3.13 Confocal images of fluorescently labeled liposomes prior to hydrogel formation (A) and released after network degradation (B). Insert: expanded view of the confocal images.

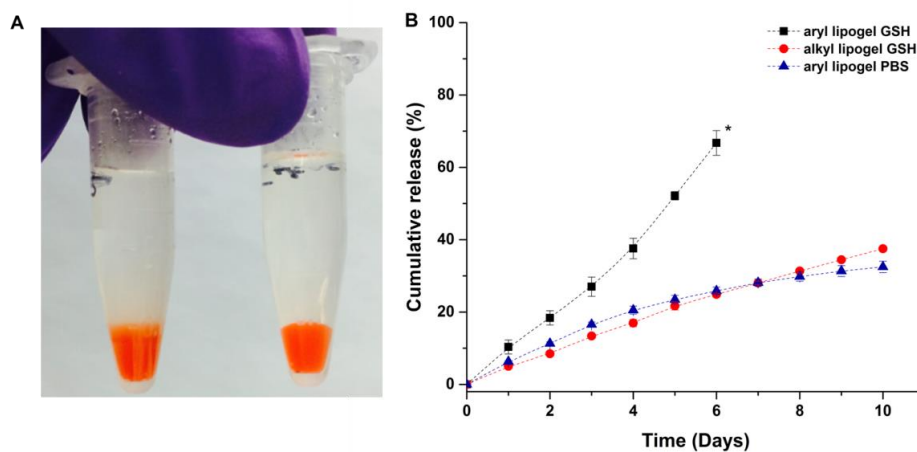


Figure 3.14 *In vitro* release of DOX from the liposome-crosslinked hydrogels at 37°C as assessed via visual inspection and fluorimetry. (A) Image of DOX-loaded liposome-crosslinked hydrogels incubated in 10 mM GSH (left, diffuse boundary observed) and PBS (right, clear boundary maintained) solutions on day 1; (B) Cumulative release profiles of DOX from liposome-crosslinked hydrogels in 10 mM GSH or in PBS solutions. *

indicates the time point where ~90% hydrogel dissolution was observed. Mean and S.D. are shown (n = 3).

3.3.7 *In Vitro* Release of DOX from Liposome-Crosslinked Hybrid Hydrogels

Doxorubicin (DOX), which is an anthracycline anticancer drug that inhibits the biosynthesis of bioactive macromolecules via interaction with DNA or RNA,^{84, 85} was used as a model drug for *in vitro* release studies. Although the release of DOX has been widely explored in various delivery systems including liposomes,^{86, 87} polymeric nanoparticles,⁸⁸⁻⁹² and hydrogels,⁹³⁻⁹⁵ significant burst release is usually observed within 12-24 h in these systems. To evaluate the potential of our liposome-crosslinked hybrid hydrogels as a matrix for controlled delivery of DOX, drug-loaded liposome-crosslinked hydrogels were prepared by first encapsulating DOX into liposomes, followed by dissolution and crosslinking of the PEG-SH precursors in the suspension of these liposomes. The DOX released from these hydrogels will be subject to a combination of diffusion barriers: first the liposomal bilayer and then the polymer network, and the presence of the two barriers may minimize burst release and prolong release over an extended period of time. To test this, the release of DOX from liposome-crosslinked hydrogels synthesized from PEG arylthiol (aryl lipogel) and alkyl PEG-SH (alkyl lipogel), respectively, was monitored as a function of time at 37°C in PBS containing 10 mM GSH (or in PBS alone), via measurement of the fluorescence intensity of the buffer in which the hydrogels were immersed (Figure 3.14).

As shown in Figure 3.14A, the aryl lipogel exhibited a diffuse boundary between the gel and the release buffer after incubation with GSH for one day, suggesting rapid GSH-mediated matrix degradation that is in agreement with the mass loss data above. In contrast, the aryl lipogel that was incubated with PBS showed a clear boundary

between the gel and the buffer, indicating hydrogel stability and the lack of any significant release of DOX at early time points (indicated to be less than 7% via fluorimetry). The release profiles of DOX from these hydrogels are presented in Figure 3.14B. For the aryl lipogel incubated in 10 mM GSH, rapid, linear release of DOX was observed, with approximately 70% of the DOX released by day 6, commensurate with the time point at which significant hydrogel degradation occurred (visual inspection indicated the loss of hydrogel integrity and the presence of suspended particulate matter) and clearly different from the two control conditions. The release of DOX is not necessarily expected to correlate exactly with hydrogel degradation, as a significant fraction of the DOX is retained in the liposomes (demonstrated below). Modeling of the release data from the aryl lipogel in GSH according to the empirical Ritger-Peppas

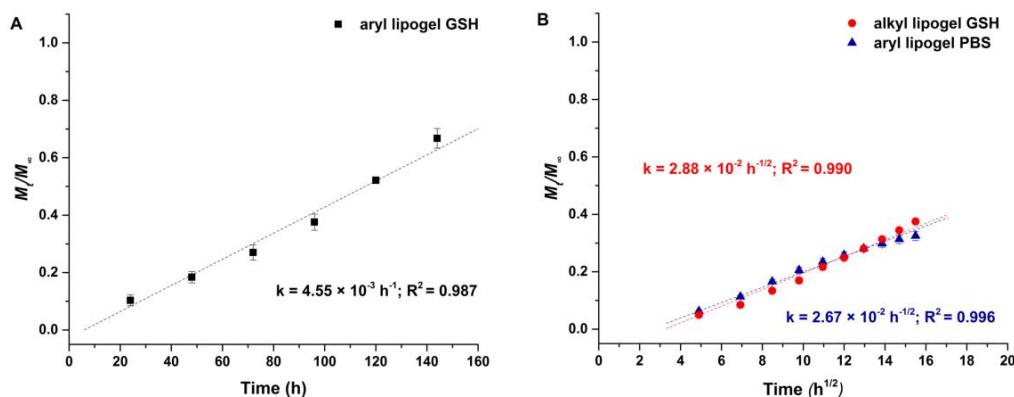


Figure 3.15 Fitting of the DOX release profiles from the liposome-crosslinked hybrid hydrogels (A) with network degradation and (B) lacking network degradation. A) Fitting of DOX release data is based on the the Ritger-Peppas equation ($n=1$). Data plotted as M_t/M_∞ versus t . B) Fitting of DOX release data is based on the early-time approximation of Fickian diffusion. Data plotted as M_t/M_∞ versus $t^{1/2}$.

equation for non-Fickian transport^{96, 97} yields a release rate constant of $4.55 \times 10^{-3} \text{ h}^{-1}$ (Figure 3.15A, equation 3.1), indicating a degradation-based mechanism. For both the GSH-insensitive control (alkyl lipogel in GSH) and the GSH-lacking control (aryl lipogel in PBS), DOX was released in a relatively slow and sustained fashion, with a total of ca. 30-35% of DOX released in 10 days. The similarity in the DOX release between these two conditions is commensurate with their lack of significant matrix degradation in both cases (ca. 35% release for the alkyl lipogel in GSH vs. ca. 30% release for the aryl lipogel in PBS at day 10, shown in Figure 3.14B).

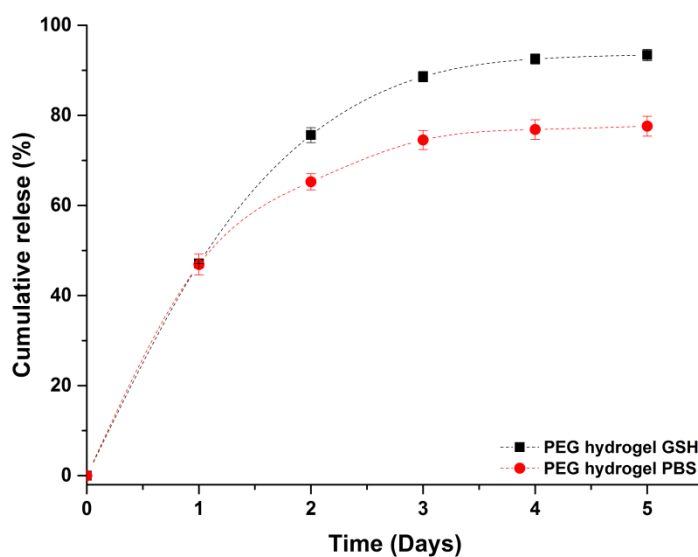


Figure 3.16 *In vitro* DOX release profiles from 6wt% PEG hydrogel control prepared by reacting 4-arm aryl PEG-SH and 4-arm PEG-maleimide. Release experiments were carried out in 10 mM GSH in PBS and PBS solutions alone respectively at 37°C. Mean and S.D. are shown (n = 2).

The diffusion-controlled release of DOX from the two control lipogels lacking degradation was analyzed by fitting the data to the early-time approximation of Fickian diffusion (Figure 3.15B, equation 3.2),^{40, 98} which also yields similar rate constants of release for the two hydrogels ($2.88 \times 10^{-2} \text{ h}^{-1/2}$ for the alkyl lipogel in 10 mM GSH and $2.67 \times 10^{-2} \text{ h}^{-1/2}$ for the aryl lipogel in PBS). The goodness of the fit ($R^2 = 0.99$) indicated a diffusion-controlled mechanism of DOX release from the alkyl lipogel (GSH-insensitive) in 10 mM GSH solutions. In contrast, burst release (nearly 50% by day 1) was observed from a DOX-loaded PEG hydrogel control (PEG-arylthiol/PEG-maleimide) prepared without liposomes (regardless of GSH concentration, Figure 3.16), indicating that incorporation of liposomes within these hydrogel systems slows drug diffusion.

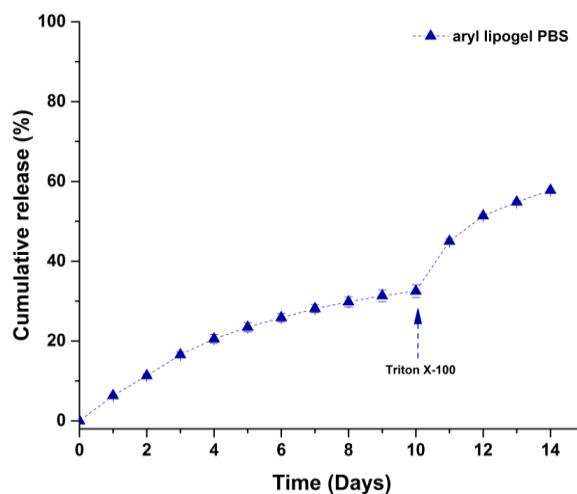


Figure 3.17 *In vitro* release of DOX from the liposome-crosslinked hydrogels at 37°C in PBS. 10% Triton™ X-100 was applied to the aryl lipogels incubated in PBS at Day 10, resulting in the liberation of more liposome-encapsulated DOX. Mean and S.D. are shown (n = 3).

The key role of the liposomes in mediating the release of DOX was indicated by the observed additional burst release (ca. 30%) of DOX from aryl lipogels upon treatment with Triton™ X-100 (Figure 3.17). In addition, the sequestration of liberated, DOX-loaded liposomes in a dialysis cup (MWCO 3500) significantly depresses the amount of DOX that can be detected from GSH-containing buffer solutions surrounding the aryl lipogel, indicating that a significant fraction of the DOX released from the aryl lipogels (ca. 65% at day 6) is located in liberated liposomes (Figure 3.18). No such reduction in the amount of detected DOX is observed for the alkyl lipogel. These results

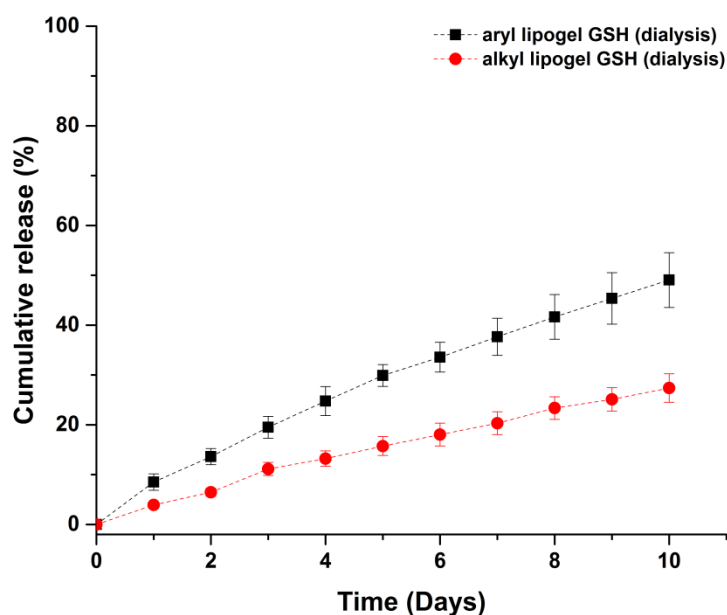


Figure 3.18 *In vitro* release of freely diffusing DOX from the liposome-crosslinked hydrogels in 10 mM GSH solutions, as monitored after dialysis in a cup-like mini dialysis device (MWCO 3.5K) at 37°C. Mean and S.D. are shown (n = 3).

in aggregate demonstrate that DOX release from the multicomponent hybrid hydrogels proceeds in a sustained manner without initial burst due to the liposome component and can be selectively triggered by thiol compounds that are known to be present in the tumor microenvironment.

3.3.8 Co-Delivery of DOX and Cytochrome c

Combined and sequential delivery of two or multiple drugs with orthogonal and possibly synergistic mechanisms might not only improve therapeutic efficacy by affecting multiple disease targets, but also minimize side effects caused by high doses of a single toxic drug and delay the generation of drug resistance.^{11, 99-101} As the liposomes constituted a structural component of the hybrid hydrogels, we anticipated that the multicomponent network would offer opportunities for dual encapsulation and differential release of multiple therapeutic cargo molecules. To examine the potential suitability of these hybrid hydrogels for such applications, cytochrome c, a small mitochondrial protein (~12 kDa) that can initiate an apoptotic cascade leading to programmed cell death upon cytoplasmic release,¹⁰²⁻¹⁰⁵ was chosen as a second therapeutic molecule. Dual encapsulation of DOX and cytochrome c in the hydrogels was carried out by dissolving cytochrome c along with the PEG-arylthiol polymers in DOX-loaded liposome suspensions. As a control, a solution of cytochrome c and PEG-arylthiol was evaluated after 1h incubation, with results demonstrating that the incubated cytochrome c electrophoresed almost identically to native cytochrome c during SDS-PAGE electrophoresis (Figure 3.19) and indicating that disulfide exchange between the protein and polymers was not significant within the timescale of the rapid crosslinking reaction.

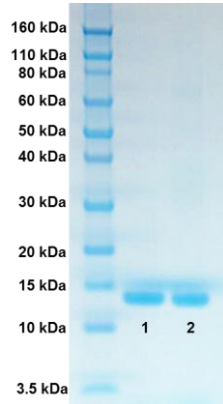


Figure 3.19 SDS-PAGE electrophoresis of cytochrome c (Lane 1) and a mixture of cytochrome c and 4-arm PEG arylthiol (Lane 2). The cytochrome c was incubated with PEG arylthiol polymers (1mg cytochrome c and 3mg of PEG polymer, the same amount as was employed in hydrogel formation, were incubated for 1h at 37°C).

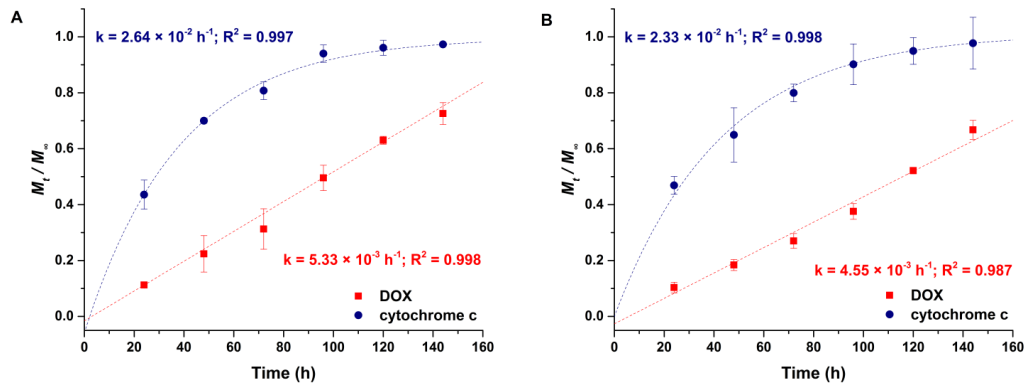


Figure 3.20 Release profiles of DOX and cytochrome c from the liposome- crosslinked hydrogels in 10 mM GSH at 37°C. A) Co-delivery of DOX and cytochrome c from a single gel. B) Individual release of DOX and cytochrome c from separate gels (DOX release data replotted from Figure 3.13). M_t/M_∞ represents the cumulative fractional mass released at time t . Dashed lines indicate the fitted curves of the release profiles. The mean and S.D. are shown ($n = 3$).

In order to probe the differential release of both cargo molecules, the simultaneous release of both molecules from the hybrid hydrogels was monitored over time in 10 mM GSH solutions; results are presented in Figure 3.17. Consistent with our hypothesis, entirely different release profiles for DOX and cytochrome c were observed from the liposome-crosslinked hybrid hydrogels (Figure 3.20A). The release profile of DOX demonstrates zero-order release kinetics, with approximately 70% release at day 6 (144h), consistent with the observed release of DOX alone from the liposome-crosslinked hybrid hydrogels (Figure 3.14), and suggesting that DOX was released via erosion-mediated release of liposomes from the hydrogel surface in GSH-containing solutions. The release of cytochrome c, however, appears to be first-order, with almost 100% release within 6 days (144h), consistent with the timescale of the GSH-induced degradation of the hydrogel (Figure 3.10). The surface erosion mechanism for the DOX, commensurate with the observation that the hydrogel decreased in size over time, may result from the localization of the arylthioether succinimide crosslinks in the sterically hindered and relatively hydrophobic environment at the polymer-liposome interface, limiting the GSH exchange reactions within the matrix and resulting in a faster degradation rate on the hydrogel surface. Similar linear, zero-order release profiles of cargo loaded in the nanoparticles were also observed as a result of surface erosion in a hybrid hydrogel system employing drug-loaded poly(ethylene glycol)-block-poly(lactic acid) nanoparticles as crosslinkers.⁵²

The release data for the DOX and the cytochrome c were modeled using the empirical Ritger-Peppas equation for non-Fickian transport^{96, 97} (DOX, equation 3.1 in SI) and the late-time approximation equation derived from Fick's second law of diffusion^{106, 107} (cytochrome c, equation 3.3). The results from these fits indicate that the

release rate constants k are $5.33 \times 10^{-3} \text{ h}^{-1}$ for DOX and $2.64 \times 10^{-2} \text{ h}^{-1}$ for cytochrome *c*, with the goodness of the fits indicating that the release of DOX from the hybrid hydrogels is dominated by a degradation-mediated release mechanism,⁵² while the release of cytochrome *c* from the hybrid hydrogels is governed by Fickian diffusion. Individual release of DOX and cytochrome *c* from separate hybrid hydrogels, measured in separate experiments and plotted together in Figure 3.20B, exhibited similar release kinetics compared to their counterparts when released simultaneously from a single gel, with release rate constants of $4.55 \times 10^{-3} \text{ h}^{-1}$ for DOX and $2.33 \times 10^{-2} \text{ h}^{-1}$ for cytochrome *c*. Statistical analysis of the release rate constants in both the simultaneous and individual release experiments shows that the release of cytochrome *c* is statistically the same in both cases. The release of DOX was suggested to be statistically slightly different ($p < 0.05$) in these experiments, which might be caused by slight batch-to-batch variations in DOX concentration in the liposomes.⁴⁹ Nevertheless, these results indicate that the release of the two therapeutic molecules is not affected substantially by their combined delivery; the sequential release of multiple therapeutic molecules is desirable for tailoring extended therapeutic regimens as well as for potentially promoting the transport and penetration of DOX-loaded liposomes to deep tissue of solid tumors through a tumor-priming mechanism.^{56, 108, 109} Similar differential release characteristics for multiple cargos have been observed in hydrogel nanocomposite drug delivery systems, where hydrophilic molecules encapsulated in the gel were released fairly rapidly while hydrophobic species encapsulated in the nanoparticles were released in a more sustained manner.^{52, 110} Consistent with these reports, our results suggest that the liposome-crosslinked hybrid hydrogels containing both nanoparticle and polymer network domains can be exploited as a functional carrier for different therapeutics to be

dually encapsulated and simultaneously released with differential profiles upon GSH-mediated degradation of the matrix.

Altogether, our studies illustrate the facile synthesis of liposome-crosslinked hybrid hydrogels for the controlled and thiol-triggered release of multiple therapeutic molecules with differential release profiles. Although nanocomposite hydrogels have been extensively studied and are widely used in the field of drug delivery and tissue engineering,^{32, 34} there have been limited studies that have explored the use of nanoparticles as crosslinkers during hydrogel formation.⁴⁹⁻⁵⁴ These hybrid hydrogels, developed based on either polymer-nanoparticle hydrophobic interactions⁴⁹⁻⁵² or polymer-nanoparticle covalent crosslinking,^{53, 54} have shown great potential in controlled drug delivery with additional engineering flexibility, although the delivery of multiple relevant therapeutic molecules with chemo-responsiveness has yet to be reported in these cases. In contrast to these existing nanoparticle-crosslinked hybrid hydrogel systems, we have demonstrated the multi-stage and sequential delivery of multiple molecules relevant for chemotherapies (as opposed to one single molecule or model drug compounds) from the liposome-crosslinked hybrid hydrogels. More importantly, the incorporation of glutathione-sensitive thioether succinimide linkages within these matrices offers great advantages for controlled and triggered release of therapeutic cargos under reducing environments similar to those in tumor microenvironments,⁶³⁻⁶⁵ making these hybrid hydrogel systems promising potential candidates in cancer drug delivery. Given the sequential release characteristics of the reported hydrogels, it may be possible that the cytochrome c released first from the hydrogels upon matrix degradation could induce partial cell apoptosis and expand the interstitial space of solid tumors, which would potentially permit the drug-loaded

liposomes to diffuse into the deep tumor tissue and slowly release the second drug for more effective cancer treatment.⁵⁶ It is also conceivable that a liposome crosslinked via this chemistry could alone be used as a delivery vehicle to transport drug to a tumor (as in current liposome-based approaches), with the added advantage that the liposome could more rapidly release its cargo upon thiol-exchange with GSH. Furthermore, the liposome-crosslinking strategy explored in this study could also be expanded to other bioactive thiolated polymer systems (e.g. low molecular weight heparin and hyaluronic acid (HA)), which have been shown to be effective in the inhibition of tumor growth via the binding of many angiogenic growth factors (such as FGF and VEGF) and the saturation of membrane-binding sites (CD44 receptors) required for the attachment of tumor cells to the extracellular matrix, respectively),¹¹¹⁻¹¹³ introducing additional biological functionalities. In addition, while not investigated here, the size, functionality, and concentration of liposomes and the identity of functional lipids, as well as the molecular weight and functionality of polymers could be easily tuned to tailor the mesh sizes, delivery properties, and degradation chemistry of the hydrogels for specific delivery applications.^{38, 114, 115} Also, the versatility of liposomes to carry both hydrophilic and hydrophobic drugs in the aqueous lumen and lipid bilayer, respectively, offers additional advantages for the delivery of multiple therapeutic molecules of differing physicochemical properties.^{11, 116}

3.4 Conclusions

We have developed an advanced hybrid hydrogel material based on the Michael-type addition between PEG polymers and liposome nanoparticles. The incorporation of arylthioether succinimide crosslinks between PEG polymers and liposome

nanoparticles enables matrix degradation in response to thiol-containing environment (i.e., GSH) relevant to physiological and pathological states. Characterization of the hybrid hydrogels confirms the role of liposomes as crosslinkers and demonstrates the GSH-mediated network degradation and triggered release of encapsulated molecules. The multiple domains within the gel allow dual loading of therapeutic molecules that can be loaded in the liposomes and the bulk polymer network. The drug delivery experiments indicate that the multiple therapeutic molecules encapsulated within the hydrogel are released in a controlled and prolonged manner, with differential release profiles that are controlled by degradation-mediated release and Fickian diffusion. These results suggest the potential of these easily synthesized liposome-crosslinked hybrid hydrogels in advanced delivery applications.

REFERENCES

1. Peer, D.; Karp, J. M.; Hong, S.; Farokhzad, O. C.; Margalit, R.; Langer, R., Nanocarriers as an emerging platform for cancer therapy. *Nat. Nanotechnol.* **2007**, *2*, (12), 751-760.
2. Davis, M. E.; Chen, Z.; Shin, D. M., Nanoparticle therapeutics: an emerging treatment modality for cancer. *Nat. Rev. Drug Discov.* **2008**, *7*, (9), 771-782.
3. Hubbell, J. A.; Chilkoti, A., Nanomaterials for Drug Delivery. *Science* **2012**, *337*, (6092), 303-305.
4. Petros, R. A.; DeSimone, J. M., Strategies in the design of nanoparticles for therapeutic applications. *Nat. Rev. Drug Discov.* **2010**, *9*, (8), 615-627.
5. Farokhzad, O. C.; Langer, R., Impact of Nanotechnology on Drug Delivery. *ACS Nano* **2009**, *3*, (1), 16-20.
6. Gao, J. H.; Gu, H. W.; Xu, B., Multifunctional Magnetic Nanoparticles: Design, Synthesis, and Biomedical Applications. *Acc. Chem. Res.* **2009**, *42*, (8), 1097-1107.
7. Ghosh, P.; Han, G.; De, M.; Kim, C. K.; Rotello, V. M., Gold nanoparticles in delivery applications. *Adv. Drug Deliver Rev.* **2008**, *60*, (11), 1307-1315.
8. Pissuwan, D.; Niidome, T.; Cortie, M. B., The forthcoming applications of gold nanoparticles in drug and gene delivery systems. *J. Controlled Release* **2011**, *149*, (1), 65-71.
9. Moon, J. J.; Suh, H.; Bershteyn, A.; Stephan, M. T.; Liu, H. P.; Huang, B.; Sohail, M.; Luo, S.; Um, S. H.; Khant, H.; Goodwin, J. T.; Ramos, J.; Chiu, W.; Irvine, D. J., Interbilayer-crosslinked multilamellar vesicles as synthetic vaccines for potent humoral and cellular immune responses. *Nat. Mater.* **2011**, *10*, (3), 243-251.
10. Joo, K. I.; Xiao, L.; Liu, S. L.; Liu, Y. R.; Lee, C. L.; Conti, P. S.; Wong, M. K.; Li, Z. B.; Wang, P., Crosslinked multilamellar liposomes for controlled delivery of anticancer drugs. *Biomaterials* **2013**, *34*, (12), 3098-3109.
11. Liu, Y. R.; Fang, J. X.; Kim, Y. J.; Wong, M. K.; Wang, P., Codelivery of Doxorubicin and Paclitaxel by Cross-Linked Multilamellar Liposome Enables Synergistic Antitumor Activity. *Mol. Pharmaceut.* **2014**, *11*, (5), 1651-1661.
12. Ding, J. X.; Chen, L. H.; Xiao, C. S.; Chen, L.; Zhuang, X. L.; Chen, X. S., Noncovalent interaction-assisted polymeric micelles for controlled drug delivery. *Chem. Commun.* **2014**, *50*, (77), 11274-11290.
13. Chen, W.; Meng, F. H.; Cheng, R.; Deng, C.; Feijen, J.; Zhong, Z. Y., Biodegradable glycopolymer-b-poly(epsilon-caprolactone) block copolymer micelles: versatile construction, tailored lactose functionality, and hepatoma-targeted drug delivery. *J. Mater. Chem. B* **2015**, *3*, (11), 2308-2317.

14. Chen, W.; Meng, F. H.; Cheng, R.; Deng, C.; Jan, F. J.; Zhong, Z., Facile construction of dual-bioresponsive biodegradable micelles with superior extracellular stability and activated intracellular drug release. *J. Controlled Release* **2015**, 210, 125-133.
15. Azagarsamy, M. A.; Alge, D. L.; Radhakrishnan, S. J.; Tibbitt, M. W.; Anseth, K. S., Photocontrolled Nanoparticles for On-Demand Release of Proteins. *Biomacromolecules* **2012**, 13, (8), 2219-2224.
16. Liang, Y.; Kiick, K. L., Multifunctional lipid-coated polymer nanogels crosslinked by photo-triggered Michael-type addition. *Polym. Chem.* **2014**, 5, (5), 1728-1736.
17. Heller, D. A.; Levi, Y.; Pelet, J. M.; Doloff, J. C.; Wallas, J.; Pratt, G. W.; Jiang, S.; Sahay, G.; Schroeder, A.; Schroeder, J. E.; Chyan, Y.; Zurenko, C.; Querbes, W.; Manzano, M.; Kohane, D. S.; Langer, R.; Anderson, D. G., Modular 'Click-in-Emulsion' Bone-Targeted Nanogels. *Adv. Mater.* **2013**, 25, (10), 1449-1454.
18. Shi, J. J.; Xiao, Z. Y.; Kamaly, N.; Farokhzad, O. C., Self-Assembled Targeted Nanoparticles: Evolution of Technologies and Bench to Bedside Translation. *Acc. Chem. Res.* **2011**, 44, (10), 1123-1134.
19. Byrne, J. D.; Betancourt, T.; Brannon-Peppas, L., Active targeting schemes for nanoparticle systems in cancer therapeutics. *Adv. Drug Deliver Rev.* **2008**, 60, (15), 1615-1626.
20. Riehemann, K.; Schneider, S. W.; Luger, T. A.; Godin, B.; Ferrari, M.; Fuchs, H., Nanomedicine-Challenge and Perspectives. *Angew. Chem. Int. Ed.* **2009**, 48, (5), 872-897.
21. Barenholz, Y., Doxil (R) - The first FDA-approved nano-drug: Lessons learned. *J. Controlled Release* **2012**, 160, (2), 117-134.
22. Allen, T. M.; Cullis, P. R., Liposomal drug delivery systems: From concept to clinical applications. *Adv. Drug Deliver Rev.* **2013**, 65, (1), 36-48.
23. Li, Y. L.; Rodrigues, J.; Tomas, H., Injectable and biodegradable hydrogels: gelation, biodegradation and biomedical applications. *Chem. Soc. Rev.* **2012**, 41, (6), 2193-2221.
24. Seliktar, D., Designing Cell-Compatible Hydrogels for Biomedical Applications. *Science* **2012**, 336, (6085), 1124-1128.
25. Censi, R.; Di Martino, P.; Vermonden, T.; Hennink, W. E., Hydrogels for protein delivery in tissue engineering. *J. Controlled Release* **2012**, 161, (2), 680-692.
26. Lin, C.-C.; Anseth, K., PEG Hydrogels for the Controlled Release of Biomolecules in Regenerative Medicine. *Pharm. Res.* **2009**, 26, (3), 631-643.
27. Vermonden, T.; Censi, R.; Hennink, W. E., Hydrogels for Protein Delivery. *Chem. Rev.* **2012**, 112, (5), 2853-2888.
28. Slaughter, B. V.; Khurshid, S. S.; Fisher, O. Z.; Khademhosseini, A.; Peppas, N. A., Hydrogels in Regenerative Medicine. *Adv. Mater.* **2009**, 21, (32-33), 3307-3329.
29. Zhu, J., Bioactive modification of poly(ethylene glycol) hydrogels for tissue engineering. *Biomaterials* **2010**, 31, (17), 4639-4656.

30. Wallace, D. G.; Cruise, G. M.; Rhee, W. M.; Schroeder, J. A.; Prior, J. J.; Ju, J.; Maroney, M.; Duronio, J.; Ngo, M. H.; Estridge, T.; Coker, G. C., A tissue sealant based on reactive multifunctional polyethylene glycol. *J. Biomed. Mater. Res.* **2001**, 58, (5), 545-555.
31. Wirostko, B.; Mann, B. K.; Williams, D. L.; Prestwich, G. D., Ophthalmic Uses of a Thiol-Modified Hyaluronan-Based Hydrogel. *Adv. Wound Care* **2014**, 3, (11), 708-716.
32. Gaharwar, A. K.; Peppas, N. A.; Khademhosseini, A., Nanocomposite Hydrogels for Biomedical Applications. *Biotechnol. Bioeng.* **2014**, 111, (3), 441-453.
33. Thoniyot, P.; Tan, M. J.; Karim, A. A.; Young, D. J.; Loh, X. J., Nanoparticle–Hydrogel Composites: Concept, Design, and Applications of These Promising, Multi-Functional Materials. *Adv. Sci.* **2015**, 2, (1-2), 140010.
34. Merino, S.; Martín, C.; Kostarelos, K.; Prato, M.; Vázquez, E., Nanocomposite Hydrogels: 3D Polymer–Nanoparticle Synergies for On-Demand Drug Delivery. *ACS Nano* **2015**, 9, (5), 4686-4697.
35. Wang, C.; Flynn, N. T.; Langer, R., Controlled structure and properties of thermoresponsive nanoparticle-hydrogel composites. *Adv. Mater.* **2004**, 16, (13), 1074-1079.
36. Shin, S. R.; Jung, S. M.; Zalabany, M.; Kim, K.; Zorlutuna, P.; Kim, S. B.; Nikkhah, M.; Khabiry, M.; Azize, M.; Kong, J.; Wan, K. T.; Palacios, T.; Dokmeci, M. R.; Bae, H.; Tang, X. W.; Khademhosseini, A., Carbon-Nanotube-Embedded Hydrogel Sheets for Engineering Cardiac Constructs and Bioactuators. *ACS Nano* **2013**, 7, (3), 2369-2380.
37. Chung, Y. I.; Ahn, K. M.; Jeon, S. H.; Lee, S. Y.; Lee, J. H.; Tae, G., Enhanced bone regeneration with BMP-2 loaded functional nanoparticle-hydrogel complex. *J. Controlled Release* **2007**, 121, (1-2), 91-99.
38. Gao, W. W.; Hu, C. M. J.; Fang, R. H.; Zhang, L. F., Liposome-like nanostructures for drug delivery. *J. Mater. Chem. B* **2013**, 1, (48), 6569-6585.
39. Popescu, M. T.; Mourtas, S.; Pampalakis, G.; Antimisariaris, S. G.; Tsitsilianis, C., pH-Responsive Hydrogel/Liposome Soft Nanocomposites For Tuning Drug Release. *Biomacromolecules* **2011**, 12, (8), 3023-3030.
40. Gao, W. W.; Vecchio, D.; Li, J. M.; Zhu, J. Y.; Zhang, Q. Z.; Fu, V.; Li, J. Y.; Thamphiwatana, S.; Lu, D. N.; Zhang, L. F., Hydrogel Containing Nanoparticle-Stabilized Liposomes for Topical Antimicrobial Delivery. *ACS Nano* **2014**, 8, (3), 2900-2907.
41. Widjaja, L. K.; Bora, M.; Chan, P. N. P. H.; Lipik, V.; Wong, T. T. L.; Venkatraman, S. S., Hyaluronic acid-based nanocomposite hydrogels for ocular drug delivery applications. *J. Biomed. Mater. Res. A* **2014**, 102, (9), 3056-3065.
42. Lopez-Noriega, A.; Hastings, C. L.; Ozbakir, B.; O'Donnell, K. E.; O'Brien, F. J.; Storm, G.; Hennink, W. E.; Duffy, G. P.; Ruiz-Hernandez, E., Hyperthermia-Induced Drug Delivery from Thermosensitive Liposomes Encapsulated in an Injectable Hydrogel for Local Chemotherapy. *Adv. Healthcare Mater.* **2014**, 3, (6), 854-859.

43. Wickremasinghe, N. C.; Kumar, V. A.; Hartgerink, J. D., Two-Step Self-Assembly of Liposome-Multidomain Peptide Nanofiber Hydrogel for Time-Controlled Release. *Biomacromolecules* **2014**, *15*, (10), 3587-3595.
44. Wickremasinghe, N. C.; Kumar, V. A.; Shi, S.; Hartgerink, J. D., Controlled Angiogenesis in Peptide Nanofiber Composite Hydrogels. *ACS Biomater. Sci. Eng.* **2015**, *1*, (9), 845-854.
45. Souza, G. R.; Christianson, D. R.; Staquicini, F. I.; Ozawa, M. G.; Snyder, E. Y.; Sidman, R. L.; Miller, J. H.; Arap, W.; Pasqualini, R., Networks of gold nanoparticles and bacteriophage as biological sensors and cell-targeting agents. *P Natl Acad Sci USA* **2006**, *103*, (5), 1215-1220.
46. Castaneda, L.; Valle, J.; Yang, N.; Pluskat, S.; Slowinska, K., Collagen Cross-Linking with Au Nanoparticles. *Biomacromolecules* **2008**, *9*, (12), 3383-3388.
47. Skardal, A.; Zhang, J. X.; McCoard, L.; Oottamasathien, S.; Prestwich, G. D., Dynamically Crosslinked Gold Nanoparticle - Hyaluronan Hydrogels. *Adv. Mater.* **2010**, *22*, (42), 4736-4740.
48. Xiao, L. X.; Tong, Z. X.; Chen, Y. C.; Pochan, D. J.; Sabanayagam, C. R.; Jia, X. Q., Hyaluronic Acid-Based Hydrogels Containing Covalently Integrated Drug Depots: Implication for Controlling Inflammation in Mechanically Stressed Tissues. *Biomacromolecules* **2013**, *14*, (11), 3808-3819.
49. Lee, J. H.; Oh, H.; Baxa, U.; Raghavan, S. R.; Blumenthal, R., Biopolymer-Connected Liposome Networks as Injectable Biomaterials Capable of Sustained Local Drug Delivery. *Biomacromolecules* **2012**, *13*, (10), 3388-3394.
50. Chen, Y. J.; Javvaji, V.; MacIntire, I. C.; Raghavan, S. R., Gelation of Vesicles and Nanoparticles Using Water-Soluble Hydrophobically Modified Chitosan. *Langmuir* **2013**, *29*, (49), 15302-15308.
51. Javvaji, V.; Dowling, M. B.; Oh, H.; White, I. M.; Raghavan, S. R., Reversible gelation of cells using self-assembling hydrophobically-modified biopolymers: towards self-assembly of tissue. *Biomater. Sci.* **2014**, *2*, (7), 1016-1023.
52. Appel, E. A.; Tibbitt, M. W.; Webber, M. J.; Mattix, B. A.; Veiseh, O.; Langer, R., Self-assembled hydrogels utilizing polymer-nanoparticle interactions. *Nat. Commun.* **2015**, *6*:6295.
53. Sekine, Y.; Moritani, Y.; Ikeda-Fukazawa, T.; Sasaki, Y.; Akiyoshi, K., A Hybrid Hydrogel Biomaterial by Nanogel Engineering: Bottom-Up Design with Nanogel and Liposome Building Blocks to Develop a Multidrug Delivery System. *Adv. Healthcare Mater.* **2012**, *1*, (6), 722-728.
54. Hashimoto, Y.; Mukai, S.; Sawada, S.; Sasaki, Y.; Akiyoshi, K., Nanogel tectonic porous gel loading biologics, nanocarriers, and cells for advanced scaffold. *Biomaterials* **2015**, *37*, 107-115.
55. Journe, F.; Chaboteaux, C.; Laurent, G.; Body, J. J., Sequence-dependent synergistic effects of ibandronate in combination with antiestrogens on growth inhibition of estrogen receptor-positive breast cancer cells. *Bone* **2006**, *38*, (3), S52-S53.
56. Hu, C. M.; Aryal, S.; Zhang, L., Nanoparticle-assisted combination therapies for effective cancer treatment. *Therapeutic delivery* **2010**, *1*, (2), 323-34.

57. Zhang, L. M.; Lu, Z. X.; Zhao, Q. H.; Huang, J.; Shen, H.; Zhang, Z. J., Enhanced Chemotherapy Efficacy by Sequential Delivery of siRNA and Anticancer Drugs Using PEI-Grafted Graphene Oxide. *Small* **2011**, 7, (4), 460-464.
58. Godsey, M. E.; Suryaprakash, S.; Leong, K. W., Materials innovation for co-delivery of diverse therapeutic cargos. *Rsc Adv* **2013**, 3, (47), 24794-24811.
59. Yilgor, P.; Tuzlakoglu, K.; Reis, R. L.; Hasirci, N.; Hasirci, V., Incorporation of a sequential BMP-2/BMP-7 delivery system into chitosan-based scaffolds for bone tissue engineering. *Biomaterials* **2009**, 30, (21), 3551-3559.
60. Chen, F. M.; Zhang, M.; Wu, Z. F., Toward delivery of multiple growth factors in tissue engineering. *Biomaterials* **2010**, 31, (24), 6279-6308.
61. Ilg, P., Stimuli-responsive hydrogels cross-linked by magnetic nanoparticles. *Soft Matter* **2013**, 9, (13), 3465-3468.
62. Baldwin, A. D.; Kiick, K. L., Tunable Degradation of Maleimide-Thiol Adducts in Reducing Environments. *Bioconjugate Chem.* **2011**, 22, (10), 1946-1953.
63. Baldwin, A. D.; Kiick, K. L., Reversible maleimide-thiol adducts yield glutathione-sensitive poly(ethylene glycol)-heparin hydrogels. *Polym. Chem.* **2013**, 4, (1), 133-143.
64. Kharkar, P. M.; Kloxin, A. M.; Kiick, K. L., Dually degradable click hydrogels for controlled degradation and protein release. *J. Mater. Chem. B* **2014**, 2, (34), 5511-5521.
65. Kharkar, P. M.; Kiick, K. L.; Kloxin, A. M., Design of thiol- and light-sensitive degradable hydrogels using Michael-type addition reactions. *Polym. Chem.* **2015**, 6, (31), 5565-5574.
66. Lyon, R. P.; Setter, J. R.; Bovee, T. D.; Doronina, S. O.; Hunter, J. H.; Anderson, M. E.; Balasubramanian, C. L.; Duniho, S. M.; Leiske, C. I.; Li, F.; Senter, P. D., Self-hydrolyzing maleimides improve the stability and pharmacological properties of antibody-drug conjugates. *Nat Biotech* **2014**, 32, (10), 1059-1062.
67. Elbert, D. L.; Pratt, A. B.; Lutolf, M. P.; Halstenberg, S.; Hubbell, J. A., Protein delivery from materials formed by self-selective conjugate addition reactions. *J. Controlled Release* **2001**, 76, (1-2), 11-25.
68. Luo, D. Y.; Smith, S. W.; Anderson, B. D., Kinetics and mechanism of the reaction of cysteine and hydrogen peroxide in aqueous solution. *J. Pharm. Sci.* **2005**, 94, (2), 304-316.
69. Fontaine, S. D.; Reid, R.; Robinson, L.; Ashley, G. W.; Santi, D. V., Long-Term Stabilization of Maleimide-Thiol Conjugates. *Bioconjugate Chem.* **2015**, 26, (1), 145-152.
70. Nie, T.; Baldwin, A.; Yamaguchi, N.; Kiick, K. L., Production of heparin-functionalized hydrogels for the development of responsive and controlled growth factor delivery systems. *J. Controlled Release* **2007**, 122, (3), 287-296.
71. Baldwin, A. D.; Robinson, K. G.; Militar, J. L.; Derby, C. D.; Kiick, K. L.; Akins, R. E., In situ crosslinkable heparin-containing poly(ethylene glycol) hydrogels for sustained anticoagulant release. *J. Biomed. Mater. Res. A* **2012**, 100A, (8), 2106-2118.

72. Lutolf, M. P.; Hubbell, J. A., Synthesis and Physicochemical Characterization of End-Linked Poly(ethylene glycol)-co-peptide Hydrogels Formed by Michael-Type Addition. *Biomacromolecules* **2003**, 4, (3), 713-722.
73. Paradee, N.; Sirivat, A.; Niamlang, S.; Prissanaroon-Ouajai, W., Effects of crosslinking ratio, model drugs, and electric field strength on electrically controlled release for alginate-based hydrogel. *J Mater Sci: Mater Med* **2012**, 23, (4), 999-1010.
74. Pakulska, M. M.; Vulic, K.; Tam, R. Y.; Shoichet, M. S., Hybrid Crosslinked Methylcellulose Hydrogel: A Predictable and Tunable Platform for Local Drug Delivery. *Adv. Mater.* **2015**, 27, (34), 5002-5008.
75. Phelps, E. A.; Enemchukwu, N. O.; Fiore, V. F.; Sy, J. C.; Murthy, N.; Sulchek, T. A.; Barker, T. H.; Garcia, A. J., Maleimide Cross-Linked Bioactive PEG Hydrogel Exhibits Improved Reaction Kinetics and Cross-Linking for Cell Encapsulation and In Situ Delivery. *Adv. Mater.* **2012**, 24, (1), 64-70.
76. Tsurkan, M. V.; Chwalek, K.; Prokoph, S.; Zieris, A.; Levental, K. R.; Freudenberg, U.; Werner, C., Defined Polymer-Peptide Conjugates to Form Cell-Instructive starPEG-Heparin Matrices In Situ. *Adv. Mater.* **2013**, 25, (18), 2606-2610.
77. Chwalek, K.; Tsurkan, M. V.; Freudenberg, U.; Werner, C., Glycosaminoglycan-based hydrogels to modulate heterocellular communication in in vitro angiogenesis models. *Sci. Rep.* **2014**, 4, 4414.
78. Mattei, B.; Franca, A. D. C.; Riske, K. A., Solubilization of Binary Lipid Mixtures by the Detergent Triton X-100: The Role of Cholesterol. *Langmuir* **2015**, 31, (1), 378-386.
79. Meng, F. H.; Hennink, W. E.; Zhong, Z., Reduction-sensitive polymers and bioconjugates for biomedical applications. *Biomaterials* **2009**, 30, (12), 2180-2198.
80. Cheng, R.; Feng, F.; Meng, F.; Deng, C.; Feijen, J.; Zhong, Z., Glutathione-responsive nano-vehicles as a promising platform for targeted intracellular drug and gene delivery. *J. Controlled Release* **2011**, 152, (1), 2-12.
81. Traverso, N.; Ricciarelli, R.; Nitti, M.; Marengo, B.; Furfaro, A. L.; Pronzato, M. A.; Marinari, U. M.; Domenicotti, C., Role of Glutathione in Cancer Progression and Chemoresistance. *Oxid Med Cell Longev* **2013**.
82. Ghosh, K.; Shu, X. Z.; Mou, R.; Lombardi, J.; Prestwich, G. D.; Rafailovich, M. H.; Clark, R. A. F., Rheological characterization of in situ cross-linkable hyaluronan hydrogels. *Biomacromolecules* **2005**, 6, (5), 2857-2865.
83. Kazakov, S.; Kaholek, M.; Teraoka, I.; Levon, K., UV-induced gelation on nanometer scale using liposome reactor. *Macromolecules* **2002**, 35, (5), 1911-1920.
84. Fornari, F. A.; Randolph, J. K.; Yalowich, J. C.; Ritke, M. K.; Gewirtz, D. A., Interference by Doxorubicin with DNA Unwinding in MCF-7 Breast-Tumor Cells. *Mol. Pharmacol.* **1994**, 45, (4), 649-656.
85. Tacar, O.; Sriamornsak, P.; Dass, C. R., Doxorubicin: an update on anticancer molecular action, toxicity and novel drug delivery systems. *J. Pharm. Pharmacol.* **2013**, 65, (2), 157-170.
86. Wang, Z. H.; Yu, Y.; Dai, W. B.; Lu, J. K.; Cui, J. R.; Wu, H. N.; Yuan, L.; Zhang, H.; Wang, X. Q.; Wang, J. C.; Zhang, X.; Zhan, Q., The use of a tumor

- metastasis targeting peptide to deliver doxorubicin-containing liposomes to highly metastatic cancer. *Biomaterials* **2012**, 33, (33), 8451-8460.
87. Zhao, Y.; Alakhova, D. Y.; Kim, J. O.; Bronich, T. K.; Kabanov, A. V., A simple way to enhance Doxil (R) therapy: Drug release from liposomes at the tumor site by amphiphilic block copolymer. *J. Controlled Release* **2013**, 168, (1), 61-69.
88. Missirlis, D.; Kawamura, R.; Tirelli, N.; Hubbell, J. A., Doxorubicin encapsulation and diffusional release from stable, polymeric, hydrogel nanoparticles. *Eur. J. Pharm. Sci.* **2006**, 29, (2), 120-129.
89. Ding, J. X.; Shi, F. H.; Xiao, C. S.; Lin, L.; Chen, L.; He, C. L.; Zhuang, X. L.; Chen, X. S., One-step preparation of reduction-responsive poly(ethylene glycol)-poly(amino acid)s nanogels as efficient intracellular drug delivery platforms. *Polym. Chem.* **2011**, 2, (12), 2857-2864.
90. Zhong, Y. N.; Yang, W. J.; Sun, H. L.; Cheng, R.; Meng, F. H.; Deng, C.; Zhong, Z. Y., Ligand-Directed Reduction-Sensitive Shell-Sheddable Biodegradable Micelles Actively Deliver Doxorubicin into the Nuclei of Target Cancer Cells. *Biomacromolecules* **2013**, 14, (10), 3723-3730.
91. Chen, W.; Zou, Y.; Meng, F. H.; Cheng, R.; Deng, C.; Feijen, J.; Zhong, Z. Y., Glyco-Nanoparticles with Sheddable Saccharide Shells: A Unique and Potent Platform for Hepatoma-Targeting Delivery of Anticancer Drugs. *Biomacromolecules* **2014**, 15, (3), 900-907.
92. Loh, X. J.; del Barrio, J.; Toh, P. P. C.; Lee, T. C.; Jiao, D. Z.; Rauwald, U.; Appel, E. A.; Scherman, O. A., Triply Triggered Doxorubicin Release From Supramolecular Nanocontainers. *Biomacromolecules* **2012**, 13, (1), 84-91.
93. Kuang, H. H.; He, H. Y.; Zhang, Z. Y.; Qi, Y. X.; Xie, Z. G.; Jinga, X. B.; Huang, Y. B., Injectable and biodegradable supramolecular hydrogels formed by nucleobase-terminated poly(ethylene oxide)s and alpha-cyclodextrin. *J. Mater. Chem. B* **2014**, 2, (6), 659-667.
94. Shi, J. B.; Guobao, W.; Chen, H. L.; Zhong, W.; Qiu, X. Z.; Xing, M. M. Q., Schiff based injectable hydrogel for in situ pH-triggered delivery of doxorubicin for breast tumor treatment. *Polym. Chem.* **2014**, 5, (21), 6180-6189.
95. Xiong, L.; Luo, Q.; Wang, Y.; Li, X.; Shen, Z.; Zhu, W., An injectable drug-loaded hydrogel based on a supramolecular polymeric prodrug. *Chem. Commun.* **2015**, 51, (78), 14644-14647.
96. Serra, L.; Domenech, J.; Peppas, N. A., Drug transport mechanisms and release kinetics from molecularly designed poly(acrylic acid-g-ethylene glycol) hydrogels. *Biomaterials* **2006**, 27, (31), 5440-5451.
97. Siepmann, J.; Peppas, N. A., Modeling of drug release from delivery systems based on hydroxypropyl methylcellulose (HPMC). *Adv. Drug Deliver Rev.* **2012**, 64, 163-174.
98. Siepmann, J.; Peppas, N. A., Higuchi equation: Derivation, applications, use and misuse. *Int. J. Pharm.* **2011**, 418, (1), 6-12.
99. Li, D.; Li, Y. B.; Xing, H. B.; Guo, J. L.; Ping, Y.; Tang, G. P., Synergistic Enhancement of Lung Cancer Therapy Through Nanocarrier-Mediated Sequential

- Delivery of Superantigen and Tyrosin Kinase Inhibitor. *Adv. Funct. Mater.* **2014**, 24, (35), 5482-5492.
100. Yoon, H. Y.; Son, S.; Lee, S. J.; You, D. G.; Yhee, J. Y.; Park, J. H.; Swierczewska, M.; Lee, S.; Kwon, I. C.; Kim, S. H.; Kim, K.; Pomper, M. G., Glycol chitosan nanoparticles as specialized cancer therapeutic vehicles: Sequential delivery of doxorubicin and Bcl-2 siRNA. *Sci. Rep.* **2014**, 4:6878.
101. Wang, W. W.; Song, H. J.; Zhang, J.; Li, P.; Li, C.; Wang, C.; Kong, D. L.; Zhao, Q., An injectable, thermosensitive and multicompartiment hydrogel for simultaneous encapsulation and independent release of a drug cocktail as an effective combination therapy platform. *J. Controlled Release* **2015**, 203, 57-66.
102. Barczyk, K.; Kreuter, M.; Pryjma, J.; Booy, E. P.; Maddika, S.; Ghavami, S.; Berdel, W. E.; Roth, J.; Los, M., Serum cytochrome c indicates in vivo apoptosis and can serve as a prognostic marker during cancer therapy. *Int. J. Cancer* **2005**, 116, (2), 167-173.
103. Santra, S.; Kaittanis, C.; Perez, J. M., Cytochrome c Encapsulating Theranostic Nanoparticles: A Novel Bifunctional System for Targeted Delivery of Therapeutic Membrane-Impermeable Proteins to Tumors and Imaging of Cancer Therapy. *Mol. Pharmaceut.* **2010**, 7, (4), 1209-1222.
104. Kim, S. K.; Foote, M. B.; Huang, L., The targeted intracellular delivery of cytochrome C protein to tumors using lipid-apolipoprotein nanoparticles. *Biomaterials* **2012**, 33, (15), 3959-3966.
105. Tang, Y. X.; Teng, Z. G.; Liu, Y.; Tian, Y.; Sun, J.; Wang, S. J.; Wang, C. Y.; Wang, J. D.; Lu, G. M., Cytochrome C capped mesoporous silica nanocarriers for pH-sensitive and sustained drug release. *J. Mater. Chem. B* **2014**, 2, (27), 4356-4362.
106. Siepmann, J.; Siepmann, F., Mathematical modeling of drug delivery. *Int. J. Pharm.* **2008**, 364, (2), 328-343.
107. Fu, Y.; Kao, W. J., Drug release kinetics and transport mechanisms of non-degradable and degradable polymeric delivery systems. *Expert Opin. Drug Del.* **2010**, 7, (4), 429-444.
108. Lu, D.; Wientjes, M. G.; Lu, Z.; Au, J. L. S., Tumor priming enhances delivery and efficacy of nanomedicines. *J. Pharmacol. Exp. Ther.* **2007**, 322, (1), 80-88.
109. Lu, Z.; Tsai, M.; Lu, D.; Wang, J.; Wientjes, M. G.; Au, J. L. S., Tumor-Penetrating Microparticles for Intraperitoneal Therapy of Ovarian Cancer. *J. Pharmacol. Exp. Ther.* **2008**, 327, (3), 673-682.
110. Baumann, M. D.; Kang, C. E.; Stanwick, J. C.; Wang, Y. F.; Kim, H.; Lapitsky, Y.; Shoichet, M. S., An injectable drug delivery platform for sustained combination therapy. *J. Controlled Release* **2009**, 138, (3), 205-213.
111. Sasisekharan, R.; Shriver, Z.; Venkataraman, G.; Narayanasami, U., Roles of heparan-sulphate glycosaminoglycans in cancer. *Nat. Rev. Cancer* **2002**, 2, (7), 521-528.
112. Liang, Y.; Kiick, K. L., Heparin-functionalized polymeric biomaterials in tissue engineering and drug delivery applications. *Acta Biomater.* **2014**, 10, (4), 1588-1600.
113. Herrera-Gayol, A.; Jothy, S., Effect of Hyaluronan on Xenotransplanted Breast Cancer. *Exp. Mol. Pathol.* **2002**, 72, (3), 179-185.

114. Tan, S.; Li, X.; Guo, Y.; Zhang, Z., Lipid-enveloped hybrid nanoparticles for drug delivery. *Nanoscale* **2013**, 5, (3), 860-872.
115. Krishnamurthy, S.; Vaiyapuri, R.; Zhang, L.; Chan, J. M., Lipid-coated polymeric nanoparticles for cancer drug delivery. *Biomater. Sci.* **2015**, 3, (7), 923-936.
116. Raemdonck, K.; Braeckmans, K.; Demeester, J.; De Smedt, S. C., Merging the best of both worlds: hybrid lipid-enveloped matrix nanocomposites in drug delivery. *Chem. Soc. Rev.* **2014**, 43, (1), 444-472.

Chapter 4

MULTIFUNCTIONAL LIPID-COATED POLYMER NANOGELS CROSSLINKED BY PHOTO-TRIGGERED MICHAEL-TYPE ADDITION

4.1 Introduction

Nanotechnology has had significant impact on the development of nanoscale vehicles and devices in the field of drug delivery and tissue engineering,¹⁻⁵ and many types of nanoparticles have been developed over the past few decades, including inorganic nanoparticles, lipid-based carriers, and polymeric nanostructures (e.g., polymer-drug conjugates and block copolymer micelles).^{6, 7} While metallic nanoparticles provide opportunities for magnetic resonance imaging (MRI)⁸ or photothermal therapy,⁹ they are not biodegradable and many are not small enough to be cleared from circulation easily, which may lead to long-term toxicity due to potential accumulation in the body. Polymeric nanoparticulate systems have attracted much attention as potential drug carriers due to enhanced therapeutic efficacy that is imparted by improvements in the solubility of hydrophobic drugs, extension of circulation half-life, reduction of immunogenicity, and sustained drug release.^{10, 11} In addition, nanoparticles that are responsive to external stimuli such as pH,¹² light,^{13, 14} temperature,^{15, 16} magnetic fields,¹⁷ and ultrasound¹⁸ have also been developed to achieve on-demand/triggered drug release.¹⁹ Particularly, nanoparticles are “small” enough (10-150 nm) to passively accumulate in specific tissues (e.g., tumors) through the enhanced permeability and retention (EPR) effect and sufficiently “large” (high

surface area-to-volume ratios) for surface functionalization with specific ligands to actively target the site of disease.^{7, 20-23}

Many polymeric nanoparticles are based on non-covalent assembly, which may render their structure unstable and lead to subsequent loss of drug when circulating in large volumes of biological fluids.²⁴⁻²⁶ To address these concerns, crosslinked polymer nanogels with improved stability have been developed.²⁷⁻³² Composed of highly crosslinked hydrophilic polymer chains, nanogels maintain structural integrity even under dilute conditions. Due to their gel-like structures, nanogels have a high degree of porosity that allows efficient encapsulation of therapeutic molecules.³³ In addition, the high water content and mechanical softness of nanogels may enhance their biocompatibility and positively impact cellular uptake and biodistribution.³⁴⁻³⁶ Nanogels have thus emerged as promising materials for the delivery of a wide range of therapeutic molecules including chemotherapeutics,^{29, 31} proteins,^{30, 32} and siRNAs.³³

A major obstacle in the preparation of nanogels is macrogelation, which ultimately promotes bulk gelation (to yield either a microgel or hydrogel).³⁷ Many procedures have been employed to avoid macrogelation during crosslinking, including microemulsion/inverse microemulsion polymerization methods.³⁸ In these approaches, each droplet of polymer solution serves as a nanoreactor, permitting isolated crosslinking of each droplet and the facile incorporation of bioactive molecules.³⁹ However, the necessary use of organic solvents in the formation of the emulsions can be detrimental for the therapeutic cargo.⁴⁰ Alternatively, preparation of nanogels from nanotemplates such as liposomes largely avoids the use of organic solvents during chemical crosslinking,⁴¹ as hydrogels are formed in the aqueous lumen of the liposome. In addition, the use of liposomes generally permits better control over the size of the

resulting nanogels, given the uniformity of liposome populations and the simplicity of the manipulation of their size via extrusion methods.⁴²

Although the preparation of nanogels using liposome-templated methods is a common approach,⁴³⁻⁴⁹ most reported strategies are based on radical polymerization of vinyl monomers/methacrylated macromers or ionic crosslinking of alginate, which exerts less control of network development and may result in heterogeneous network structures. While Michael-type addition reactions have been widely used as a crosslinking strategy for hydrogel preparation under mild, physiologically relevant conditions,^{50, 51} they have not been as commonly employed in the field of nanogel synthesis,⁵² owing to their spontaneous reaction kinetics.⁵³ The application of photolabile protecting groups and photo-catalyzed chemistries provides spatial and temporal regulation of the physical and chemical properties of materials.⁵⁴⁻⁵⁷ The photocleavage reaction has been widely used in photodegradable crosslinkers,⁵⁸⁻⁶⁰ side chain functionalization of photoresponsive block copolymers,⁶¹⁻⁶³ and photo-activated bioconjugates.⁶⁴⁻⁶⁷ Recently, photolabile chemistry has also been utilized as a strategy for light-triggered crosslinking of alginate hydrogels, which displayed improved mechanical properties and homogeneity.⁶⁸ The application of these strategies to yield photolabile, protected precursors for Michael-type additions would permit the light-dependent production of homogeneous network structures with more precise control of the reaction, which would thus expand the utility of Michael-type additions in the synthesis of nanogels.

We report here the production of novel lipid-coated polymer nanogels, which are crosslinked by photo-triggered Michael-type additions of thiols and maleimides, via liposome-templated methods. Specifically, photolabile *o*-nitrobenzyl protecting groups

have been employed to protect PEG-thiols and to thus permit triggering of nanogel formation upon photo-irradiation; the *o*-nitrobenzyl groups undergo photoisomerization into *o*-nitrosobenzaldehyde upon irradiation with UV light, releasing free thiols for subsequent crosslinking reactions with maleimides.^{54, 69} The photo-triggered chemistry provides temporal control of the reaction and avoids macroscale gelation during nanogel synthesis, while the lipid coating offers additional functional features to the nanogels by preventing burst release of therapeutic molecules and providing surface versatility. The photo-triggered gelation of bulk hydrogels was monitored via oscillatory rheology and the size distribution and colloidal stability of the nanogels were measured via dynamic light scattering and electrophoretic light scattering, respectively. The morphology and size of the nanogels were confirmed via transmission electron microscopy (TEM). The chemical reactivity of the nanogels was probed via their modification with a fluorescent dye. Owing to the ability to control degradation of the resulting polymeric networks, these nanogels have potential application as targeted drug-delivery vehicles and imaging probes.

4.2 Materials and Methods

4.2.1 Materials

Four-arm, thiol-functionalized PEG (PEG-SH, Mn 10000 g/mol) and four-arm, maleimide-functionalized PEG (PEG-Mal, Mn 10000 g/mol) were purchased from JenKem Technology USA Inc. (Allen, TX, USA). 1- α -Phosphatidylcholine from egg (egg-PC), cholesterol, *o*-nitrobenzyl bromide, N-(3-dimethylaminopropyl)-N'-ethylcarbodiimide hydrochloride (EDC·HCl) and N-hydroxysulfosuccinimide (sulfo-

NHS) were purchased from Sigma-Aldrich (St. Louis, MO, USA). DSPE-PEG2000 carboxylic acid was purchased from Nanocs Inc. (New York, NY, USA). 1-Aminomethylpyrene hydrochloride was purchased from AnaSpec Inc. (Fremont, CA, USA). All other reagents and materials were purchased from Fisher Scientific unless otherwise noted (Pittsburgh, PA, USA). ¹H NMR spectra were acquired under standard quantitative conditions at ambient temperature on a Bruker AV400 NMR spectrometer (Billerica, MA, USA). All samples were dissolved in CDCl₃.

4.2.2 Synthesis of Photolabile, Protected PEG-SH

Four-arm PEG-SH, protected with *o*-nitrobenzyl groups, was synthesized via previously published methods, with some modifications.^{62,70} Four-arm thiol-terminated PEG (150 mg) was dissolved in 5 mL of DMF, and then neutralized with 100 μL TEA. The solution was cooled down to 0 °C and a solution of 2-nitrobenzyl bromide (50 mg in 5 mL acetone) was added dropwise over 15 min. The reaction mixture was stirred vigorously at 0 °C for 1 h and then at room temperature for 24 h. The resulting solution was dialyzed against DI water for 24 hrs (MWCO 1000) and then lyophilized to afford a white powder product. The functionality of the resulting polymers was determined via ¹H NMR (in CDCl₃), with an average value of 71 ± 5%. ¹H NMR (Fig. S1) (400 MHz, CDCl₃) δ 7.99 (d, 4H, Ar), 7.55 (dd, 8H, Ar), 7.45 (d, 4H, Ar), 4.17 (s, 8H, CH₂), 3.90-3.40 (d, 900H, CH₂CH₂O), 2.64 (t, 8H, CH₂).

4.2.3 Bulk Gel Preparation via Photo-Triggered Michael-type Addition and Subsequent Rheological Analysis

The PEG hydrogel was prepared by the photo-triggered Michael-type addition of protected PEG-SH and PEG-Mal (at a final concentration of 5 wt% or 15 wt%). The solution was well mixed by vortexing and then was exposed for 2 hours to UV light

(365nm; Black-Ray[®] mercury lamp) at an intensity of 10 mW/cm². Oscillatory rheology experiments conducted on a stress-controlled AR-G2 rheometer (TA Instruments, New Castle, DE, USA) were used to characterize the photo-triggered cross-linking and subsequent mechanical properties of the bulk PEG hydrogels. Experiments were conducted at room temperature using an 8 mm-diameter, steel plate geometry with 100 μ m gap distance, with oscillatory time, frequency and strain sweeps performed. Strain sweeps were performed on samples from 0.1% to a maximum strain of 1000% to determine the limit of the linear viscoelastic region. Dynamic oscillatory time sweeps were collected at angular frequencies of 6 rad/s and 1% strain chosen from the linear viscoelastic region. Rheological properties were examined by frequency sweep experiments ($\omega = 0.1$ to 100 rad/s) at a fixed strain amplitude of 1%. The protected PEG-SH and PEG-Mal precursors were dissolved in water separately with a concentration of 15 wt%. The precursors were then combined, vortexed, and loaded onto the rheometer stage. Hydrogels were formed by exposing the solution to UV light continuously for 2 hours (365 nm at 10 mW/cm²; OmniCure[®] S2000, 200 W UV lamp with bandpass filters and high power fiber light guide) or periodically by shuttering the light (365 nm at 10 mW/cm²; light on for 5 min, light off for 20 min); the G' and G'' values were monitored throughout the crosslinking experiments.

4.2.4 Synthesis of Lipid-Coated Nanogels (NG)

A chloroform solution (1 mL) with 5 mg egg-PC and 0.5 mg of cholesterol was placed in a round-bottom flask, with evaporation of the chloroform under nitrogen flushing to yield a thin film of the lipid that was then dried under vacuum overnight at room temperature to remove organic solvent. A 15 wt% PEG solution was prepared by dissolving 75 mg PEG-Mal and 75 mg *o*-nitrobenzyl-protected PEG-SH in 1 mL DI

water; this solution was used to hydrate to the lipid film, with ten alternating cycles of 30s vortexing and 5 min quiescent incubation at room temperature.⁴⁸ The solution was then sonicated for 30 min to completely solubilize the lipid. The resulting multilamellar liposomes were extruded 20 times through a 0.8 μm polycarbonate membrane (Whatman, Piscataway, NJ, USA), 20 times through a 0.2 μm membrane, and finally 21 times through a 0.1 μm membrane using an Avanti[®] Mini-Extruder (Avanti Polar Lipids Inc., Alabaster, AL, USA). The resulting unilamellar liposomes were then diluted 5 times (to avoid macroscale gelation upon UV irradiation). The solutions were irradiated under UV light (365nm) for 2 hours with a light intensity of 10 mW/cm². The nanogels were stored at 4°C until further use.

4.2.5 Surface Functionalization of Lipid-Coated Nanogels

Chloroform solution (1 mL) with 4 mg egg-PC, 1mg DSPE-PEG₂₀₀₀-COOH and 0.5 mg cholesterol was placed in a round-bottom flask, with nitrogen flushing and drying to yield a thin film. Carboxylic-acid-functionalized liposomes, and then lipid-coated nanogels (COOH-NGs), were produced as described above and stored at 4°C until further use. A solution of COOH-NG (1 mL, 1.2 mg/mL) was then added to EDC/sulfo-NHS solution (50mM EDC and 25mM sulfo-NHS dissolved in phosphate buffer pH=7.2) to yield a total final volume of 2.5 mL. The solution was stirred for 45 min at 4°C to activate the carboxylic acid groups and then 0.5 mg 1-aminomethylpyrene (dissolved in 50 μL DMSO) was added dropwise to achieve a final dye concentration of 0.2 mg/mL. The solution was subsequently stirred for 4 hours at room temperature. The resulting dye-conjugated nanogels (dye-conjugated NGs, 2.5 mL) were then dialyzed against 2 L water overnight and washed 3 times with water at 4,000 rpm for 20 min using Amicon Ultra-15 Centrifugal Filter Units (MWCO: 30kDa, Millipore,

Billerica, MA) to remove unconjugated dye molecules. The emission fluorescence spectrum of the dye-conjugated nanogels was measured from 350-600 nm with a slit width of 1.5 nm (after excitation at 333 nm with a slit width of 3 nm) using a HORIBA Jobin Yvon SPEX FluoroMax-4 spectrofluorometer. Microscopy images of the fluorescently labeled NGs were obtained via confocal laser scanning microscopy (CLSM, Zeiss, 510 NLO, Germany). A COOH-NG control was prepared under identical reaction conditions and procedures, without the coupling reagents, to confirm that non-reacted dye was removed under the reported conditions.

4.2.6 Dynamic Light Scattering (DLS) and Zeta Potential Analysis

The average size and size distribution of the nanogels were analyzed via dynamic light scattering (DLS) and the zeta potential determined via analysis of light scattering on a Malvern Zetasizer Nano ZS apparatus with Malvern Instruments DTS software (v.6.01) (Malvern Instruments, UK). The analyses were conducted on solutions of the nanogels in DI water and at 25°C. For the stability measurement, analyses were conducted in PBS buffer at different temperatures. The mean hydrodynamic diameter of the nanogels (d_h) was computed from the intensity of the scattered light using the Malvern software package based on the theory of Brownian motion and the Stokes-Einstein equation. The zeta potential of the nanogels was analyzed using the electrophoretic light scattering spectrophotometer of the instrument.

4.2.7 Transmission Electron Microscopy (TEM) Characterization of Nanogel Morphology

Transmission electron microscopy (TEM) images were acquired using a FEI Tecnai-12 microscope operating at an accelerating voltage of 120 kV. Images were collected on a Gatan CCD camera. TEM samples were prepared by applying a drop of

nanogel solution ($\sim 3 \mu\text{L}$) onto a carbon-coated copper TEM grid (300 mesh size). The excess solution was wicked away after 1 min using a piece of filter paper. A droplet of 1% phosphotungstic acid aqueous solution ($\sim 3 \mu\text{L}$) was then added onto the grid and wicked away after 1 min using a piece of filter paper. The samples were dried under room temperature for 3 hours before imaging.

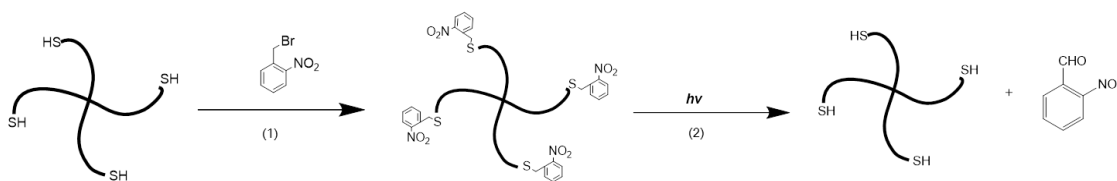


Figure 4.1 Schematic of the protection of 4-arm PEG-thiol with photolabile groups: 1) DMF, 24h, R.T.; 2) water, 365nm, 10 mW/cm².

4.3 Results and Discussion

4.3.1 Photodeprotection and Photo-Triggered Gelation

The photolabile, protected PEG-SH was synthesized as shown in Figure 4.1. The thiols from the PEG chains were protected by the photolabile *o*-nitrobenzyl groups to yield *o*-nitrobenzyl thioether moieties. ¹H NMR spectroscopy was used to confirm the functionality of the polymer protection by *o*-nitrobenzyl groups. The data shown in Figure 4.2 indicate the presence of both aromatic protons (7.4-8.0 ppm) of the *o*-nitrobenzyl group, and the ethylene protons (3.4-3.9 ppm) of the polymer, which is consistent with results reported in similar photoprotection systems.^{65, 69-71} Based on the integration of the aromatic and ethylene group protons, a functionality of $71 \pm 5\%$ was obtained; this functionality was consistently obtained across multiple syntheses. Upon

UV irradiation, the *o*-nitrobenzyl groups undergo photoisomerization into *o*-nitrosobenzaldehyde, releasing free thiols for subsequent *in situ* Michael-type additions.

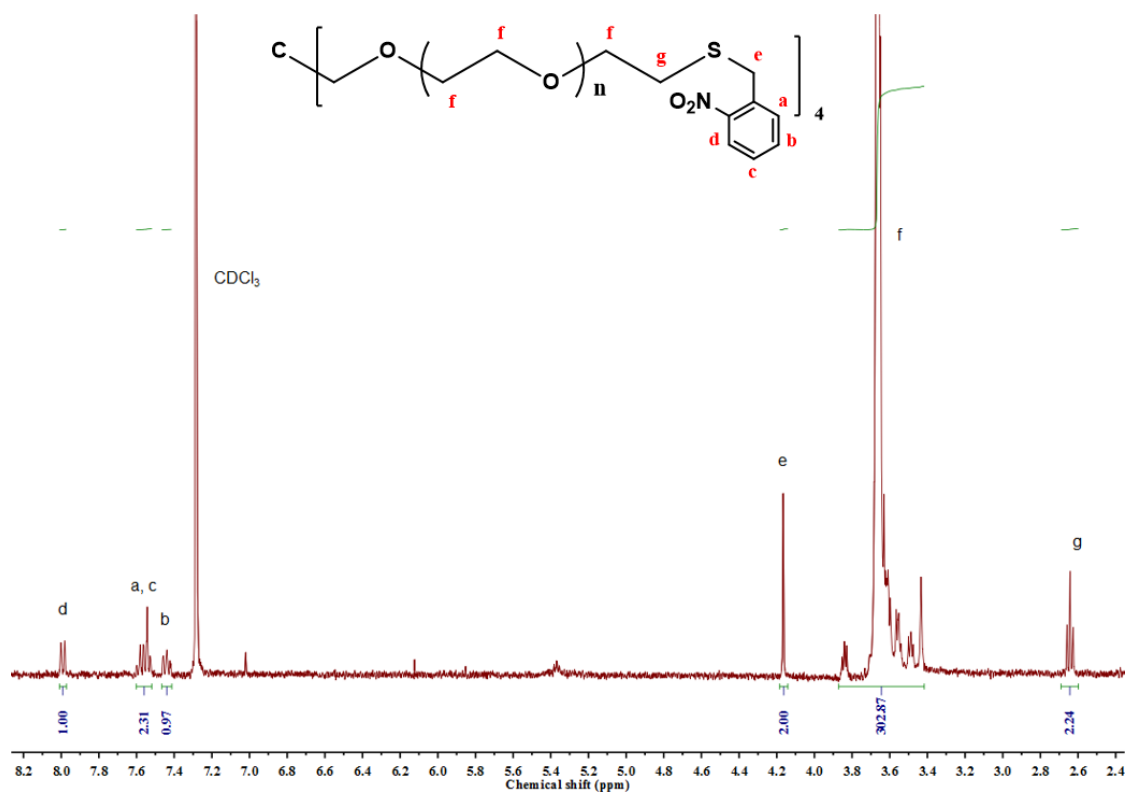


Figure 4.2 ^1H NMR spectrum of four-arm thiolated PEG protected with the nitrobenzyl group. Functionality is calculated based on the integration of the aromatic protons of the protecting group relative to the methylene protons of the polymer.

during network development (Figure 4.4). The data in Figure 4.4a show that homogeneous solutions of protected PEG-SH and PEG-Mal in water did not exhibit any increase in the elastic modulus (G') before UV irradiation, while the Michael-type addition between thiol and maleimide usually occur within seconds under similar conditions.^{50, 72} After 5 min irradiation, a rapid increase in G' was observed, confirming gelation and supporting the expected photo-triggered crosslinking mechanism.

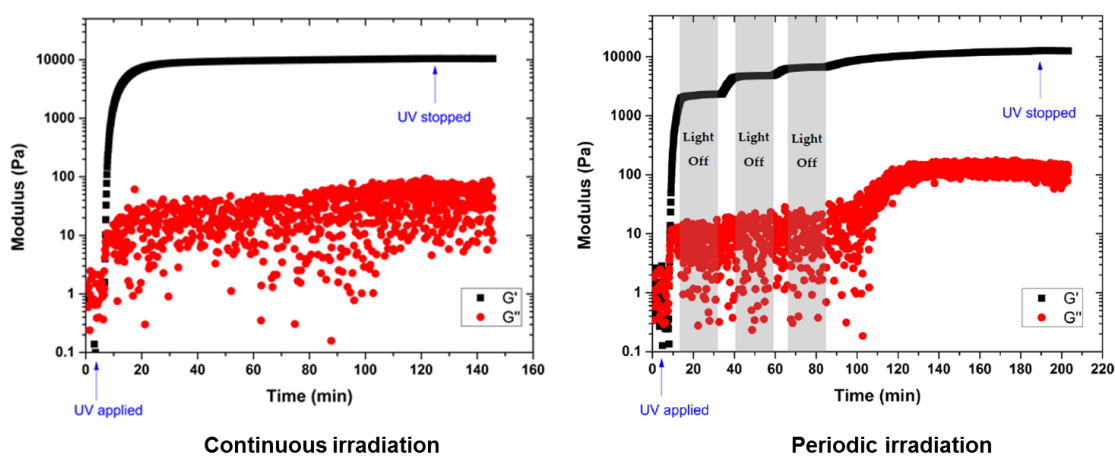


Figure 4.5 Oscillatory rheology time sweeps of 15wt% PEG hydrogels formed by photo-triggered Michael-type addition (plotted in log scale).

The rheology results are also plotted in log scale as shown in Figure 4.5, to better show that the viscous modulus (G'') remained essentially unchanged before UV irradiation and ultimately increased to approximately 100 Pa when irradiation was completed. The slow increase of G' at later time points during the measurement is likely a result of some continued polymerization (owing to the slow deprotection kinetics) and in part due to the radical polymerization of remaining PEG-Mal functional groups that have not yet reacted with thiol.⁷³ In order to demonstrate that the crosslinking reaction

between thiol and maleimide groups occurs mainly as a result of UV exposure, the polymerization was interrupted at approximately 15, 40 and 65 min, for a period of 20 min each time, simply by shuttering the UV light source. The data in Figure 4.4b illustrate that little or no increase in elastic modulus was observed during the periods when there is no UV irradiation, indicating the temporal control of this light-dependent crosslinking strategy. Similar to other light-dependent thiol-ene polymerization strategies as those previously reported by Bowman, Anseth and co-workers,⁷⁴ the photo-triggered Michael-type addition might also have significant potential in the preparation of biomimetic hydrogels. The temporal control achieved by this strategy would allow premixing and appropriate positioning (e.g., in a tissue defect) of hydrogel precursors prior to crosslinking. The spatial control enabled by this chemistry, while not investigated here, might extend the capability of Michael-type additions to create patterned devices, materials and structures.

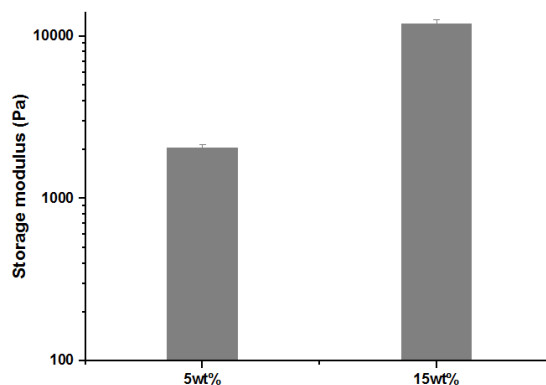


Figure 4.6 Comparison of storage moduli of PEG-SH/Mal hydrogels at different concentrations, after irradiation at 365 nm, 10 mW/cm² in aqueous solution, characterized via oscillatory rheology.

It should be noted that the mechanical properties of these hydrogels can be readily tuned not only by varying UV irradiation time, but also by changing polymer concentration. As is shown in Figure 4.6, an expected increase in elastic modulus was observed upon an increase in polymer concentration. Specifically, the measured G' of the 5 wt% gels is 2 kPa, while that of the 15 wt% gels increased to approximately 12 kPa. Such changes in hydrogel properties with variation in crosslinking density have been regularly employed to modify the delivery properties of various hydrogels, which could be potentially applied to these nanogel systems.^{50, 75}

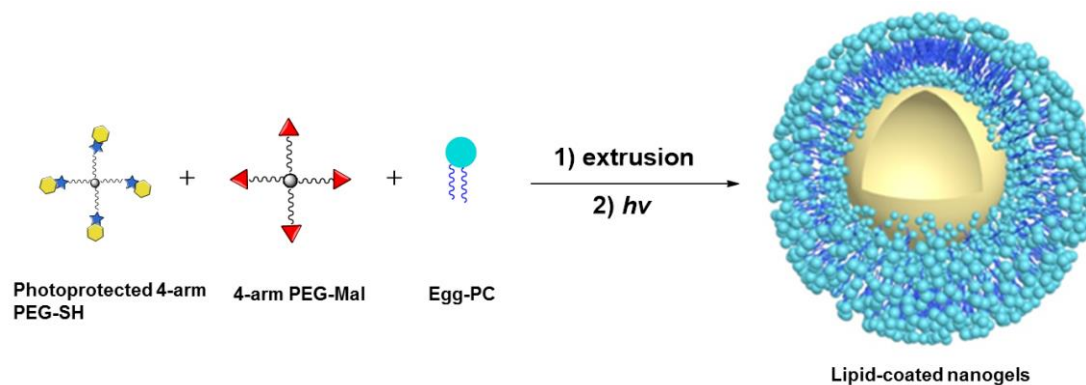


Figure 4.7 Schematic representation of the synthesis of PEG-based nanogels via liposome templates in aqueous solutions. 1) DI water, polycarbonate membrane; 2) 2h, 365 nm, 10 mW/cm².

4.3.2 Synthesis and Characterization of Lipid-Coated Nanogels (NGs)

The lipid-coated PEG nanogels were prepared via a liposome-templated method as shown in Figure 4.7. Upon hydration of a lipid thin film with the polymer solutions, multilamellar liposomes form with hydrogel precursors encapsulated in the aqueous lumen. By extrusion of the multilamellar liposome suspension through polycarbonate

membranes of specific pore size, small unilamellar liposomes with well-defined size distribution can be prepared.⁴⁴ The solutions of the unilamellar liposomes, prepared via these accepted strategies, were then diluted to prevent the potential macrogelation of any unencapsulated precursors outside the liposomes. After UV irradiation, precursors were crosslinked by photo-triggered Michael-type addition inside the lipid vesicles, forming lipid-coated nanogels.

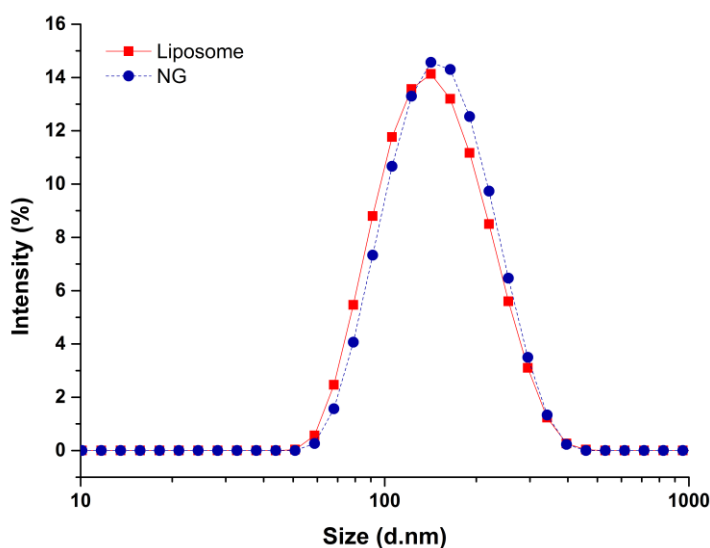


Figure 4.8 Dynamic light scattering analysis of the hydrodynamic size of liposomes and lipid-coated nanogels in water at room temperature.

The hydrodynamic diameter and surface charge of the lipid-coated nanogels in aqueous solution were determined via dynamic light scattering (DLS) and zeta potential measurements, respectively. As is shown in Figure 4.8, the lipid-coated nanogels have an average diameter of 160 nm with a polydispersity index (PDI) of 0.25, which is very

close to that of the liposomes prepared under the same conditions (154 nm, PDI 0.14). The similarity in size between the lipid-coated nanogels and liposomes confirmed the successful use of the template to form nanogels of prescribed size as expected based on the use of other liposome-templated nanogel systems.^{42, 45} For example, work reported by An *et al.* demonstrated the size control and monodispersity of nanogels prepared from liposome templates by varying the polycarbonate membrane with specific pore sizes. The lipid-coated nanogels exhibited slightly negative zeta potentials (-7.1 mV), which may be attributed to the lipid layer since the surface charge of bare nanogels became neutral when the lipid layer was removed by detergent such as Triton X-100 (data not shown). Work reported by Wang *et al.*⁷⁶ also indicated that conventional liposomes composed of egg-PC and cholesterol (2:1 molar ratio) demonstrate a zeta potential value of -2.7 mV (average diameter: 110nm), which is in good agreement with our results. Retention of the lipid layer offers advantages for the subsequent use of these hydrogel nanoparticles; the slight negative charge introduced by the lipid layer should improve the stability of the nanogels in solution (and in circulation) by preventing self-aggregation and non-specific cellular uptake, based on electrostatic repulsion.^{77, 78}

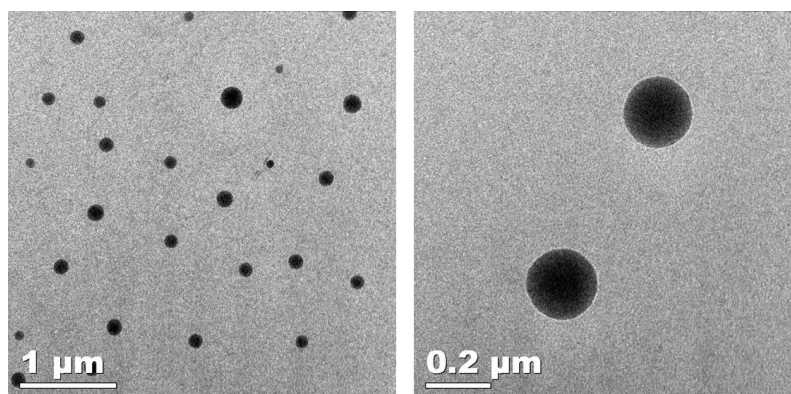


Figure 4.9 TEM images of the lipid-coated nanogels dried from aqueous solution.

The morphology of the lipid-coated nanogels dried from aqueous solution was confirmed via transmission electron microscopy (TEM); representative data from these experiments are shown in Figure 4.9. As illustrated in the images, the lipid-coated nanogels showed a reasonably well-defined spherical morphology. The average diameter of the nanogels (calculated from analysis of the TEM images by ImageJ) is 130 ± 30 nm, which is in good agreement with results obtained from the DLS measurements presented in Figure 4.8. The relatively smaller size observed from the TEM images compared with DLS results is likely due to the dehydration of the nanogels during the TEM sample preparation, which has been commonly observed.^{30, 31, 79}

The stability of these nanogels under physiologically-relevant buffer conditions was evaluated via DLS at different temperatures. The data shown in Figure 4.10 indicate that changes in hydrodynamic size of the nanogels upon temperature changes are almost negligible between 25°C to 50°C, suggesting their stability against aggregation at physiological temperatures and also suggesting a lack of detectable network degradation (which would result in a swelling of the gel). The nanogel solutions were also stable and showed no significant aggregation for several months when stored at 4°C.

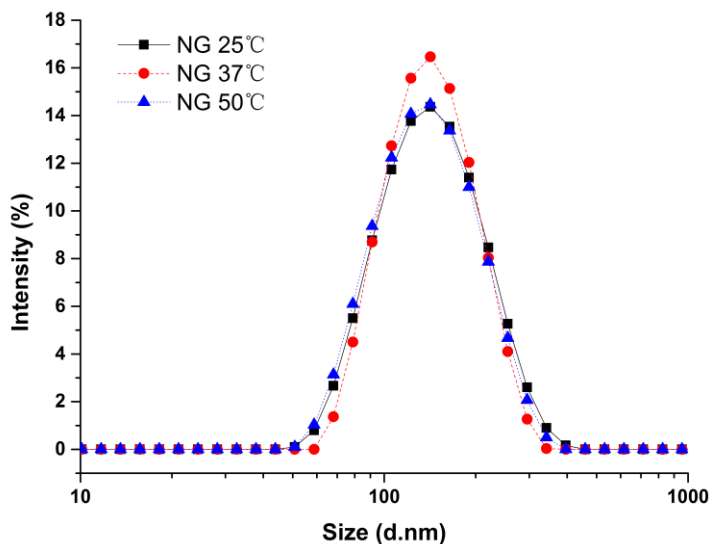


Figure 4.10 Dynamic light scattering analysis of the hydrodynamic size of lipid-coated nanogels in PBS at different temperatures.

4.3.3 Surface Functionalization of Lipid-coated Nanogels

Owing to their high surface area-to-volume ratio, the therapeutic effect of nanoparticles can be enhanced by surface modification with ligands that allow targeting of specific tissues and/or fluorescence imaging.^{7, 80} To examine the potential suitability of these lipid-coated nanogels for such applications, carboxylic lipid-coated nanogels (COOH-NGs) composed of PEG based nanogels and a mixture of egg-PC and DSPE-PEG₂₀₀₀-COOH in a 4:1 ratio (w/w) were formulated. Poly(ethylene glycol) (PEG) on nanogel surfaces has been demonstrated to prolong circulation and improve evasion of immune clearance.⁸¹ A reactive fluorescent dye, 1-aminomethylpyrene, was then introduced onto the surface of the COOH-NGs via an EDC/sulfo-NHS coupling reaction to yield dye-conjugated nanogels (dye-conjugated NGs) (Figure 4.11).

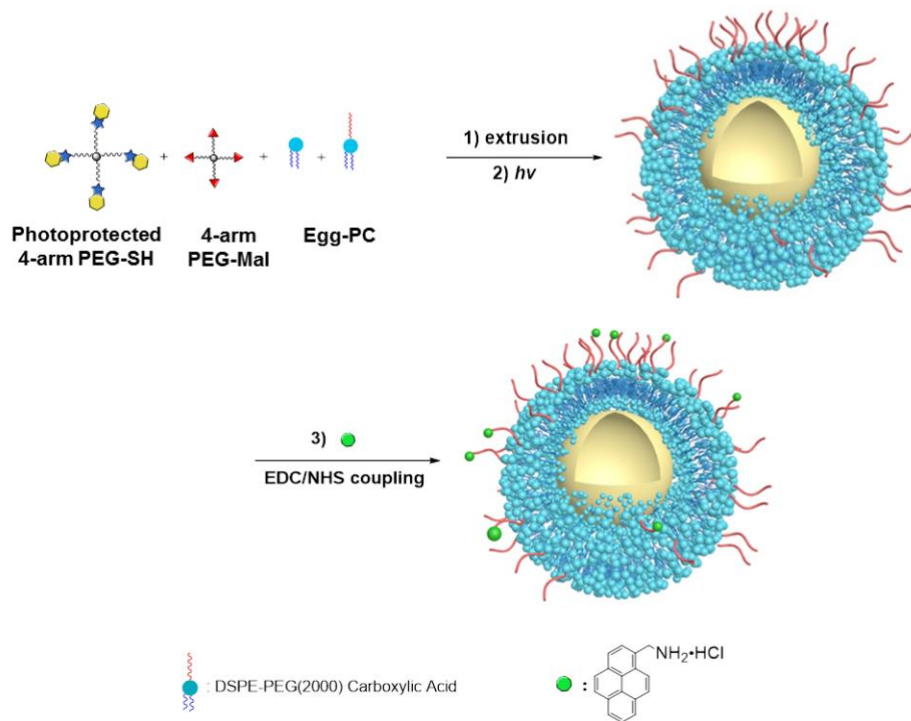


Figure 4.11 Schematic representation of the synthesis of carboxylic-acid-functionalized, lipid-coated nanogels and the surface conjugation of a reactive fluorescent dye. 1) DI water, polycarbonate membrane; 2) 2h, 365 nm, 10 mW/cm²; 3) EDC/sulfo-NHS solution, 1-aminomethylpyrene (dissolved in DMSO), pH = 7.2, 4h, R.T..

A control experiment was performed on COOH-NGs under identical conditions and procedures, without the coupling reagents, to demonstrate that unconjugated pyrene can be removed under such conditions. The chemical conjugation of pyrene was confirmed by fluorescence spectroscopy; data from these experiments are presented in Figure 4.12. As illustrated in the data, the COOH-NGs control showed no obvious fluorescence emission from 425 nm to 525 nm, while the solution of dye-conjugated nanogels displayed the characteristic excimer emissions of pyrene molecules at approximately 450 nm and 490 nm.⁸²⁻⁸⁴

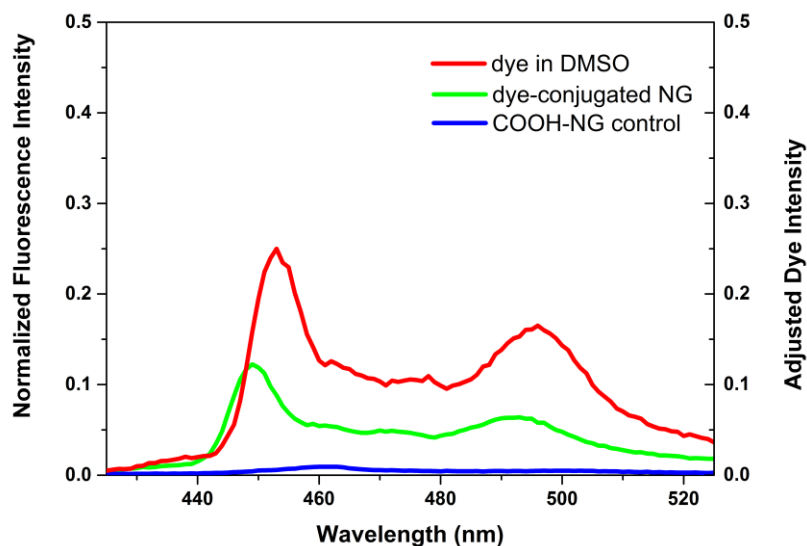


Figure 4.12 Fluorescence spectra of carboxylic-acid-functionalized, lipid-coated nanogels and dye-conjugated nanogels in aqueous solution; $\lambda_{exc}=333$ nm, 20°C; spectra of nanogels were normalized to the *o*-nitrosobenzaldehyde peak at 360 nm, which should be of similar intensity for the various nanogels.

The emission from the dye-conjugated NGs closely matches the spectrum of pyrene dissolved in DMSO, suggesting that the chromophore remains intact after conjugation. These results illustrate that pyrene has been covalently conjugated to the surface of nanogels via EDC/sulfo-NHS coupling; the fact that no significant signal was observed in the same region from the COOH-NGs control demonstrates that unbound pyrene molecules were removed under these experimental conditions.

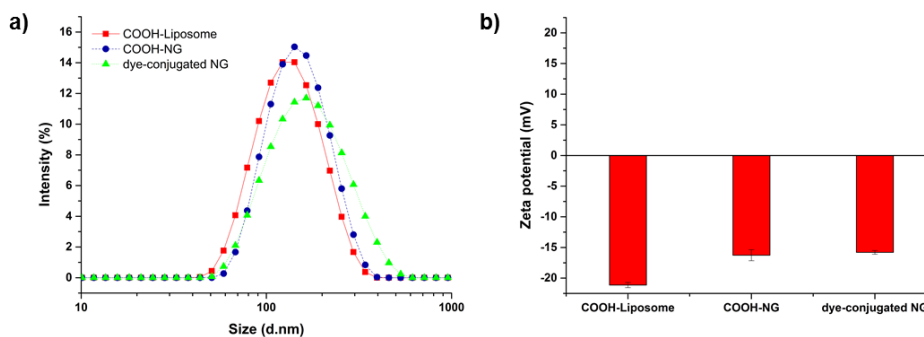


Figure 4.13 Dynamic light scattering and zeta potential analysis of functional lipid-coated nanogels. Size distribution (a) and surface charge density (b) of carboxylic-acid-functionalized liposomes, carboxylic-acid-functionalized lipid-coated nanogels and dye-conjugated nanogels in water at room temperature.

The hydrodynamic diameter and surface charge of the COOH-NGs and dye-conjugated NGs in aqueous solution were also measured by dynamic light scattering (DLS) and electrophoretic light scattering, respectively, as shown in Figure 4.13. The COOH-NGs have an average diameter of 156 nm with a PDI of 0.17, which closely matches that of the COOH-functionalized liposome (141 nm, PDI: 0.12), as expected. The size analysis of the dye-conjugated NGs revealed that they have an average diameter of 181 nm with a PDI of 0.23, illustrating the lack of significant change in hydrodynamic diameter after conjugation of the dye. The slight increase in size could be explained by slight swelling of the nanogels due to the retention of a small amount of DMSO from the reaction (Figure 4.13a).³¹ As shown in Figure 4.13b, the COOH-NGs exhibit a slightly greater negative surface charge (-16.3 mV) than the NGs, as expected owing to the presence of the carboxylic acid group. The negative zeta potential of dye-conjugated NGs (-15.8 mV) became only slightly less negative after the

conjugation of pyrene, which is likely due to the relatively low coupling efficiency of EDC-mediated reactions at pH = 7.2.⁸⁵

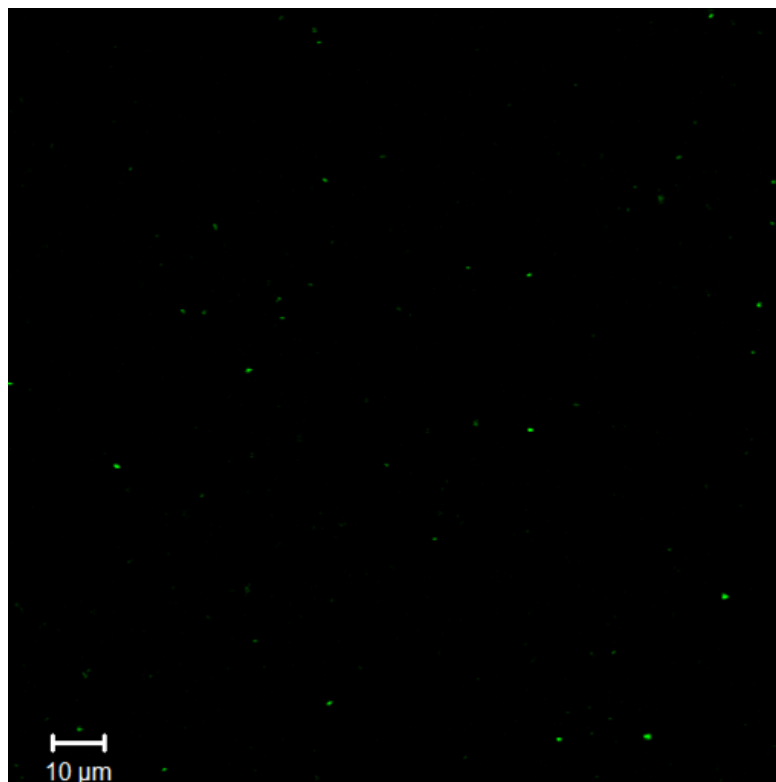


Figure 4.14 Fluorescence microscopy image of dye-conjugated nanogels in aqueous solution, characterized by confocal laser scanning microscopy (CLSM).

The surface modification was also confirmed via fluorescence microscopy of the pyrene-modified NGs; a representative image from confocal laser scanning microscopy is shown in Figure 4.14. As shown in the figure, the dye-conjugated nanogels appear as individual green dots on the dark background, while no green particles were observed in the fluorescence microscopy image of the COOH-NG control (data not shown). Work recently reported by Singh *et al.*³² also confirmed the conjugation of

carboxyfluorescein-labeled model peptide to nanogels and the removal of unbound peptide via similar methods. Consistent with this report, these confocal microscopy data are consistent with the spectroscopy data and confirm the successful conjugation of pyrene. These results also suggest that the nanogels likely have the capacity to be functionalized with a broad range of biomolecules to enhance therapeutic efficacy.

In contrast to traditional radical-chain-growth photo-polymerization of polymers modified with acrylate or methacrylate moieties, formation of hydrogels via the step-growth mechanism of Michael-type addition may afford networks of greater homogeneity and improved mechanical integrity.⁸⁶ Also, compared to step-growth thiol-ene chemistry⁷⁴ and the recently developed photocaged amine-catalyzed thiol-Michael addition,⁵⁶ the photolabile-protection strategy of thiol groups permits triggering of subsequent crosslinking reactions without the addition of any initiators or catalysts, and might thus positively affect the integrity and bioactivity of encapsulated therapeutic agents. In addition to the *o*-nitrobenzyl moiety employed here, similar photolabile-protection of thiols or amines could be achieved by coumarin and *p*-methoxyphenacyl moieties.^{66, 67, 71} Therefore, this photo-triggered Michael-type addition crosslinking strategy provides an initiator/catalyst-free photo-crosslinking method for polymer network formation with the associated advantages of homogeneity and spatiotemporal control, potentially diversifying the uses for the photo-mediated click reaction toolbox.

Compared with other existing nanogel systems, the lipid-coated nanogels synthesized from photo-triggered Michael-type addition in this report provide mild reaction conditions during and control of the network development, offering new strategies in the design of nanogel materials. The surface charge and functionality introduced by the lipid coating may increase circulation stability and offer versatility of

the nanogels in multiple applications, making them promising candidates as nanoparticle therapeutics.

As stimuli-triggered drug delivery systems are becoming more and more attractive, several chemically labile linkages have been employed in the synthesis of nanogels to allow on-demand or targeted release of therapeutic molecules.^{30-32, 75, 79} In particular, our group has exploited the reversibility of Michael-type reactions in the presence of glutathione (GSH), a thiol-containing tripeptide localized in cellular compartments or tumor microenvironments.⁸⁷ Hydrogels prepared with arylthiol-modified PEGs based on thiol-maleimide Michael-type addition showed significantly more rapid degradation under conditions similar to those in intracellular compartments and tumor microenvironments (10 mM GSH) than under reducing conditions in blood circulation (10 μ M GSH).⁷² Therefore, the incorporation of these GSH-responsive arylthiol-maleimide linkages in nanogel synthesis suggests potential opportunities in the development of nanoparticles for intracellular or targeted delivery of therapeutics with increased stability in blood circulation. Considering the hydrophilic nature of these nanogels, hydrophilic drugs and proteins could be incorporated into these systems via physical encapsulation or chemical conjugation. Our ongoing studies have also preliminarily shown that these nanogels have higher drug encapsulation efficiency compared to liposome carriers due to their crosslinked network structure. Investigations of such nanogel systems with stimuli responsiveness are underway and will be the subject of future reports.

4.4 Conclusions

Novel, well-defined lipid-coated polymer nanogels were successfully synthesized via photo-triggered Michael-type addition using liposome templates. The nanotemplate method offers facile control of the size of the nanogels and mild synthetic conditions. The photo-triggered crosslinking and temporal control achieved by these chemical strategies, confirmed by oscillatory rheology experiments, permit the synthesis of these nanogel templates and suggest opportunities for expanding the toolbox for photo-triggered Michael-type additions and patterning bulk gels via these methods. Through surface modification with functional ligands such as targeting moieties and cell penetration peptides, these nanogels provide a promising platform for nanoparticle therapeutics.

REFERENCES

1. Farokhzad, O. C.; Langer, R., Impact of Nanotechnology on Drug Delivery. *ACS Nano* **2009**, 3, (1), 16-20.
2. Shi, J. J.; Votruba, A. R.; Farokhzad, O. C.; Langer, R., Nanotechnology in Drug Delivery and Tissue Engineering: From Discovery to Applications. *Nano Lett.* **2010**, 10, (9), 3223-3230.
3. Riehemann, K.; Schneider, S. W.; Luger, T. A.; Godin, B.; Ferrari, M.; Fuchs, H., Nanomedicine--challenge and perspectives. *Angew Chem Int Ed Engl* **2009**, 48, (5), 872-97.
4. Shi, J. J.; Xiao, Z. Y.; Kamaly, N.; Farokhzad, O. C., Self-Assembled Targeted Nanoparticles: Evolution of Technologies and Bench to Bedside Translation. *Acc. Chem. Res.* **2011**, 44, (10), 1123-1134.
5. Dvir, T.; Timko, B. P.; Kohane, D. S.; Langer, R., Nanotechnological strategies for engineering complex tissues. *Nat. Nanotechnol.* **2011**, 6, (1), 13-22.
6. Lammers, T.; Hennink, W. E.; Storm, G., Tumour-targeted nanomedicines: principles and practice. *Brit J Cancer* **2008**, 99, (3), 392-397.
7. Davis, M. E.; Chen, Z.; Shin, D. M., Nanoparticle therapeutics: an emerging treatment modality for cancer. *Nat. Rev. Drug Discov.* **2008**, 7, (9), 771-782.
8. Gao, J. H.; Gu, H. W.; Xu, B., Multifunctional Magnetic Nanoparticles: Design, Synthesis, and Biomedical Applications. *Acc. Chem. Res.* **2009**, 42, (8), 1097-1107.
9. Murphy, C. J.; Gole, A. M.; Stone, J. W.; Sisco, P. N.; Alkilany, A. M.; Goldsmith, E. C.; Baxter, S. C., Gold Nanoparticles in Biology: Beyond Toxicity to Cellular Imaging. *Acc. Chem. Res.* **2008**, 41, (12), 1721-1730.
10. Gref, R.; Minamitake, Y.; Peracchia, M. T.; Trubetskoy, V.; Torchilin, V.; Langer, R., Biodegradable Long-Circulating Polymeric Nanospheres. *Science* **1994**, 263, (5153), 1600-1603.
11. Langer, R., Drug delivery and targeting. *Nature* **1998**, 392, (6679), 5-10.
12. Gao, W. W.; Chan, J. M.; Farokhzad, O. C., pH-Responsive Nanoparticles for Drug Delivery. *Mol Pharmaceut* **2010**, 7, (6), 1913-1920.
13. Yan, B.; Boyer, J.-C.; Branda, N. R.; Zhao, Y., Near-Infrared Light-Triggered Dissociation of Block Copolymer Micelles Using Upconverting Nanoparticles. *J Am Chem Soc* **2011**, 133, (49), 19714-19717.
14. Tong, R.; Hemmati, H. D.; Langer, R.; Kohane, D. S., Photoswitchable Nanoparticles for Triggered Tissue Penetration and Drug Delivery. *J. Am. Chem. Soc.* **2012**, 134, (21), 8848-8855.

15. Wei, H.; Zhang, X.-Z.; Zhou, Y.; Cheng, S.-X.; Zhuo, R.-X., Self-assembled thermoresponsive micelles of poly(N-isopropylacrylamide-b-methyl methacrylate). *Biomaterials* **2006**, 27, (9), 2028-2034.
16. Nakayama, M.; Okano, T.; Miyazaki, T.; Kohori, F.; Sakai, K.; Yokoyama, M., Molecular design of biodegradable polymeric micelles for temperature-responsive drug release. *J Control Release* **2006**, 115, (1), 46-56.
17. de Cogan, F.; Booth, A.; Gough, J. E.; Webb, S. J., Spatially controlled apoptosis induced by released nickel(ii) within a magnetically responsive nanostructured biomaterial. *Soft Matter* **2013**, 9, (7), 2245-2253.
18. Gao, Z.-G.; Fain, H. D.; Rapoport, N., Controlled and targeted tumor chemotherapy by micellar-encapsulated drug and ultrasound. *J Control Release* **2005**, 102, (1), 203-222.
19. Timko, B. P.; Dvir, T.; Kohane, D. S., Remotely Triggerable Drug Delivery Systems. *Adv Mater* **2010**, 22, (44), 4925-4943.
20. Peer, D.; Karp, J. M.; Hong, S.; Farokhzad, O. C.; Margalit, R.; Langer, R., Nanocarriers as an emerging platform for cancer therapy. *Nat. Nanotechnol.* **2007**, 2, (12), 751-760.
21. Ferrari, M., Cancer nanotechnology: Opportunities and challenges. *Nat. Rev. Cancer* **2005**, 5, (3), 161-171.
22. Maeda, H.; Wu, J.; Sawa, T.; Matsumura, Y.; Hori, K., Tumor vascular permeability and the EPR effect in macromolecular therapeutics: a review. *J Control Release* **2000**, 65, (1-2), 271-284.
23. Byrne, J. D.; Betancourt, T.; Brannon-Peppas, L., Active targeting schemes for nanoparticle systems in cancer therapeutics. *Adv. Drug Deliver Rev.* **2008**, 60, (15), 1615-1626.
24. Bae, Y. H.; Yin, H., Stability issues of polymeric micelles. *J. Controlled Release* **2008**, 131, (1), 2-4.
25. Kim, S.; Shi, Y. Z.; Kim, J. Y.; Park, K.; Cheng, J. X., Overcoming the barriers in micellar drug delivery: loading efficiency, in vivo stability, and micelle-cell interaction. *Expert Opin. Drug Del.* **2010**, 7, (1), 49-62.
26. Jiwanich, S.; Ryu, J. H.; Bickerton, S.; Thayumanavan, S., Noncovalent Encapsulation Stabilities in Supramolecular Nanoassemblies. *J Am Chem Soc* **2010**, 132, (31), 10683-10685.
27. Ryu, J.-H.; Chacko, R. T.; Jiwanich, S.; Bickerton, S.; Babu, R. P.; Thayumanavan, S., Self-Cross-Linked Polymer Nanogels: A Versatile Nanoscopic Drug Delivery Platform. *J. Am. Chem. Soc.* **2010**, 132, (48), 17227-17235.
28. Heller, D. A.; Levi, Y.; Pelet, J. M.; Doloff, J. C.; Wallas, J.; Pratt, G. W.; Jiang, S.; Sahay, G.; Schroeder, A.; Schroeder, J. E.; Chyan, Y.; Zurenko, C.; Querbes, W.; Manzano, M.; Kohane, D. S.; Langer, R.; Anderson, D. G., Modular 'Click-in-Emulsion' Bone-Targeted Nanogels. *Adv. Mater.* **2013**, 25, (10), 1449-1454.
29. Chen, Y.; Wilbon, P. A.; Zhou, J. H.; Nagarkatti, M.; Wang, C. P.; Chu, F. X.; Tang, C. B., Multifunctional self-fluorescent polymer nanogels for label-free imaging and drug delivery. *Chem. Commun.* **2013**, 49, (3), 297-299.

30. Azagarsamy, M. A.; Alge, D. L.; Radhakrishnan, S. J.; Tibbitt, M. W.; Anseth, K. S., Photocontrolled Nanoparticles for On-Demand Release of Proteins. *Biomacromolecules* **2012**, 13, (8), 2219-2224.
31. Li, M. Q.; Tang, Z. H.; Sun, H.; Ding, J. X.; Song, W. T.; Chen, X. S., pH and reduction dual-responsive nanogel cross-linked by quaternization reaction for enhanced cellular internalization and intracellular drug delivery. *Polym. Chem.* **2013**, 4, (4), 1199-1207.
32. Singh, S.; Topuz, F.; Hahn, K.; Albrecht, K.; Groll, J., Embedding of Active Proteins and Living Cells in Redox-Sensitive Hydrogels and Nanogels through Enzymatic Cross-Linking. *Angew. Chem. Int. Ed.* **2013**, 52, (10), 3000-3003.
33. Smith, M. H.; Lyon, L. A., Multifunctional Nanogels for siRNA Delivery. *Accounts Chem Res* **2012**, 45, (7), 985-993.
34. Beningo, K. A.; Wang, Y. L., Fc-receptor-mediated phagocytosis is regulated by mechanical properties of the target. *J Cell Sci* **2002**, 115, (4), 849-856.
35. Banquy, X.; Suarez, F.; Argaw, A.; Rabanel, J.-M.; Grutter, P.; Bouchard, J.-F.; Hildgen, P.; Giasson, S., Effect of mechanical properties of hydrogel nanoparticles on macrophage cell uptake. *Soft Matter* **2009**, 5, (20), 3984-3991.
36. Merkel, T. J.; Jones, S. W.; Herlihy, K. P.; Kersey, F. R.; Shields, A. R.; Napier, M.; Luft, J. C.; Wu, H. L.; Zamboni, W. C.; Wang, A. Z.; Bear, J. E.; DeSimone, J. M., Using mechanobiological mimicry of red blood cells to extend circulation times of hydrogel microparticles. *P Natl Acad Sci USA* **2011**, 108, (2), 586-591.
37. Yallapu, M. M.; Jaggi, M.; Chauhan, S. C., Design and engineering of nanogels for cancer treatment. *Drug Discovery Today* **2011**, 16, (9-10), 457-463.
38. Nayak, S.; Lyon, L. A., Soft Nanotechnology with Soft Nanoparticles. *Angew. Chem. Int. Ed.* **2005**, 44, (47), 7686-7708.
39. Klinger, D.; Landfester, K., Photo-sensitive PMMA microgels: light-triggered swelling and degradation. *Soft Matter* **2011**, 7, (4), 1426-1440.
40. Raemdonck, K.; Demeester, J.; De Smedt, S., Advanced nanogel engineering for drug delivery. *Soft Matter* **2009**, 5, (4), 707-715.
41. Sasaki, Y.; Akiyoshi, K., Nanogel engineering for new nanobiomaterials: from chaperoning engineering to biomedical applications. *The Chemical Record* **2010**, 10, (6), 366-376.
42. An, S. Y.; Bui, M. P. N.; Nam, Y. J.; Han, K. N.; Li, C. A.; Choo, J.; Lee, E. K.; Katoh, S.; Kumada, Y.; Seong, G. H., Preparation of monodisperse and size-controlled poly(ethylene glycol) hydrogel nanoparticles using liposome templates. *J. Colloid Interface Sci.* **2009**, 331, (1), 98-103.
43. Kazakov, S.; Kaholek, M.; Teraoka, I.; Levon, K., UV-induced gelation on nanometer scale using liposome reactor. *Macromolecules* **2002**, 35, (5), 1911-1920.
44. Kazakov, S.; Kaholek, M.; Kudasheva, D.; Teraoka, I.; Cowman, M. K.; Levon, K., Poly(N-isopropylacrylamide-co-1-vinylimidazole) hydrogel nanoparticles prepared and hydrophobically modified in liposome reactors: Atomic force microscopy and dynamic light scattering study. *Langmuir* **2003**, 19, (19), 8086-8093.

45. Van Thienen, T. G.; Lucas, B.; Flesch, F. M.; van Nostrum, C. F.; Demeester, J.; De Smedt, S. C., On the Synthesis and Characterization of Biodegradable Dextran Nanogels with Tunable Degradation Properties. *Macromolecules* **2005**, *38*, (20), 8503-8511.
46. Schillemans, J. P.; Flesch, F. M.; Hennink, W. E.; van Nostrum, C. F., Synthesis of Bilayer-Coated Nanogels by Selective Cross-Linking of Monomers inside Liposomes. *Macromolecules* **2006**, *39*, (17), 5885-5890.
47. Van Thienen, T. G.; Raemdonck, K.; Demeester, J.; De Smedt, S. C., Protein Release from Biodegradable Dextran Nanogels. *Langmuir* **2007**, *23*, (19), 9794-9801.
48. Park, J.; Wrzesinski, S. H.; Stern, E.; Look, M.; Criscione, J.; Ragheb, R.; Jay, S. M.; Demento, S. L.; Agawu, A.; Limon, P. L.; Ferrandino, A. F.; Gonzalez, D.; Habermann, A.; Flavell, R. A.; Fahmy, T. M., Combination delivery of TGF-beta inhibitor and IL-2 by nanoscale liposomal polymeric gels enhances tumour immunotherapy. *Nat. Mater.* **2012**, *11*, (10), 895-905.
49. Hong, J. S.; Vreeland, W. N.; DePaoli Lacerda, S. H.; Locascio, L. E.; Gaitan, M.; Raghavan, S. R., Liposome-templated supramolecular assembly of responsive alginate nanogels. *Langmuir* **2008**, *24*, (8), 4092-4096.
50. Nie, T.; Baldwin, A.; Yamaguchi, N.; Kiick, K. L., Production of heparin-functionalized hydrogels for the development of responsive and controlled growth factor delivery systems. *J Control Release* **2007**, *122*, (3), 287-296.
51. Nie, T.; Akins, R. E.; Kiick, K. L., Production of heparin-containing hydrogels for modulating cell responses. *Acta Biomater* **2009**, *5*, (3), 865-875.
52. Scott, E. A.; Nichols, M. D.; Cordova, L. H.; George, B. J.; Jun, Y. S.; Elbert, D. L., Protein adsorption and cell adhesion on nanoscale bioactive coatings formed from poly(ethylene glycol) and albumin microgels. *Biomaterials* **2008**, *29*, (34), 4481-4493.
53. Oh, J. K.; Drumright, R.; Siegwart, D. J.; Matyjaszewski, K., The development of microgels/nanogels for drug delivery applications. *Progress in Polymer Science* **2008**, *33*, (4), 448-477.
54. Zhao, H.; Sterner, E. S.; Coughlin, E. B.; Theato, P., o-Nitrobenzyl Alcohol Derivatives: Opportunities in Polymer and Materials Science. *Macromolecules* **2012**, *45*, (4), 1723-1736.
55. Adzima, B. J.; Tao, Y. H.; Kloxin, C. J.; DeForest, C. A.; Anseth, K. S.; Bowman, C. N., Spatial and temporal control of the alkyne-azide cycloaddition by photoinitiated Cu(II) reduction. *Nat. Chem.* **2011**, *3*, (3), 256-259.
56. Xi, W. X.; Krieger, M.; Kloxin, C. J.; Bowman, C. N., A new photoclick reaction strategy: photo-induced catalysis of the thiol-Michael addition via a caged primary amine. *Chem. Commun.* **2013**, *49*, (40), 4504-4506.
57. Thomas, S. W., New Applications of Photolabile Nitrobenzyl Groups in Polymers. *Macromol Chem Phys* **2012**, *213*, (23), 2443-2449.
58. Kloxin, A. M.; Kasko, A. M.; Salinas, C. N.; Anseth, K. S., Photodegradable Hydrogels for Dynamic Tuning of Physical and Chemical Properties. *Science* **2009**, *324*, (5923), 59-63.

59. Kloxin, A. M.; Tibbitt, M. W.; Anseth, K. S., Synthesis of photodegradable hydrogels as dynamically tunable cell culture platforms. *Nat Protoc* **2010**, 5, (12), 1867-1887.
60. Kloxin, A. M.; Tibbitt, M. W.; Kasko, A. M.; Fairbairn, J. A.; Anseth, K. S., Tunable Hydrogels for External Manipulation of Cellular Microenvironments through Controlled Photodegradation. *Adv. Mater.* **2010**, 22, (1), 61-+.
61. Jiang, J. Q.; Tong, X.; Morris, D.; Zhao, Y., Toward photocontrolled release using light-dissociable block copolymer micelles. *Macromolecules* **2006**, 39, (13), 4633-4640.
62. Liu, G.; Dong, C. M., Photoresponsive Poly(S-(o-nitrobenzyl)-L-cysteine)-b-PEO from a L-Cysteine N-Carboxyanhydride Monomer: Synthesis, Self-Assembly, and Phototriggered Drug Release. *Biomacromolecules* **2012**, 13, (5), 1573-1583.
63. Jiang, X.; Lavender, C. A.; Woodcock, J. W.; Zhao, B., Multiple micellization and dissociation transitions of thermo- and light-sensitive poly(ethylene oxide)-b-poly(ethoxytri(ethylene glycol) acrylate-co-o-nitrobenzyl acrylate) in water. *Macromolecules* **2008**, 41, (7), 2632-2643.
64. Luo, Y.; Shoichet, M. S., A photolabile hydrogel for guided three-dimensional cell growth and migration. *Nat. Mater.* **2004**, 3, (4), 249-253.
65. Luo, Y.; Shoichet, M. S., Light-activated immobilization of biomolecules to agarose hydrogels for controlled cellular response. *Biomacromolecules* **2004**, 5, (6), 2315-2323.
66. Wosnick, J. H.; Shoichet, M. S., Three-dimensional chemical Patterning of transparent hydrogels. *Chem Mater* **2008**, 20, (1), 55-60.
67. Wylie, R. G.; Shoichet, M. S., Two-photon micropatterning of amines within an agarose hydrogel. *J Mater Chem* **2008**, 18, (23), 2716-2721.
68. Cui, J.; Wang, M.; Zheng, Y.; Rodríguez Muñiz, G. M.; del Campo, A., Light-Triggered Cross-Linking of Alginates with Caged Ca²⁺. *Biomacromolecules* **2013**, 14, (5), 1251-1256.
69. Delaittre, G.; Pauloehrl, T.; Bastmeyer, M.; Barner-Kowollik, C., Acrylamide-Based Copolymers Bearing Photoreleasable Thiols for Subsequent Thiol-Ene Functionalization. *Macromolecules* **2012**, 45, (4), 1792-1802.
70. Pauloehrl, T.; Delaittre, G.; Bastmeyer, M.; Barner-Kowollik, C., Ambient temperature polymer modification by in situ phototriggered deprotection and thiol-ene chemistry. *Polym. Chem.* **2012**, 3, (7), 1740-1749.
71. Hensarling, R. M.; Hoff, E. A.; LeBlanc, A. P.; Guo, W.; Rahane, S. B.; Patton, D. L., Photocaged pendent thiol polymer brush surfaces for postpolymerization modifications via thiol-click chemistry. *J Polym Sci Pol Chem* **2013**, 51, (5), 1079-1090.
72. Baldwin, A. D.; Kiick, K. L., Reversible maleimide-thiol adducts yield glutathione-sensitive poly(ethylene glycol)-heparin hydrogels. *Polym Chem-Uk* **2013**, 4, (1), 133-143.
73. Ng, L.-T.; Jönsson, S.; Swami, S.; Lindgren, K., Synthesis of hydrogel for drug delivery studies utilizing photoinitiator-free photopolymerization based on the

- donor/acceptor pair, N-vinylpyrrolidinone and hydroxypentyl maleimide. *Polym. Int.* **2002**, 51, (12), 1398-1403.
74. Fairbanks, B. D.; Schwartz, M. P.; Halevi, A. E.; Nuttelman, C. R.; Bowman, C. N.; Anseth, K. S., A Versatile Synthetic Extracellular Matrix Mimic via Thiol-Norbornene Photopolymerization. *Adv. Mater.* **2009**, 21, (48), 5005-+.
75. Chen, W.; Zheng, M.; Meng, F. H.; Cheng, R.; Deng, C.; Jan, F. J.; Zhong, Z. Y., In Situ Forming Reduction-Sensitive Degradable Nanogels for Facile Loading and Triggered Intracellular Release of Proteins. *Biomacromolecules* **2013**, 14, (4), 1214-1222.
76. Wang, X. Y.; Ishida, T.; Ichihara, M.; Kiwada, H., Influence of the physicochemical properties of liposomes on the accelerated blood clearance phenomenon in rats. *J. Controlled Release* **2005**, 104, (1), 91-102.
77. Tatur, S.; Maccarini, M.; Barker, R.; Nelson, A.; Fragneto, G., Effect of Functionalized Gold Nanoparticles on Floating Lipid Bilayers. *Langmuir* **2013**, 29, (22), 6606-6614.
78. He, C.; Hu, Y.; Yin, L.; Tang, C.; Yin, C., Effects of particle size and surface charge on cellular uptake and biodistribution of polymeric nanoparticles. *Biomaterials* **2010**, 31, (13), 3657-3666.
79. Ding, J. X.; Shi, F. H.; Xiao, C. S.; Lin, L.; Chen, L.; He, C. L.; Zhuang, X. L.; Chen, X. S., One-step preparation of reduction-responsive poly(ethylene glycol)-poly(amino acid)s nanogels as efficient intracellular drug delivery platforms. *Polym Chem-Uk* **2011**, 2, (12), 2857-2864.
80. Petros, R. A.; DeSimone, J. M., Strategies in the design of nanoparticles for therapeutic applications. *Nat. Rev. Drug Discov.* **2010**, 9, (8), 615-627.
81. Huang, C.; Neoh, K. G.; Wang, L.; Kang, E.-T.; Shuter, B., Magnetic nanoparticles for magnetic resonance imaging: modulation of macrophage uptake by controlled PEGylation of the surface coating. *J. Mater. Chem.* **2010**, 20, (39), 8512-8520.
82. Ossipov, D. A.; Yang, X.; Varghese, O.; Kootala, S.; Hilborn, J., Modular approach to functional hyaluronic acid hydrogels using orthogonal chemical reactions. *Chem. Commun.* **2010**, 46, (44), 8368-8370.
83. Li, M.-C.; Ho, R.-M.; Lee, Y.-D., Photo-induced excimer formation of pyrene-labeled polymers for optical recording. *J. Mater. Chem.* **2011**, 21, (8), 2451-2454.
84. Yang, J.-S.; Lin, C.-S.; Hwang, C.-Y., Cu²⁺-Induced Blue Shift of the Pyrene Excimer Emission: A New Signal Transduction Mode of Pyrene Probes. *Org. Lett.* **2001**, 3, (6), 889-892.
85. Freudenberg, U.; Hermann, A.; Welzel, P. B.; Stirl, K.; Schwarz, S. C.; Grimmer, M.; Zieris, A.; Panyanuwat, W.; Zschoche, S.; Meinhold, D.; Storch, A.; Werner, C., A star-PEG-heparin hydrogel platform to aid cell replacement therapies for neurodegenerative diseases. *Biomaterials* **2009**, 30, (28), 5049-5060.
86. Tibbitt, M. W.; Kloxin, A. M.; Sawicki, L. A.; Anseth, K. S., Mechanical Properties and Degradation of Chain and Step-Polymerized Photodegradable Hydrogels. *Macromolecules* **2013**, 46, (7), 2785-2792.

87. Baldwin, A. D.; Kiick, K. L., Tunable Degradation of Maleimide-Thiol Adducts in Reducing Environments. *Bioconjugate Chem.* **2011**, 22, (10), 1946-1953.

Chapter 5

CONCLUSIONS AND FUTURE DIRECTIONS

5.1 Conclusions and Significance

Polyethylene glycol (PEG) hydrogels have been extensively used as matrices for controlling drug delivery due to the versatility of the PEG macromer chemistry and its excellent biocompatibility. In addition, the FDA approval of PEG has propelled the use of PEG hydrogel-based materials in a number of medical products including wound healing matrices, medical implants, and drug delivery depots. Spurred by these advances, the overall goal of this dissertation work is to develop PEG-based hydrogel matrices from bulk to nanoscale with unique physicochemical properties that are tailored to different specific delivery applications, including local delivery, sequential delivery and systemic delivery.

In the first part of this dissertation, hydrophilic and hydrolytically degradable poly (ethylene glycol) (PEG) hydrogels were formed via Michael-type addition and employed for sustained delivery of a monoclonal antibody against the protective antigen of anthrax. Taking advantage of the PEG-induced precipitation of the antibody, burst release from the matrix was avoided. These hydrogels were able to release active antibodies in a controlled manner from 14 days to as long as 56 days *in vitro* by varying the polymer architectures and molecular weights of the precursors. Analysis of the secondary and tertiary structure and the *in vitro* activity of the released antibody showed that the encapsulation and release did not affect the protein conformation or functionality. These hydrolytically degradable PEG hydrogel systems, present a simple

yet efficient strategy to provide protein stabilization and sustained release of protein over an extended period of time, suggesting significant potential of such PEG-based carriers in the long-term delivery of therapeutic molecules.

Subsequently, an advanced, stimuli-responsive hybrid hydrogel system was developed by integrating liposome nanoparticles and PEG polymers into a unifying hydrogel construct. The hybrid hydrogels were prepared by the Michael-type addition of thiols with maleimides, via the use of maleimide-functionalized liposome cross-linkers and thiolated PEG polymers. Gelation of the materials and the liposome-crosslinking strategy were confirmed by oscillatory rheology experiments. These hybrid hydrogels are rendered degradable upon exposure to thiol-containing molecules such as glutathione (GSH), via the incorporation of selected thioether succinimide crosslinks between PEG polymers and liposome nanoparticles. Dynamic light scattering (DLS) characterization confirmed that intact liposomes were released upon network degradation. Owing to the hierarchical structure of the network, multiple cargo molecules relevant for chemotherapies, namely doxorubicin (DOX) and cytochrome c, were encapsulated and simultaneously released from the hybrid hydrogels, with differential release profiles that were driven by degradation-mediated release and Fickian diffusion, respectively. This work introduces a facile approach for the development of glutathione-responsive, liposome-crosslinked hybrid hydrogel system with unique physical and chemical properties that are absent in the individual building block, providing a promising platform for the triggered and temporal release of multiple therapeutic molecules.

Finally, novel, multifunctional lipid-coated polymer nanogels were prepared via the use of liposome templates. With the incorporation of a photolabile *o*-nitrobenzyl

protecting group, an initiator/catalyst-free, photo-triggered, Michael-type addition was employed as the crosslinking method for nanogel network production. The photo-sensitive gelation and temporal control of the crosslinking reaction were confirmed by oscillatory rheology experiments of bulk hydrogels. The production of nanogels was confirmed via dynamic light scattering and transmission electron microscopy. The surface functionality of the lipid-coated nanogels was demonstrated by surface modification with a reactive fluorescent dye. These multifunctional lipid-coated nanogels, given the mild preparation conditions, ease of size control, and versatility of the chemical linkages used as cross-links, have significant potential for use in polymeric nanoparticulate drug delivery systems.

5.2 Future Directions

Recently, on-demand drug delivery is becoming feasible through the design of stimuli-responsive systems that can respond to their microenvironment in a precise and controlled way based on dynamic molecular interactions and reversible chemical linkages.¹⁻³ The glutathione-responsive, retro Michael reaction of arylthioether succinimide linkages explored in the design of liposome-crosslinked hybrid hydrogels in this work could be potentially applied to a wide range of other material platforms for triggered and targeted release applications. Several prospective areas are described below in details.

5.2.1 Dual Responsive PEG-Collagen-Like Peptide Physical Hydrogels

Synthetic collagen-like peptides (CLPs) have been shown to mimic the triple helix conformation of native collagen and exhibit thermally reversible melting

behavior.^{4,5} When heated above their melting temperature (T_m), the CLPs exist as single strands that will completely reform the triple helix structure when cooled down below the melting temperature.⁶ The temperature-sensitive folding of CLP has been employed to create hydrogels with temperature-sensitive macroscopic stability.^{7, 8} Via the conjugation of CLPs to other polymer systems (e.g. PEG), the triple helix formation between different CLP molecules below T_m could lead to the physical crosslinking of the polymer system, forming a self-supporting gel.^{9, 10} The non-covalent crosslinking nature of these systems provides a route to fabricate hydrogel materials with shear-thinning and self-healing properties, enabling minimally invasive injection applications in controlled drug delivery.^{11, 12} Further, reversible, temperature-sensitive gelation can be achieved based on the melting of the triple helical crosslinks. Additionally, the thermal stability of the collagen peptide-polymer hydrogel system can be modulated by varying the CLP sequences.¹³

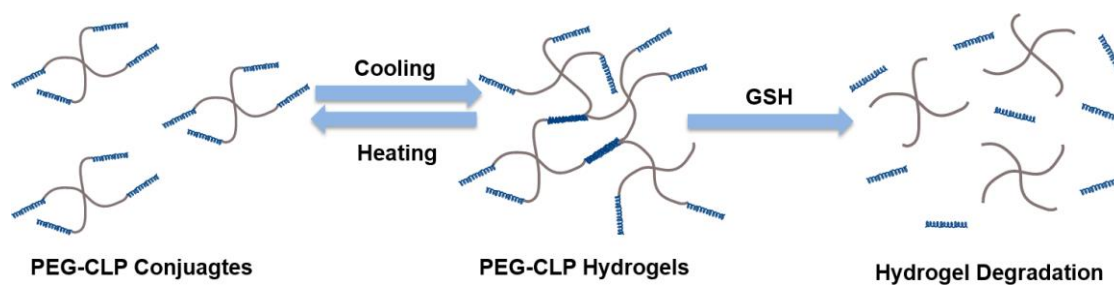


Figure 5.1 Schematic illustration of the thermo-reversible gelling behaviors and chemical degradation of the PEG-CLP physical hydrogels.

With the incorporation of glutathione-sensitive arylthioether succinimide linkages between collagen-like peptides and PEG polymers, dual responsive PEG-CLP physical hydrogels can be developed (Figure 5.1). Similar to other existing PEG-CLP

hybrid systems, the hydrogels can display reversible formation of a liquid-like state near the melting temperature (T_m) of the collagen triple helix. More importantly, the physical crosslinked network can undergo permanent chemical degradation at the presence of glutathione (GSH), allowing targeted delivery of the encapsulated therapeutic molecules and achieving clearance of the device when release is completed.

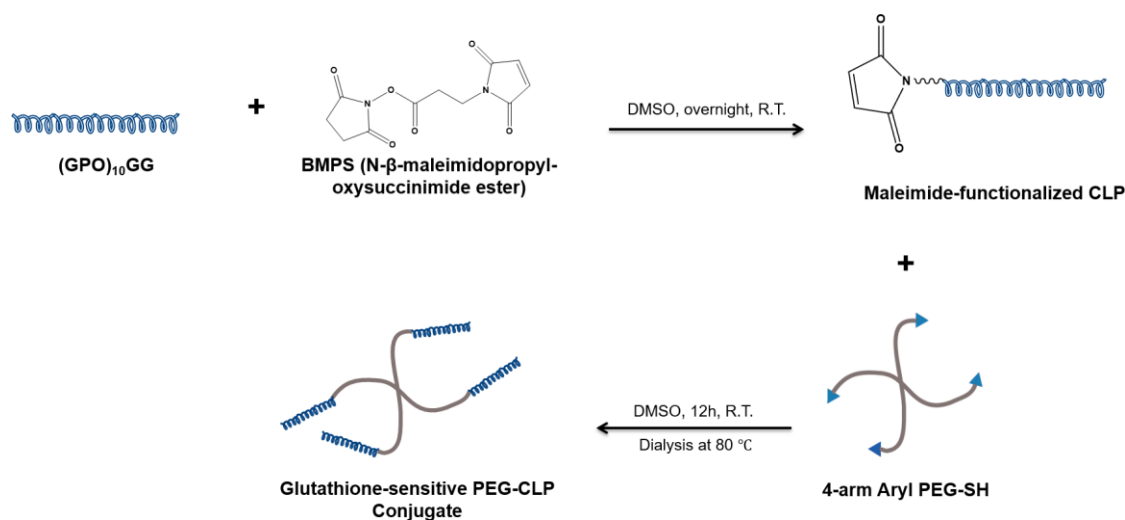


Figure 5.2 Schematic illustration of the synthesis of glutathione(GSH)-sensitive PEG-CLP conjugates.

As shown in Figure 5.2, the design of the dual responsive PEG-CLP hydrogels is based on two major components: 4-arm arylthiolated PEG polymers (20 kDa) and maleimide-functionalized CLPs. Specifically, CLPs with a (GPO)₁₀ sequence (G = glycine, P = proline, O = hydroxyproline) will be modified with maleimide moieties via the NHS ester reaction. The maleimide-functionalized CLPs will be subsequently treated with 4-arm arylthiolated PEG polymers to produce PEG-CLP conjugates via the thiol-maleimide Michael-type addition.

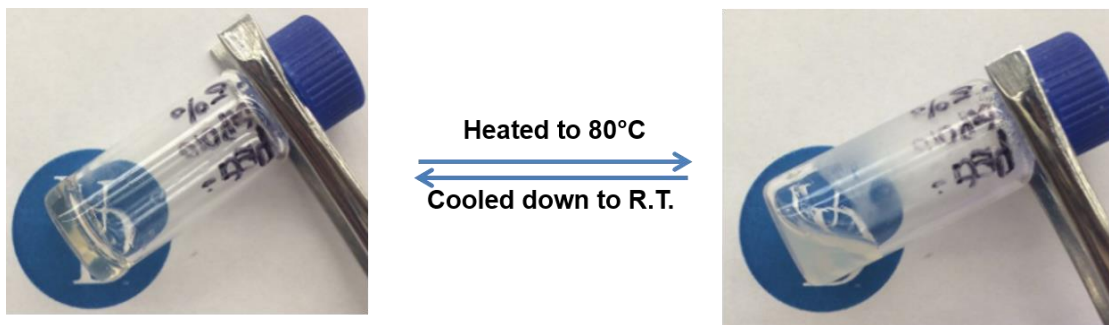


Figure 5.3 Visual inspection of the reversible thermal gelling behaviors of the 5wt% PEG-CLP hydrogels. The hydrogel is weakened into a liquid-like state at 80°C. Upon cooling, the liquid-like state rapidly transforms into a solid-like, self-standing gel.

Preliminary studies of the hydrogels prepared from the resulting peptide-polymer conjugates have shown reversible gelation behaviors when heated above 70°C (the melting temperature of (GPO)₁₀ sequence)¹⁰ and cooled down to room temperature. As shown in Figure 5.3, the triple helices formed by the CLPs on the peptide-polymer conjugates unfold at elevated temperature and completely liquefy at 80°C due to disassembly of the physical crosslinks within the polymer network. Upon cooling, the unfolded CLP population can re-anneal into stable triple helices, forming a self-standing, elastic network. These results illustrate the physical crosslinking nature of the polymer systems based on collagen triple helix structures and suggest opportunities for tuning the degrees of crosslinking and delivery characteristics of the hydrogels at elevated temperatures. Furthermore, the arylthioether succinimide linkages between CLP and PEG can undergo the retro-Michael and thiol-exchange reactions in the presence of GSH, introducing chemo-responsive degradability to this physical-crosslinked network system. Images in Figure 5.4 have shown that the PEG-CLP hydrogels exhibit matrix degradation overnight in 10 mM GSH solutions while remaining stable in PBS under

the same timescale, confirming the GSH-sensitivity of the hydrogels. It is envisioned that the temperature dependent elasticity and the GSH-triggered degradation of the hydrogels could be leveraged to modulate the release properties of the materials and achieve targeted delivery of therapeutic molecules under exogenous (temperature) and endogenous (GSH) stimuli respectively.

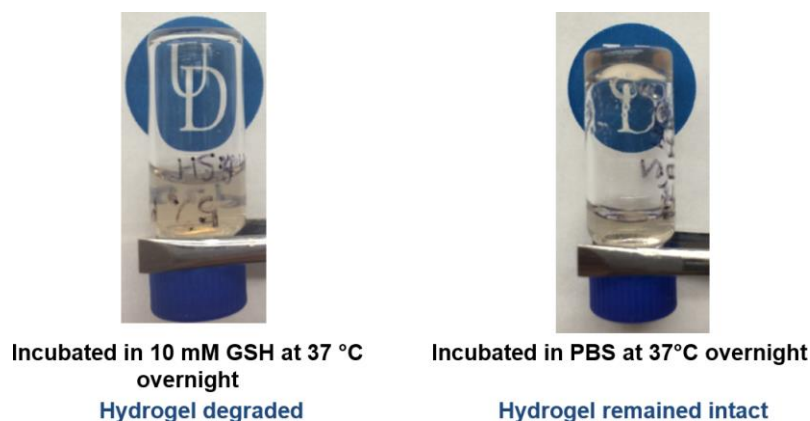


Figure 5.4 Visual inspection of the GSH-triggered degradation of the 5wt% PEG-CLP hydrogels. Matrix degradation is observed in 10 mM GSH solutions after incubation at 37°C overnight whereas the hydrogels remain intact and stable in PBS under the same conditions.

5.2.2 Glutathione(GSH)-Sensitive Crosslinked Liposomes

Owing to their encapsulation capacity, chemical versatility and formulation flexibility, liposomes have become a leading drug delivery platform with a wide range of formulations and products under clinical use, such as Doxil and Myocet.^{14, 15} Recently, crosslinked multilamellar liposomes have been developed to offer stable encapsulation of various proteins and small molecule drugs and achieve a controlled and sustained rate of release over the course of weeks to months.¹⁶⁻¹⁸ Considering the abundance and overproduction of GSH (~10 mM, 1000-fold increase comparing to the concentration

in blood circulation) in tumor microenvironments due to increased cellular proliferation,^{19, 20} the arylthioether succinimide linkages can be used as GSH-sensitive crosslinks within liposomes, offering triggered release characteristics for enhanced therapeutic efficacy. Furthermore, the cleavage rate of the arylthioether succinimide adducts has been demonstrated to be significantly lower than that of the analogous cleavage of disulfide linkages (10-100 times reduction in rate),^{21, 22} enabling expanded timescales of therapeutic release from these nanocarriers. It is anticipated that these GSH-sensitive crosslinked liposomes could serve as a delivery vehicle to transport therapeutics to a tumor via intravenous injection, providing a useful alternative and addition to the locally injectable liposome-crosslinked hybrid hydrogels discussed in Chapter 3.

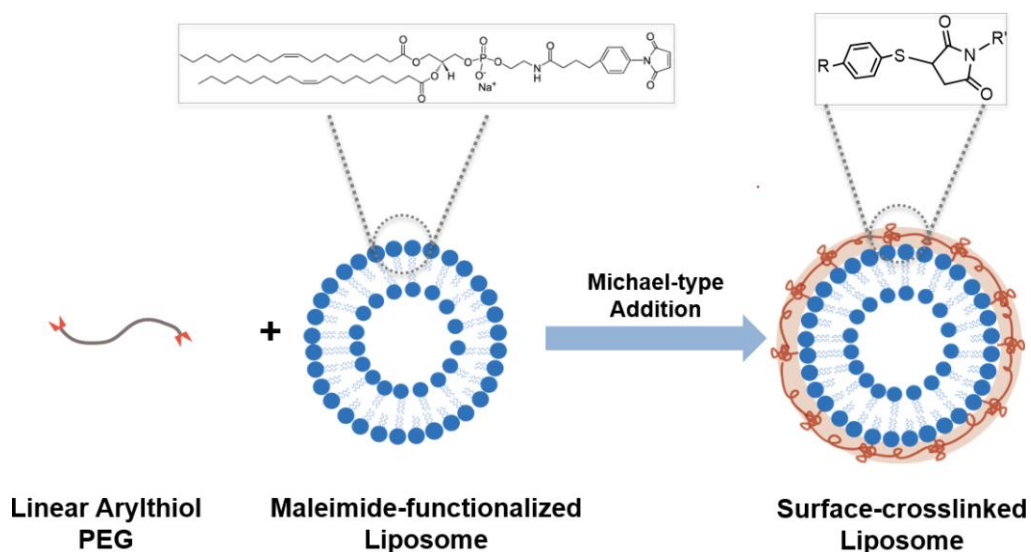


Figure 5.5 Schematic illustration of the design of GSH-sensitive, surface-crosslinked liposomes.

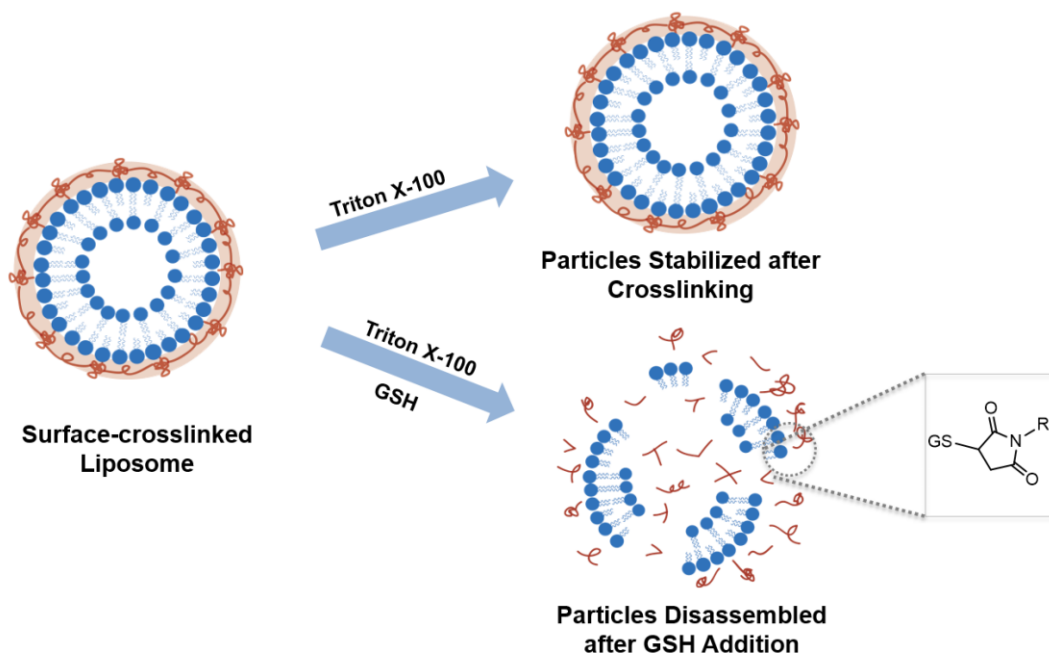


Figure 5.6 Schematic illustration of the stability of surface-crosslinked liposomes against Triton X-100 and GSH-triggered particle disassembly in Triton X-100.

Similar to the formation of liposome-crosslinked hybrid hydrogels, the design of GSH-sensitive, surface-crosslinked liposomes is based on arylthiolated PEG polymers and maleimide-functionalized liposomes. Specifically, linear arylthiolated PEG polymers (3.4 kDa) will be used as crosslinkers to react with maleimide-modified liposomes (1.5 mM) via Michael-type addition (SH:Mal = 2:1 molar ratio), creating a crosslinked polymer layer on the surface of the liposomes (Figure 5.5). Due to the reversibility of the arylthioether succinimide linkages, the crosslinked PEG polymers, which creates a diffusion barrier at the liposome surface, can be degraded in the presence of GSH, achieving triggered and targeted release of therapeutic molecules encapsulated in the liposomes. The successful crosslinking of the liposomes and their

GSH sensitivity will be explored via the addition of Triton X-100, a nonionic detergent that solubilizes lipid bilayers. We hypothesize that the liposomes with surface crosslinking features will remain stable after the addition of Triton, while the crosslinked polymer surface will undergo degradation in GSH, leading to particle disassembly as a result of lipid solubilization with the addition of Triton. (Figure 5.6).

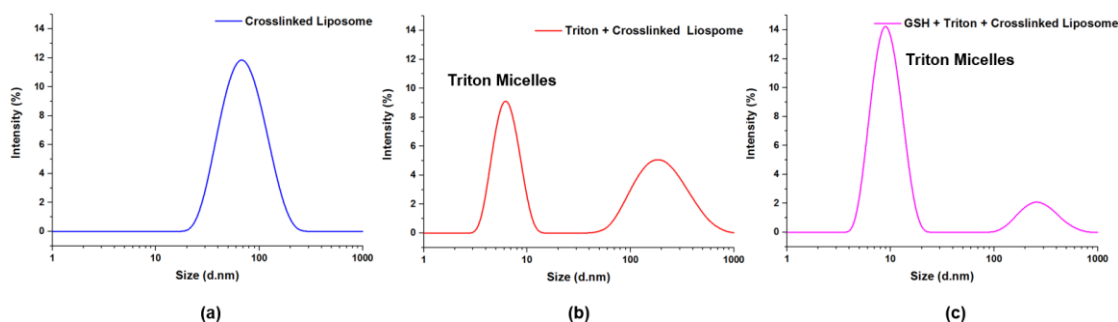


Figure 5.7 Dynamic light scattering (DLS) characterization of various liposome samples: a) surface crosslinked liposomes; b) surface crosslinked liposomes with 5 mM Triton X-100; c) surface crosslinked liposomes with 5 mM Triton X-100 and 10 mM GSH.

Preliminary DLS studies of the liposomes shown in Figure 5.7 have confirmed the surface crosslinking strategy and GSH-responsiveness. The crosslinked liposomes exhibit a monodispersed size distribution with an average diameter of approximately 75 nm (Figure 5.7a). After the addition of Triton, the liposome peak remains, confirming the increased particle stability and the success of surface crosslinking (Figure 5.7b). The size increase of the liposomes after Triton addition could be explained by the possible aggregation of mixed bilayers and mixed micelles. With the simultaneous addition of Triton and GSH, the intensity of the liposome peak decreases significantly, indicative of the disassembly of the crosslinked liposomes at the presence of GSH (Figure 5.7c).

Exploratory drug delivery studies will be carried out by loading the crosslinked liposomes with doxorubicin (DOX, drug-to-lipid ratio of ~1:1.5) and monitoring the *in vitro* release profiles via dialysis in GSH and PBS respectively. As shown in Figure 5.8, DOX is released rapidly in 10 mM GSH solutions, with approximately 85% release in 4 weeks, commensurate with the degradation of crosslinked PEG polymers on the surface. On the other hand, DOX is released in a more sustained manner in PBS, with merely 30% release under the same timescale, confirming the GSH-selectivity of the release process. It is expected that these surface-crosslinked liposomes can maintain their stability in circulation and rapidly release their payloads upon arrival at the site of disease where GSH is at elevated levels, offering significant opportunities for targeted delivery of therapeutics in cancer therapy.

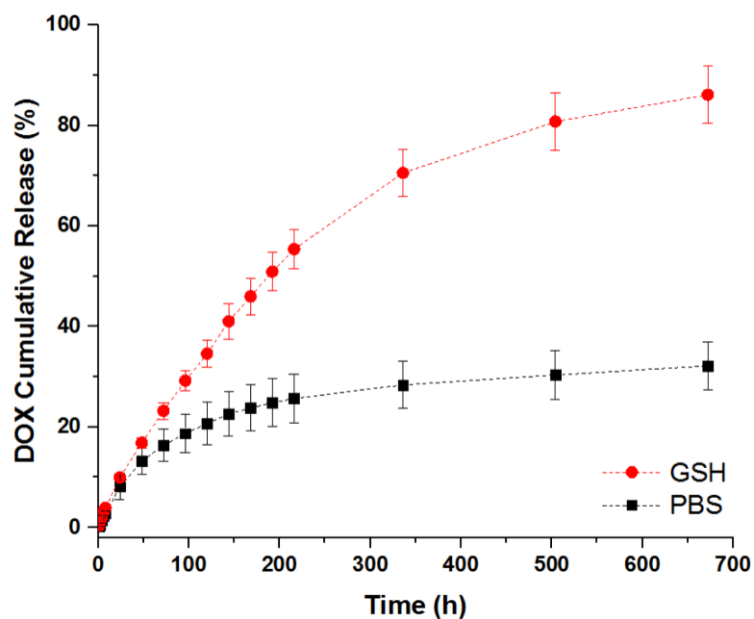


Figure 5.8 *In vitro* DOX release profiles from surface crosslinked liposomes at 37°C in 10 mM GSH and PBS respectively.

REFERENCES

1. Mura, S.; Nicolas, J.; Couvreur, P., Stimuli-responsive nanocarriers for drug delivery. *Nat. Mater.* **2013**, 12, (11), 991-1003.
2. Delplace, V.; Nicolas, J., Degradable vinyl polymers for biomedical applications. *Nat. Chem.* **2015**, 7, (10), 771-784.
3. Stuart, M. A. C.; Huck, W. T. S.; Genzer, J.; Muller, M.; Ober, C.; Stamm, M.; Sukhorukov, G. B.; Szleifer, I.; Tsukruk, V. V.; Urban, M.; Winnik, F.; Zauscher, S.; Luzinov, I.; Minko, S., Emerging applications of stimuli-responsive polymer materials. *Nat. Mater.* **2010**, 9, (2), 101-113.
4. Holmgren, S. K.; Taylor, K. M.; Bretscher, L. E.; Raines, R. T., Code for collagen's stability deciphered. *Nature* **1998**, 392, (6677), 666-667.
5. Kotch, F. W.; Raines, R. T., Self-assembly of synthetic collagen triple helices. *P Natl Acad Sci USA* **2006**, 103, (9), 3028-3033.
6. Mo, X.; An, Y. J.; Yun, C. S.; Yu, S. M., Nanoparticle-assisted visualization of binding interactions between collagen mimetic peptide and collagen fibers. *Angew. Chem. Int. Ed.* **2006**, 45, (14), 2267-2270.
7. Stahl, P. J.; Romano, N. H.; Wirtz, D.; Yu, S. M., PEG-Based Hydrogels with Collagen Mimetic Peptide-Mediated and Tunable Physical Cross-Links. *Biomacromolecules* **2010**, 11, (9), 2336-2344.
8. Perez, C. M. R.; Panitch, A.; Chmielewski, J., A Collagen Peptide-Based Physical Hydrogel for Cell Encapsulation. *Macromol. Biosci.* **2011**, 11, (10), 1426-1431.
9. Yamazaki, C. M.; Asada, S.; Kitagawa, K.; Koide, T., Artificial Collagen Gels via Self-Assembly of De Novo Designed Peptides. *Biopolymers* **2008**, 90, (6), 816-823.
10. Matsusaki, M.; Amekawa, R.; Matsumoto, M.; Tanaka, Y.; Kubota, A.; Nishida, K.; Akashi, M., Physical and Specific Crosslinking of Collagen Fibers by Supramolecular Nanogelators. *Adv. Mater.* **2011**, 23, (26), 2957-2961.
11. Yu, L.; Ding, J. D., Injectable hydrogels as unique biomedical materials. *Chem. Soc. Rev.* **2008**, 37, (8), 1473-1481.

12. Webber, M. J.; Appel, E. A.; Meijer, E. W.; Langer, R., Supramolecular biomaterials. *Nat. Mater.* **2016**, 15, (1), 13-26.
13. Perez, C. M. R.; Rank, L. A.; Chmielewski, J., Tuning the thermosensitive properties of hybrid collagen peptide-polymer hydrogels. *Chem. Commun.* **2014**, 50, (60), 8174-8176.
14. Torchilin, V. P., Recent advances with liposomes as pharmaceutical carriers. *Nat. Rev. Drug Discov.* **2005**, 4, (2), 145-160.
15. Gao, W. W.; Hu, C. M. J.; Fang, R. H.; Zhang, L. F., Liposome-like nanostructures for drug delivery. *J. Mater. Chem. B* **2013**, 1, (48), 6569-6585.
16. Moon, J. J.; Suh, H.; Bershteyn, A.; Stephan, M. T.; Liu, H. P.; Huang, B.; Sohail, M.; Luo, S.; Um, S. H.; Khant, H.; Goodwin, J. T.; Ramos, J.; Chiu, W.; Irvine, D. J., Interbilayer-crosslinked multilamellar vesicles as synthetic vaccines for potent humoral and cellular immune responses. *Nat. Mater.* **2011**, 10, (3), 243-251.
17. Joo, K. I.; Xiao, L.; Liu, S. L.; Liu, Y. R.; Lee, C. L.; Conti, P. S.; Wong, M. K.; Li, Z. B.; Wang, P., Crosslinked multilamellar liposomes for controlled delivery of anticancer drugs. *Biomaterials* **2013**, 34, (12), 3098-3109.
18. Liu, Y. R.; Fang, J. X.; Kim, Y. J.; Wong, M. K.; Wang, P., Codelivery of Doxorubicin and Paclitaxel by Cross-Linked Multilamellar Liposome Enables Synergistic Antitumor Activity. *Mol. Pharmaceut.* **2014**, 11, (5), 1651-1661.
19. Yeh, C. C.; Hou, M. F.; Wu, S. H.; Tsai, S. M.; Lin, S. K.; Hou, L. A.; Ma, H.; Tsai, L. Y., A study of glutathione status in the blood and tissues of patients with breast cancer. *Cell Biochem. Funct.* **2006**, 24, (6), 555-559.
20. Traverso, N.; Ricciarelli, R.; Nitti, M.; Marengo, B.; Furfaro, A. L.; Pronzato, M. A.; Marinari, U. M.; Domenicotti, C., Role of Glutathione in Cancer Progression and Chemoresistance. *Oxid Med Cell Longev* **2013**.
21. Baldwin, A. D.; Kiick, K. L., Tunable Degradation of Maleimide-Thiol Adducts in Reducing Environments. *Bioconjugate Chem.* **2011**, 22, (10), 1946-1953.
22. Baldwin, A. D.; Kiick, K. L., Reversible maleimide-thiol adducts yield glutathione-sensitive poly(ethylene glycol)-heparin hydrogels. *Polym. Chem.* **2013**, 4, (1), 133-143.

Appendix

COPYRIGHT PERMISSION FOR REPRINT OF PUBLISHED ARTICLES

Chapter 1

Figure 1.2.

Title: Emerging Frontiers in Drug Delivery

Author: Mark W. Tibbitt, James E. Dahlman, Robert Langer

Publication: Journal of the American Chemical Society

Publisher: American Chemical Society

Date: Jan 1, 2016

Copyright © 2016, American Chemical Society

PERMISSION/LICENSE IS GRANTED FOR YOUR ORDER AT NO CHARGE

This type of permission/license, instead of the standard Terms & Conditions, is sent to you because no fee is being charged for your order. Please note the following:

Permission is granted for your request in both print and electronic formats, and translations.

If figures and/or tables were requested, they may be adapted or used in part.

Please print this page for your records and send a copy of it to your publisher/graduate school.

Appropriate credit for the requested material should be given as follows: "Reprinted (adapted) with permission from (COMPLETE REFERENCE CITATION). Copyright

(YEAR) American Chemical Society." Insert appropriate information in place of the capitalized words.

One-time permission is granted only for the use specified in your request. No additional uses are granted (such as derivative works or other editions). For any other uses, please submit a new request.

Figure 1.3

Figure 1.3 A

Licensee: Yingkai Liang

License Date: May 24, 2016

License Number: 3875540368950

Publication: Nature Communications

Title: Moving from static to dynamic complexity in hydrogel design

Type of Use: reuse in a dissertation / thesis

Total: 0.00 USD

Your order details and publisher terms and conditions are available by clicking the

link below:

<http://s100.copyright.com/CustomerAdmin/PLF.jsp?ref=620831b0-656e-4bbf-808d-7d6664eb6e41>

Figure 1.3 B

Title: Selective Proteolytic Degradation of Guest–Host Assembled, Injectable Hyaluronic Acid Hydrogels

Author: Christopher B. Rodell, Ryan J. Wade, Brendan P. Purcell, et al

Publication: ACS Biomaterials Science & Engineering

Publisher: American Chemical Society

Date: Apr 1, 2015

Copyright © 2015, American Chemical Society

PERMISSION/LICENSE IS GRANTED FOR YOUR ORDER AT NO CHARGE

This type of permission/license, instead of the standard Terms & Conditions, is sent to you because no fee is being charged for your order. Please note the following:

Permission is granted for your request in both print and electronic formats, and translations.

If figures and/or tables were requested, they may be adapted or used in part.

Please print this page for your records and send a copy of it to your publisher/graduate school.

Appropriate credit for the requested material should be given as follows: "Reprinted (adapted) with permission from (COMPLETE REFERENCE CITATION). Copyright (YEAR) American Chemical Society." Insert appropriate information in place of the capitalized words.

One-time permission is granted only for the use specified in your request. No additional uses are granted (such as derivative works or other editions). For any other uses, please submit a new request.

Figure 1.3 C

Licensee: Yingkai Liang

License Date: May 24, 2016

License Number: 3875541102863

Publication: Soft Matter

Title: Dextran based photodegradable hydrogels formed via a Michael addition

Type of Use: Thesis/Dissertation

Total: 0.00 USD

Your order details and publisher terms and conditions are available by clicking the link below:

<http://s100.copyright.com/CustomerAdmin/PLF.jsp?ref=a176cc44-9060-4755-b1b5-92d916cce4a5>

Figure 1.3 D

Licensee: Yingkai Liang

License Date: May 24, 2016

License Number: 3875541193581

Publication: Polymer Chemistry

Title: Reversible maleimide-thiol adducts yield glutathione-sensitive poly(ethylene glycol)-heparin hydrogels

Type of Use: Thesis/Dissertation

Total: 0.00 USD

Your order details and publisher terms and conditions are available by clicking the link below:

<http://s100.copyright.com/CustomAdmin/PLF.jsp?ref=9931d6c6-f3da-4d6c-931f-c0a59714ed7e>

Figure 1.5

Figure 1.5 A

This ACS article is provided to You under the terms of this Standard ACS AuthorChoice/Editors' Choice usage agreement between You and the American Chemical Society ("ACS"), a federally-chartered nonprofit located at 1155 16th Street NW, Washington DC 20036. Your access and use of this ACS article means that you have accepted and agreed to the Terms and Conditions of this Agreement. ACS and You are collectively referred to in this Agreement as "the Parties").

1. SCOPE OF GRANT

ACS grants You non-exclusive and nontransferable permission to access and use this ACS article subject to the terms and conditions set forth in this Agreement.

2. PERMITTED USES

a. For non-commercial research and education purposes only, You may access, download, copy, display and redistribute articles as well as adapt, translate, text and data mine content contained in articles, subject to the following conditions:

i. The authors' moral right to the integrity of their work under the Berne Convention (Article 6bis) is not compromised.

ii. Where content in the article is identified as belonging to a third party, it is your responsibility to ensure that any reuse complies with copyright policies of the owner.

iii. Copyright notices or the display of unique Digital Object Identifiers (DOI's), ACS or journal logos, bibliographic (e.g. authors, journal, article title, volume, issue, page numbers) or other references to ACS journal titles, web links, and any other journal-specific “branding” or notices that are included in the article or that are provided by the ACS with instructions that such should accompany its display, should not be removed or tampered with in any way. The display of ACS AuthorChoice or ACS Editors’ Choice articles on non-ACS websites must be accompanied by prominently displayed links to the definitive published versions of those articles on the ACS website.

iv. Any adaptations for non-commercial purposes must prominently link to the definitive published version on the ACS website and prominently display the statement: “This is an unofficial adaptation of an article that appeared in an ACS publication. ACS has not endorsed the content of this adaptation or the context of its use.”

v. Any translations for non-commercial purposes, for which a prior translation agreement with ACS has not been established, must prominently link to the definitive published version on the ACS website and prominently display the statement: “This is

an unofficial translation of an article that appeared in an ACS publication. ACS has not endorsed the content of this translation or the context of its use.”

b. Each time You distribute this ACS article or an adaptation, ACS offers to the recipient a license to this ACS article on the same terms and conditions as the license granted to You under this License.

c. For permission to use ACS copyrighted articles beyond that permitted here, visit:
<http://pubs.acs.org/copyright/permissions.html>

Figure 1.5 B

Licensee: Yingkai Liang

License Date: May 24, 2016

License Number: 3875550631554

Publication: Nature Communications

Title: Self-assembled hydrogels utilizing polymer-nanoparticle interactions

Type of Use: reuse in a dissertation / thesis

Total: 0.00 USD

Your order details and publisher terms and conditions are available by clicking the link below:

<http://s100.copyright.com/CustomAdmin/PLF.jsp?ref=c7cfff05-ede6-42e7-8424-40763878d74f>

Figure 1.5 C

Licensee: Yingkai Liang

License Date: May 24, 2016

License Number: 3875550763714

Publication: Advanced Healthcare Materials

Title: A Hybrid Hydrogel Biomaterial by Nanogel Engineering: Bottom-Up Design with Nanogel and Liposome Building Blocks to Develop a Multidrug Delivery System

Type of Use: Dissertation/Thesis

Total: 0.00 USD

Your order details and publisher terms and conditions are available by clicking the link below:

<http://s100.copyright.com/CustomAdmin/PLF.jsp?ref=03aa083b-832c-4f1c-a85f-89715c327182>

Figure 1.6

Licensee: Yingkai Liang

License Date: May 24, 2016

License Number: 3875550896576

Publication: Nature Nanotechnology

Title: Nanocarriers as an emerging platform for cancer therapy

Type of Use: reuse in a dissertation / thesis

Total: 0.00 USD

Your order details and publisher terms and conditions are available by clicking the link below:

<http://s100.copyright.com/CustomerAdmin/PLF.jsp?ref=b1285f8f-b7a8-4df1-86e7-56e409871247>

Figure 1.7

Figure 1.7 A

Title: Multifunctional Nanogels for siRNA Delivery

Author: Michael H. Smith, L. Andrew Lyon

Publication: Accounts of Chemical Research

Publisher: American Chemical Society

Date: Jul 1, 2012

Copyright © 2012, American Chemical Society

PERMISSION/LICENSE IS GRANTED FOR YOUR ORDER AT NO CHARGE

This type of permission/license, instead of the standard Terms & Conditions, is sent to you because no fee is being charged for your order. Please note the following:

Permission is granted for your request in both print and electronic formats, and translations.

If figures and/or tables were requested, they may be adapted or used in part.

Please print this page for your records and send a copy of it to your publisher/graduate school.

Appropriate credit for the requested material should be given as follows: "Reprinted (adapted) with permission from (COMPLETE REFERENCE CITATION). Copyright (YEAR) American Chemical Society." Insert appropriate information in place of the capitalized words.

One-time permission is granted only for the use specified in your request. No additional uses are granted (such as derivative works or other editions). For any other uses, please submit a new request.

Figures 1.7 B and 1.7 C

Licensee: Yingkai Liang

License Date: May 24, 2016

License Number: 3875560132784

Publication: The Chemical Record

Title: Nanogel engineering for new nanobiomaterials: from chaperoning engineering to biomedical applications

Type of Use: Dissertation/Thesis

Total: 0.00 USD

Your order details and publisher terms and conditions are available by clicking the link below:

<http://s100.copyright.com/CustomAdmin/PLF.jsp?ref=3294a26e-3b73-41ff-91e8-b3c7f183dc0b>

Chapter 2

Reproduced in its entirety from:

Licensee: Yingkai Liang

License Date: May 24, 2016

License Number: 3875560685958

Publication: Journal of Biomedical Materials Research

Title: Controlled release of an anthrax toxin-neutralizing antibody from hydrolytically degradable polyethylene glycol hydrogels

Type of Use: Dissertation/Thesis

Total: 0.00 USD

Your order details and publisher terms and conditions are available by clicking the link below:

<http://s100.copyright.com/CustomAdmin/PLF.jsp?ref=b87f1d61-8fc4-4672-bafa-29ed6bda4b77>

Chapter 3

Reproduced in its entirety from:

Title: Liposome-Cross-Linked Hybrid Hydrogels for Glutathione-Triggered Delivery of Multiple Cargo Molecules

Author: Yingkai Liang, Kristi L. Kiick

Publication: Biomacromolecules

Publisher: American Chemical Society

Date: Feb 1, 2016

PERMISSION/LICENSE IS GRANTED FOR YOUR ORDER AT NO CHARGE

This type of permission/license, instead of the standard Terms & Conditions, is sent to you because no fee is being charged for your order. Please note the following:

Permission is granted for your request in both print and electronic formats, and translations.

If figures and/or tables were requested, they may be adapted or used in part.

Please print this page for your records and send a copy of it to your publisher/graduate school.

Appropriate credit for the requested material should be given as follows: "Reprinted (adapted) with permission from (COMPLETE REFERENCE CITATION). Copyright (YEAR) American Chemical Society." Insert appropriate information in place of the capitalized words.

One-time permission is granted only for the use specified in your request. No additional uses are granted (such as derivative works or other editions). For any other uses, please submit a new request.

Chapter 4

Reproduced in its entirety from:

Multifunctional lipid-coated polymer nanogels crosslinked by photo-triggered Michael-type addition

Y. Liang and K. L. Kiick, Polym. Chem., 2014, 5, 1728

DOI: 10.1039/C3PY01269G

This article is licensed under a Creative Commons Attribution 3.0 Unported Licence.
Material from this article can be used in other publications provided that the correct acknowledgement is given with the reproduced material.

Reproduced material should be attributed as follows:

For reproduction of material from NJC:

[Original citation] - Published by The Royal Society of Chemistry (RSC) on behalf of the Centre National de la Recherche Scientifique (CNRS) and the RSC.

For reproduction of material from PCCP:

[Original citation] - Published by the PCCP Owner Societies.

For reproduction of material from PPS:

[Original citation] - Published by The Royal Society of Chemistry (RSC) on behalf of the European Society for Photobiology, the European Photochemistry Association, and RSC.

For reproduction of material from all other RSC journals:

[Original citation] - Published by The Royal Society of Chemistry.

Information about reproducing material from RSC articles with different licences is available on our [Permission Requests](#) page.